# The PID Consortium

**From TOF:** * Contact/Coordinator email: chiu@bnl.gov

M.Alfred[2], M.Awadi[2], B.Azmoun[1], M.Chiu[1*] (co-PI), I.Choi[3], C.Han[3], Y.Kulinich[3], M.Grosse-Perdekamp[3] (co-PI), E.Kistenev[1], J.Lindesay[2], R.Pisani[1], S.Rescia[1], A.Sukhanov[1], J.Toh[3], R.Towell[4], T.Tsang[1], C.Woody[1]

*[1)] Brookhaven National Laboratory*
*[2)] Howard University*
*[3)] University of Illinois at Urbana-Champaign*
*[4)] Abilene Christian University*

**From RICH:** * Contact/Coordinator email: hubert@lanl.gov

F.Barbosa[e], W.Brooks[i], M.Contalbrigo[d], A.Datta[h], M.Demarteau[a], C.L. da Silva[f], J.M.Durham[f], D.Fields[h], X.He[c], H.van Hecke[f,*] (co-PI), J.Huang[b], M.Liu[f], J.McKisson[e], P.Rossi[e], Yi Qiang[e], M.Sarsour[c], R.Wagner[a], W.Xi[e], L.Xue[c], Z.Zhao[g](co-PI), C.Zorn[e] , B.Zihlmann[e] (co-PI)

a. *Argonne National Lab, Argonne, IL 60439*
b. *Brookhaven National Lab, Riverhead, NY 11901*
c. *Georgia State University, Atlanta, GA 30303*
d. *INFN, Sezione di Ferrara, 44100 Ferrara, Italy*
e. *Jefferson Lab, Newport News, VA 23606*
f. *Los Alamos National Lab, Los Alamos, NM 87545*
g. *Duke University, Durham, NC 27708*
h. *The University of New Mexico, Albuquerque, NM 87131*
i. *Universidad Tecnica Federico Santa Maria, Valparaiso, Chile*

**From DIRC:** * Contact/Coordinator emails: turonski@jlab.org, jordanka@jlab.org

L.Allison[1], T.Cao[2], R.Dzhygadlo[3], T.Horn[4] (co-PI), C.Hyde[1] (co-PI), Y.Ilieva[2] (co-PI), G.Kalicy[1], P.Nadel-Turonski[5,*] (co-PI), K.Park[1], K.Peters[3], C.Schwarz[3], J.Schwiening[3] (co-PI), J.Stevens[5], W.Xi[5], and C.Zorn[5].

*[1)] Old Dominion University, Norfolk, VA 23529*
*[2)] University of South Carolina, Columbia, SC 29208*
*[3)] GSI Helmholtzzentrum für Schwerionenforschung GmbH, 64291 Darmstadt, Germany*
*[4)] The Catholic University of America, Washington, DC 20064*
*[5)] Thomas Jefferson National Accelerator Facility, Newport News, VA 23606*

**From LAPPD/MCP** * Contact/Coordinators email: carl.zorn@jlab.org, chiu@bnl.gov

F.Barbosa[3], W.Brooks[5], M.Chiu[2]* (co-PI), M.Demarteau[1], J.Harris[6], M.Grosse-Perdekamp[4], R.Majka[6], R.Mendez[5], N.Smirnov[6], T.Tsang[2], R.Wagner[1], Ji.Wang[1], J.Xie[1], B.Zihlmann[3], C.Zorn[3]* (co-PI)

*[1)] Argonne National Laboratory*
*[2)] Brookhaven National Laboratory*
*[3)] Jefferson Lab*
*[4)] University of Illinois at Urbana-Champaign*
*[5)] Universidad Tecnica Federico Santa Maria, Valparaiso, Chile*
*[6)] Yale University*

## Abstract

An R&D consortium is proposed for an integrated program of Particle Identification (PID) challenges and opportunities for a future Electron Ion Collider (EIC). This consortium is the fusion of three previous collaborations: eRD10 (TOF), eRD11 (RICH), and eRD4 (DIRC). Each collaboration proposes to continue their work, as presented in the respective chapters of this proposal. In addition, the consortium will work together to address the issues of integrating the various proposed detectors into a PID system that will address the full range of physics goals of the EIC. Areas of common interest between the three collaborations will be coordinated. These include high magnetic field tests of photosensors and evaluation of LAPPD prototypes.

The four collaborations of this consortium are studying the following subjects:

- Picosecond Time-of-Flight (TOF). High resolution Time of Flight detection is crucial in all regions of an EIC detector. This program explores the frontier of 10 ps timing resolution, with a dual track of multi-gap Resistive Plate Chambers (mRPC) and the new Large Area Picosecond PhotoDectectors (LAPPD).
- Ring Imaging Cherenkov (RICH) detectors are essential for the hadron particle identification in the endcap region of the future Electron-Ion Collider (EIC). Both the dual-radiator RICH option and a modular RICH concept will be investigated and the associated special optics design will be carried out. In particular, LAPPDs will be carefully evaluated as the readout of the RICH detector. If feasible, the excellent timing resolution provided by this new readout will greatly improve the PID capability of the RICH detector. A GEM-based readout option will be investigated as well. At the end, the project will be able to determine the best detector technology and provide a conceptual design of the RICH detector for the EIC.
- Detection of Internally Reflected Cherenkov light (DIRC) detectors can provide high performance PID in a very compact depth. This makes them ideal for the central (barrel) region of a solenoid-based detector, as well as a possible supplement to other detectors in the EndCap regions. We propose to continue our R&D efforts to explore the intrinsic momentum limits of the DIRC concept, with a specific goal of extending $3\sigma$ $\pi/K$ separation from 4 GeV/*c* (BaBAR) to 6 GeV/*c*. Our innovations include focussing, a compact expansion volume and a highly segmented photo-sensor array.
- Large Area Picosecond Photon Detectors (LAPPD) are an exciting new technology with the prospect of lower cost, compact format, and excellent time resolution using an innovative Micro-Channel Plate (MCP) technology. This effort potentially has applications in all three PID areas.

# 1. Motivation and Introduction

The future Electron-Ion Collider (EIC) [2] will target multiple topics that are crucial to understanding the QCD structure of matter. These include: Three-dimensional imaging of quarks and gluons in the nucleon and nuclei via both deeply virtual exclusive processes (Generalized Parton Distributions) and transverse-momentum dependent parton distributions (TMDs) measured in semi-inclusive deep inelastic scattering (SIDIS); The parton to hadron transition of the current and target jets produced in deep inelastic scattering (DIS); Hadron spectroscopy, and; The elucidation of gluon saturation in heavy nuclei. This physics program requires particle identification (PID), particularly e/π/K/p over a wide kinematic range. A dedicated EIC detector is currently under development and its conceptual schematic is shown in Fig. 1.1. It is very clear that new detector technologies are crucial to help achieve the ultimate physics goals.

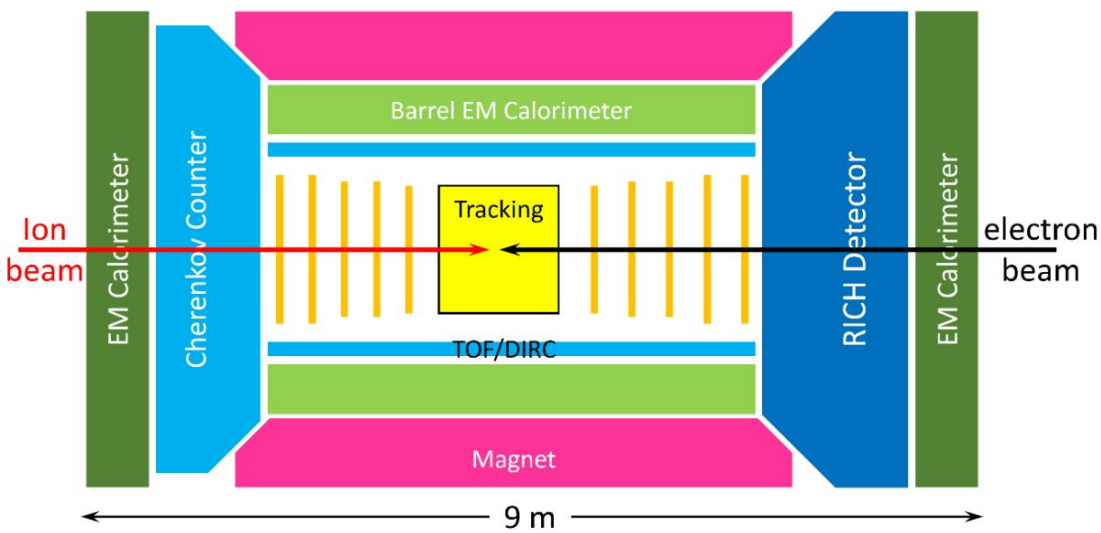


**Figure 1.1:** A schematic view of an EIC detector package.

In this PID Consortium proposal, we intend to further pursue several key PID technologies, and to start the integration of the individual detectors into a PID system. We are currently developing three basic technologies:

- Ultrafast Time-of-Flight (< 10 ps). Time-of-flight (TOF) is essential in all parts of the detector. It provides direct PID at momenta below ~3 GeV/*c*, and it provides an essential reference time for both DIRC and RICH detectors. We are currently studying both multi-gap Resistive Plate Chambers (mRPC) and prototypes from the Large Area Picosecond PhotoDetector (LAPPD) collaboration.
- Gas and Aerogel Ring-Imaging Cherenkov (RICH) detectors. We have a novel concept for a compact modular aerogel RICH counter. We are also studying how to integrate a

dual or triple radiator RICH counter into the overall detector system. A key challenge is to design a system within the geometrical constraints of a nearly hermetic detector and the strong and non-uniform magnetic field at both the radiator and photo-detector regions.

- Detector of Internally Reflected Cherenkov-light (DIRC). This is an ideal system for PID in the central region, as the DIRC detector is radially compact (≤ 5 cm) and the high performance photon-detectors occupy only a fraction of the surface area of the total detector. Unique aspects of this project include focussing in a compact expansion volume, photon-sensors in magnetic fields from 1 to 3 Tesla, and 3σ π/K separation beyond 4 GeV/*c*.

The particle detection and identification challenge naturally separates into 3 generic regions, two of which are illustrated in Fig. 1.1. The exact boundaries depend upon the specific detector design, but the general features are common to all active EIC concepts:

- The central (or barrel) region is characterized by a uniform solenoidal magnetic field and covers a kinematic region defined roughly by $|y| \leq 1$, where y is the rapidity. In this region we need to identify primarily electrons pions and kaons, but as we can see in Fig. 1.2, the momentum requirements are more modest than in the forward region.
- The forward ($4 > y > 1$) and backward ($-4<y<-1$) regions (or Endcap regions). In the forward direction the hadrons extend to much higher momenta (10 – 20 GeV/*c*). In the backward direction the primary concern is to identify electrons, but there is still a significant flux of hadrons from low-x DIS events.
- The far-forward (and backward) regions are not illustrated in Fig. 1.1, but they include detection (or veto) of beam fragments ( target fragmentation in DIS) in the far forward direction, and quasi-real photon-tagging (via detection of zero-degree scattered electrons) in the far-backward direction.

In this proposal, we are mainly concerned with hadron identification in the first two regions listed above ($|y| <4$). Using the semi-inclusive DIS (SIDIS) as an example, SIDIS is a powerful tool for disentangling the distributions for different quark and antiquark flavors. It is also the golden channel to study the TMDs and further allow us to investigate the full three-dimensional dynamics of the nucleon. While detection of pions provides information mainly regarding light quarks, kaon identification is particularly important to study both sea quark and gluon distributions (the latter via semi-inclusive and exclusive phi-meson production). The momentum distributions for pions are illustrated in Fig. 1.2 for a variety of beam configurations. In the central region ($|y| <1$) most of the pion momenta are less than 2 GeV/*c*, but there is a tail extending up to 6 or 8 GeV/*c*, depending on beam parameters. These high momentum pions (and other hadrons) are the motivation for our exploration of the limits of DIRC technology for PID. In the forward direction ($1<|y| <4$), the pion momenta typically range from less than 1 GeV to about 15 GeV, with the limits strongly correlated with angle (equivalently rapidity). From Fig. 1.3 we can see that pions greatly outnumber kaons over the whole kinematic region. In most of the momentum range the kaon yield is about 10 – 15% of the pion yield. Therefore, a 3$\sigma$ to 4$\sigma$ π/K separation is desirable for clean kaon identification.

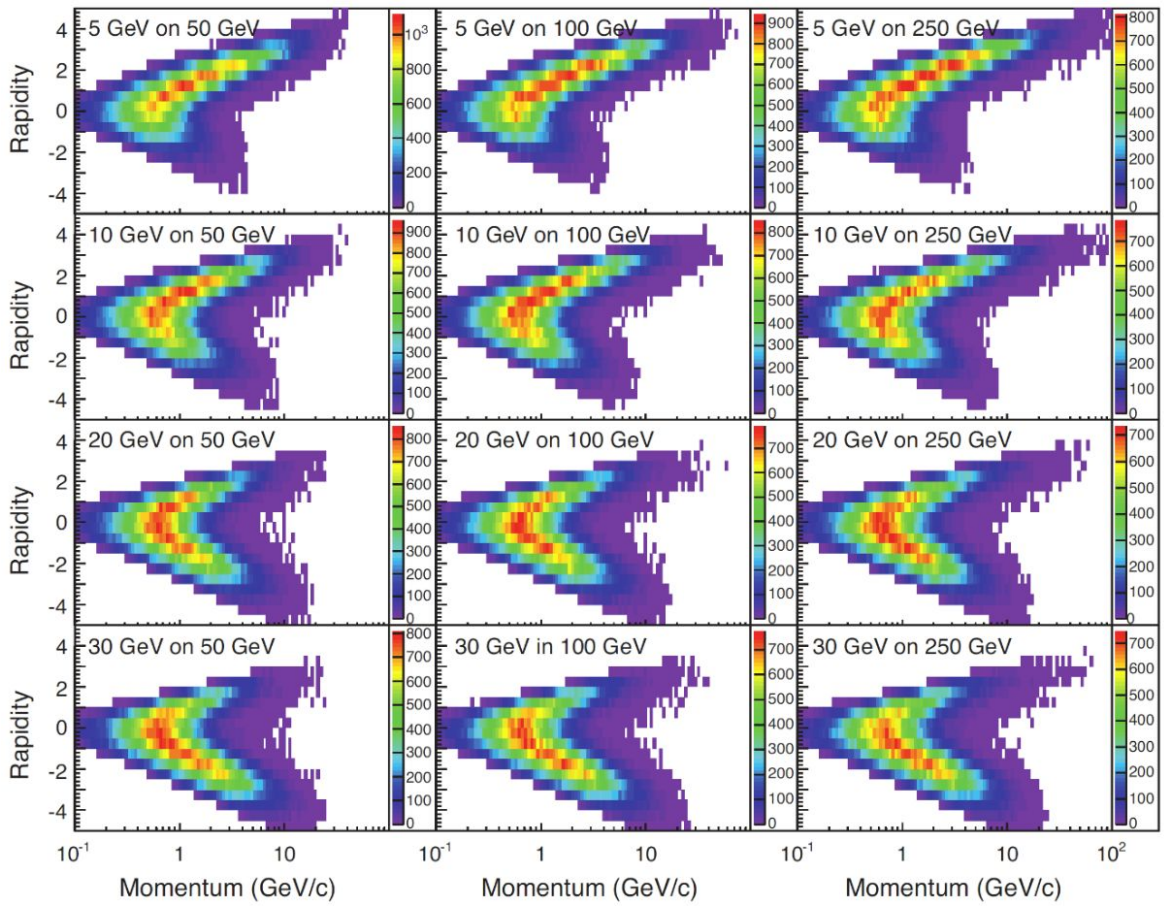


**Figure 1.2:** Momentum vs. rapidity in the laboratory frame for pions from semi-inclusive deep inelastic scattering (SIDIS) reactions [1]. The following cuts have been applied: $Q^2 > 1$ GeV$^2$, $0.01 < y < 0.95$ and $z > 0.1$.

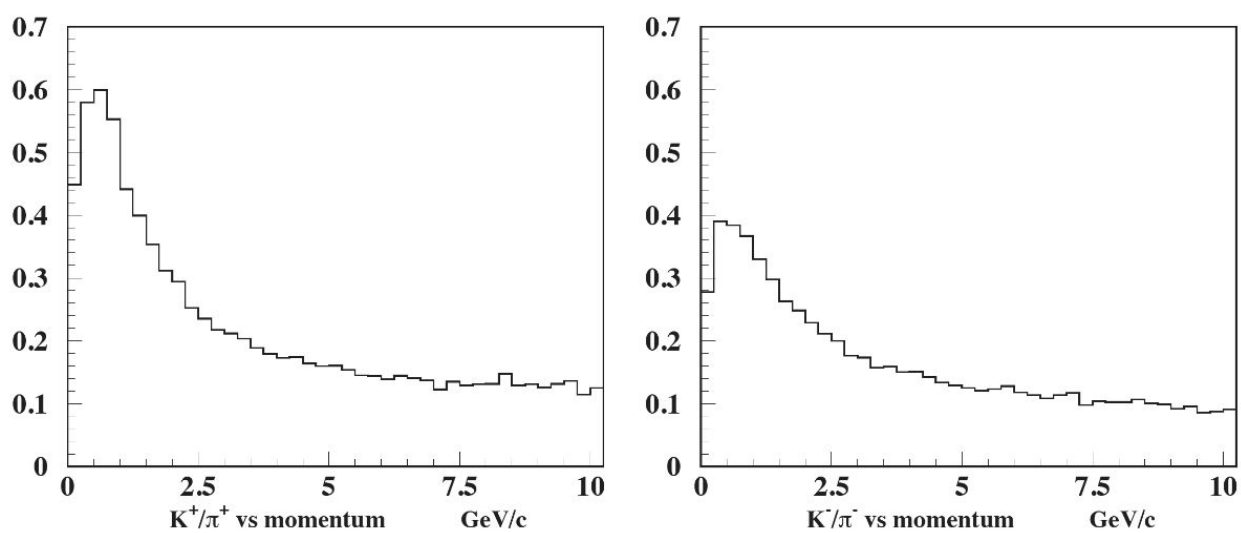


**Figure 1.3:** Kaon/pion ratio vs. momentum in the laboratory system from SIDIS events in the forward region (rapidity > 1 and for a 10×100 GeV configuration).

In order to cover such a large momentum range a combination of various particle identification technologies is needed.

- Endcap region:

  Time-of-flight benefits from a large path length in this region. TOF with resolution $\sigma(t) = \pm 50$ ps and a 4 m flight path will achieve 4σ π/K separation up to 2.7 GeV/*c*. On the other hand, if the rms timing resolution can be improved to 10 ps, the 4σ π/K separation is pushed to 6 GeV/*c*. This program is described in Chapter 2.

  Meanwhile, for the higher momentum range (3 – 15 GeV), the most viable detector options are Ring Imaging Cherenkov (RICH) detectors with dual radiators, or two RICH detectors with radiators of different refractive indices. Each radiator will provide unique sensitivities to different kinematic regions. As illustrated in Fig. 1.4, an aerogel RICH detector would provide kaon identification for the intermediate $x$ and $Q^2$ region, and a gas radiator would provide unique coverage in the high $x$ and $Q^2$ region. In Chapter 3, we discuss in more detail the R&D program of different radiators and readout options.

- Central (Barrel) Region

  Here the flight path is much shorter. At 90°, with a flight path of 1 m, 50 ps TOF resolution yields 3σ π/K separation up to 1.50 GeV/*c*, whereas 10 ps resolution pushes this to 3 GeV/*c*. In this region, 3σ separation from both the TOF and DIRC will provide 4σ π/K separation.

  The program described in Chapter 4 is an R&D program of simulations, sensor tests, and in-beam tests, to push the envelope of DIRC performance, with a specific goal of achieving 3σ π/K separation up to 6 GeV/*c*.

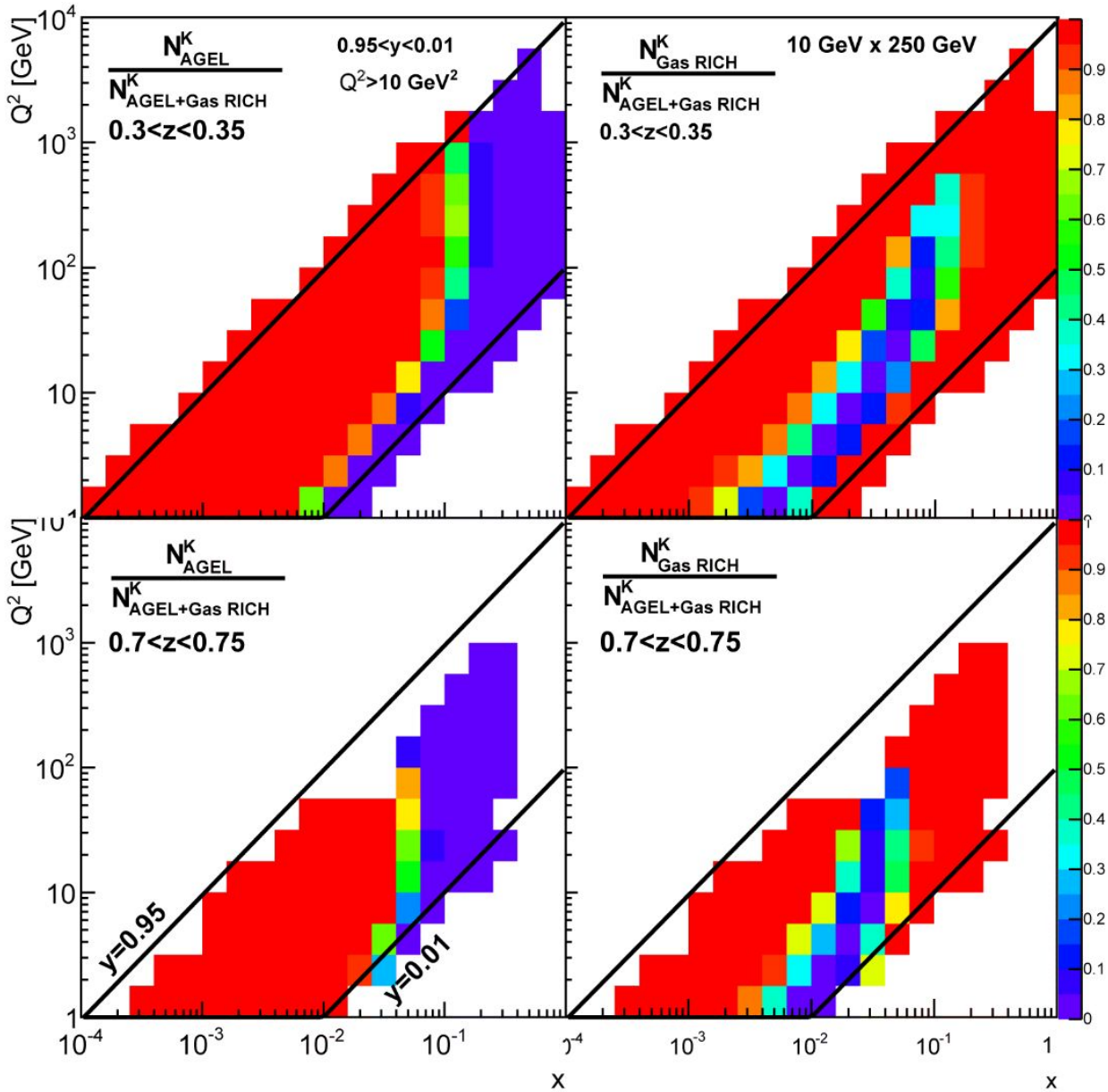


**Figure 1.4:** Yield ratios for SIDIS events with identified Kaons as function of *x* and $Q^2$, for an EIC detector with a barrel PID detector, a forward gas RICH and a forward aerogel RICH. Shown are the ratios when the forward gas RICH (left) or the forward aerogel RICH (right) are removed. Higher and lower z-ranges are shown in the top and bottom rows. This particular study is from the ePHENIX collaboration [3] for a 10×250 GeV beam configuration.

The physics goals of high performance PID are also illustrated in Fig. 1.5. The specific kinematics and detector region boundaries are for the MEIC, but the general features are generic. In this figure, the hadron three-momentum is approximated as $p_h = z(x_{Bj}P + q)$. Two examples from Fig. 1.5 illustrate the physics reach:

- For hadrons emitted at 90°, π/K separation up to 6 GeV allows full flavor separation of

SIDIS up to the exclusive limit (z=1) for x ≤ 0.05 and $Q^2 \leq 64$ GeV$^2$ and separation for *z<0.6, 0.05<x<0.1,* and 64 GeV$^2$ < $Q^2$ < 128 GeV$^2$. This range of moderate $x \approx m_\pi/M_N$ is crucial for understanding the role of chiral symmetry breaking in nucleon structure.

- For hadrons in the ion-side endcap, even for low-*x*, the hadron momenta rise rapidly at angles below 20°. Particle ID in this region is essential for achieving full flavor separations at large $Q^2$ and small *x.*

In addition to direct flavor tagging, and the sensitivity to glue through phi-production and open charm, the extended PID reach in *x* and $Q^2$ is essential for QCD evolution studies of gluon structure in both transverse momentum and coordinate space.

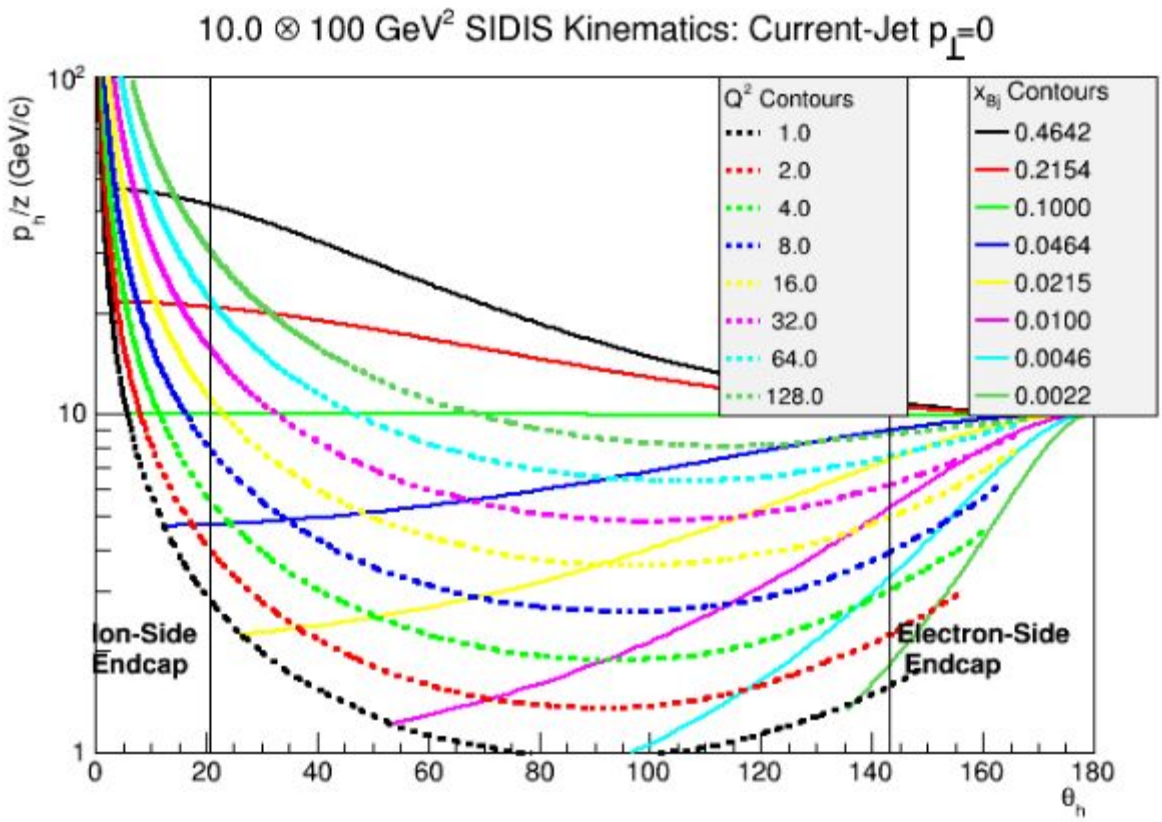


Figure 1.5: Normalized hadron three-momentum $p_h$ / z = *(xP+q)* versus angular direction of the vector *xP+q*. The solid lines are contours of constant Bjorken-*x*. The dashed lines are contours of constant $Q^2$. High momentum PID in each angular range is required to extend the physics reach to the maximal x, $Q^2$, and z ranges. The boundaries of the detector regions are illustrated for the MEIC design.

## References


[1] RICH Detector for the EIC's Forward Region Particle Identification, M. Contalbrigo et al., RD 2013-4, https://wiki.bnl.gov/conferences/images/2/27/RD2013-4_Qiang.pdf

[2] *Electron Ion Collider: The Next QCD Frontier*, A. Accardi *et al.*, arXiv nucl-ex/1212.1701 (2012)

[3] *Concept for and Electron Ion Collider (EIC) detector built around the BaBar solenoid*, PHENIX Collaboration, arXiv:1402.1170

# 2. Ten-Picosecond Time-of-Flight R&D

Marcus Alfred[2], Majed Awadi[2], Bob Azmoun[1], Mickey Chiu[1] (co-PI), Ihnjea Choi[3], Chong Han[3], Yakov Kulinich[3], Matthias Grosse-Perdekamp[3] (co-PI), Edouard Kistenev[1], James Lindesay[2], Rob Pisani[1], Sergio Rescia[1], Andrey Sukhanov[1], Jun Hui See Toh[3], Rusty Towell, Thomas Tsang[1], Craig Woody[1]

*[1)] Brookhaven National Laboratory*
*[2)]Howard University*
*[3)]University of Illinois at Urbana-Champaign*
*[4)]Abilene Christian University*

Typical time-of-flight detectors today are capable of ~100 ps resolution. Our group is working on developing detectors which we hope will improve the resolution by an order of magnitude, to a level of around 10 picosecond resolution (or better). This will allow the maximum momenta of particle identification via time-of-flight to increase by a factor of 3σ compared to existing TOF detectors. This increase in capability makes them attractive candidates for a PID detector covering the lower momentum range in both the forward (hadron-going) and barrel regions. Most of the hadrons produced will be at these lower momenta, so this is an important kinematic region to cover. It will give the best statistics for much of the x range for SIDIS measurements, for example.

Using ePHENIX as an example, in the forward direction the TOF wall would be placed at a distance of 3 m. At this location the 3 π/K separation would be at ~6.5 GeV, and the K/p separation is at ~11 GeV. This is for a TOF measurement with a total resolution of 10 ps. In the barrel region, one could place the TOF at about 1 m from the beam-pipe, with a resulting π/K and K/p separation at 3.5 and 6 GeV, respectively. Note that with 100 ps resolution, *i.e.*, using current TOF technology, one would have only $1/\sqrt{10}$ times the momentum reach. Thus previously one could only reach about 1 and 2 GeV for the π/K and K/p separation, respectively, which isn't very compelling.

A TOF detector is compact and would therefore fit in well as part of the overall suite of detectors at an experiment for the EIC. This helps reduce any space conflicts that might arise. We expect a TOF can be designed to take up no more than 10-20 cm of space, even after tilting them to be projective towards the interaction point, leaving more room for a gas-based RICH, for instance. A TOF may also help with electron-hadron discrimination, particularly when combined with dE/dx such as from a TPC.

We have identified two different detector approaches that we believe are very promising to achieve the goal of 10 picosecond, or hopefully better. One is based on multi-gap resistive plate chambers (mRPC) that have thinner gas gaps, as well as more gaps than the current designs in use at Alice, STAR, and PHENIX. The other approach is based on using a 1 cm

quartz cerenkov radiator read out by micro-channel plate PMTs (MCP-PMT's) built by the LAPPD collaboration. MCP-PMT's have extremely good timing performance of ~50 ps transit time spread (TTS) or better. The key attribute besides this superlative performance for the LAPPD MCP-PMTs is that they are expected to have a cost that is within reason. Current commercial MCP-PMTs from vendors such as Photonis or Hamamatsu are more than $1 million per square meter, and the hope is that the cost will be reduced by at least a factor of 3-5. Between the two detector approaches, the mRPC is expected to be cheaper, but the timing resolution will be worse when compared to MCP-PMTs. The MCP-PMTs are also expected to perhaps be more tolerant of magnetic fields than the mRPCs, though both are expected to be able to work in high fields (this needs further confirmation however). The cost, magnetic field tolerance, as well as the better performance makes the MCP-PMT a possibly better choice for the barrel region, where the flight path is the shortest and therefore performance is at a premium. The larger area that must be covered in the forward region may be a better option for the mRPC since it will be cheaper.

For the past year our group's effort has mostly concentrated on building and testing glass mRPCs in a cosmic ray stand, and testing the high bandwidth preamps and waveform digitizing electronics that are needed. We have also embarked on simulations of SIDIS production of kaons in e+A collisions as a motivation for the TOF detector that we propose. The code for detailed detector design simulations with Garfield++ has also been started but are only halfway done. The details for these accomplishments over the past year are in the eRD10 Progress Report. We believe our results with the mRPC are very promising, and we would like to continue this effort over the next year since we have ideas for improving the result further.

For our proposed LAPPD MCP-PMT effort, we have not made much progress, but within the context of this new PID consortium we are very eager to begin collaborating on the MCP-PMT R&D in the upcoming year.

# 2.1 Multi-Gap Resistive Plate Chambers (mRPC) R&D

mRPCs are in widespread use as TOF detectors for heavy ion experiments, and are installed in Alice, Star, and PHENIX. These devices are made of float glass, fishing line, PCB, and graphite, so they are fairly cheap to construct. Their low cost makes them suitable for covering large areas (175 $m^2$ in the case of Alice), and with decent performance. The typical reported resolutions from the above experiments are in the range of ~60-100 ps, which has been the typical resolution for TOF detectors over the past several decades (without much improvement over that time).

By going to smaller gap sizes (250 um to 150 um), and doubling the number of gaps from 12 to 24, and reducing the thickness of the glass, Crispin Williams, et al have shown that a resolution as good as ~20 ps is achievable [1,2]. Over the past year our group has been working to reproduce this result. A picture of a prototype 24 gap mRPC built at UIUC is shown in Fig. 2-1, where you can see the stack of 24 gaps, each 150 um wide, and grouped into 4 layers. Two identical prototypes were built, and their performance was assumed to be the same in order to determine the resolution for one detector.

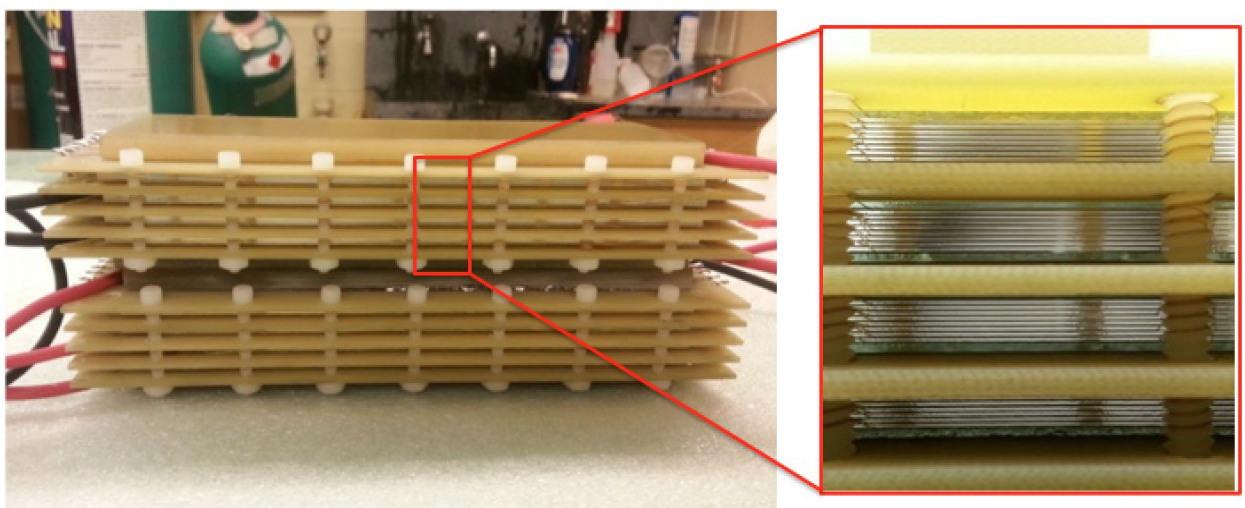

**Figure 2.1:** Prototype mRPC with 24 gaps, 150 um each.

The device was tested in a cosmic ray test stand made of scintillators with a lead brick to remove lower energy muons. A Drift Chamber was also read out in coincidence to provide tracking of the muons, so that we could determine the angle of incidence and where the muons hit on the mRPC. The resulting time difference between the two prototypes is shown in fig. 2-2. There seem to be two contributions to the time difference of the two prototypes, one with a narrow peak with a $\Delta t$ of 32.5 ps, and a much broader distribution underneath. We believe the wider distribution may come from cross-talk between the copper strips, or from streamer events. Assuming identical mRPC's, the resolution of one detector is $\Delta t/\sqrt{2}$ ~ 18 ps. The figure includes

corrections for the angle of incidence, which changes the path length between the two detectors. This analysis is still on-going and we expect to have updated results by the EIC R&D meeting in July 2015.

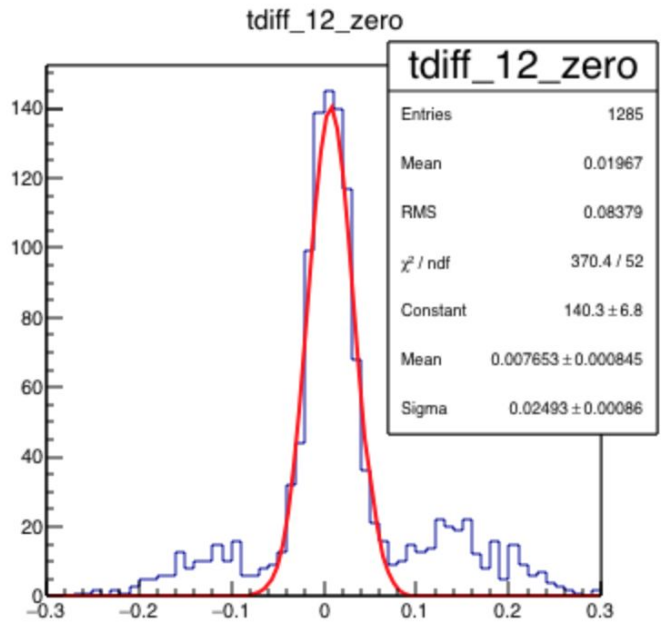


**Figure 2.2:** Distribution of $\Delta t = t_1 - t_2$ of the measured times from a cosmic muon incident on the two mRPCs.

# Further Improvements to mRPC Performance

One possibility we have considered for improving mRPCs is to replace the glass material with another dielectric. The advantage of going to different materials is that one can make them much thinner, thus bringing the signals generated in the gas gaps closer to the cathode pickup. This will increase the magnitude of the signal on the cathode pickup strips, and therefore increase the signal to noise ratio as well as improving the risetime. Both changes will serve to improve the timing resolution since the time resolution is proportional to the SNR/risetime. Also with new thinner materials one can create many more gaps in the same volume, increasing further the signal to noise ratio, and improving efficiency.

Replacing the dielectric may also reduce the cost, and make building a mRPC much easier since one doesn't have to worry about glass breakage. For alternative materials we have considered mylar and kapton. Also recently the UIUC group has explored 3D printing the gas gap structure entirely, as in fig. 2-3. In the 3D printing case, not only would the materials be much cheaper, but also the assembly and production will be vastly simplified since one

produces the entire gas gap structure pre-built. This should dramatically reduce the costs for building the detector.

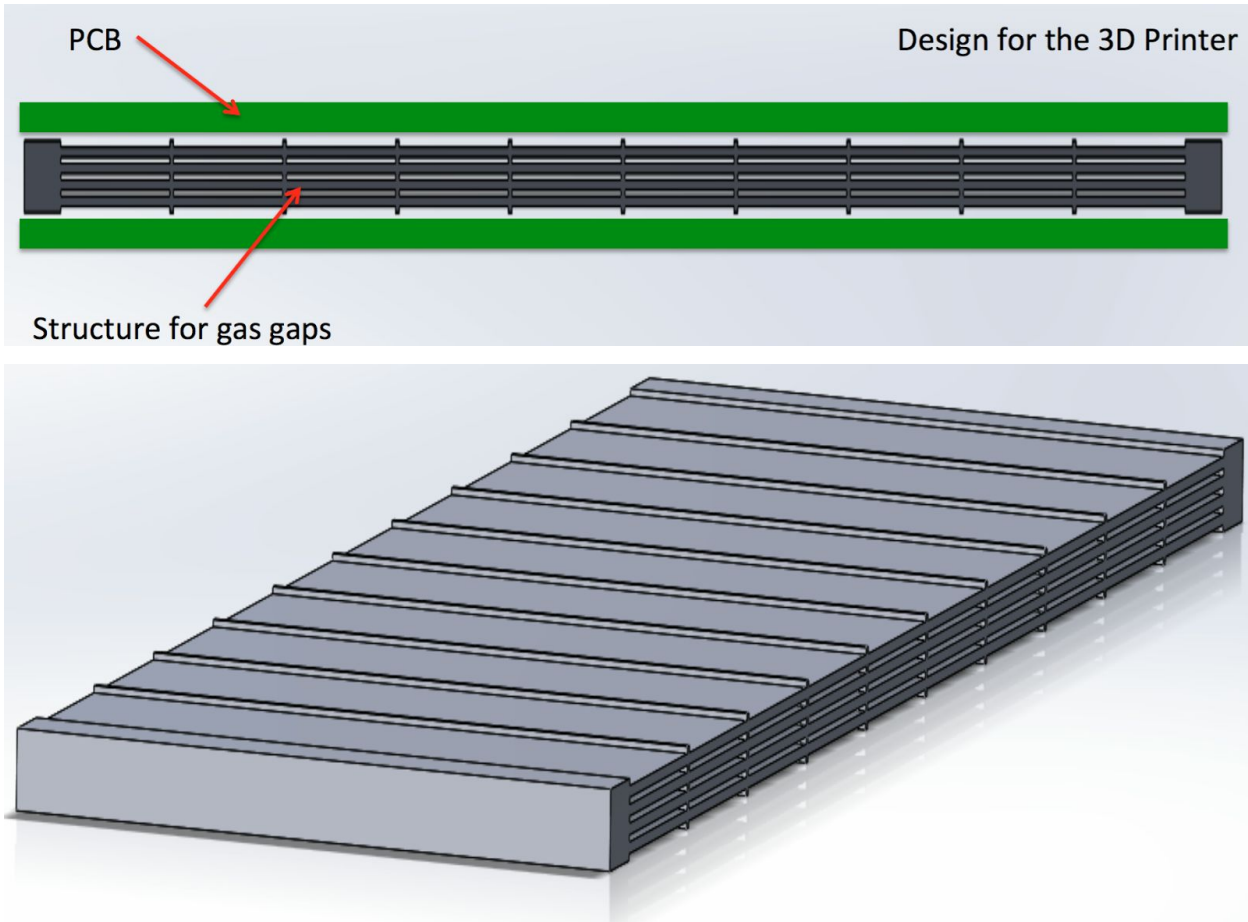


**Figure 2.3:** 3D printed design of a gas gap structure for a mRPC

In table 2-1, various 3D printers available at UIUC are listed. There are a variety of printers that will print layers that are 100 um thick with a surface uniformity of about 10 um, which should be adequate for the mRPC gap. The costs listed are just for the raw printer materials, and there will not be an additional cost at UIUC for using the printer. There are a wide variety of materials that can be used in the printing, from ABS plastics to nylon. Each of these has different resistivities and will have to be tested to determine their rate capabilities. Another important criteria are to make sure the materials do not outgas. Some baking may be required before they can be used in an mRPC gas volume. We expect to compare a few different 3D printed materials to see how well they perform in mRPCs. In particular, there is an open question about how the electron recombination occurs in mRPCs. A resolution of this question will be helped by these studies using new materials for the dielectrics.

| Type | Formiga P 100 Selective Laser Sintering System (SLS) (EOS) | Fortus 360MC (FDM) | Viper si Stereo Lithography Apparatus (SLA) (3D Systems) | Eden 350 (Objet Geometries, Ltd.) | MakerBot Replicator 2 |
|---|---|---|---|---|---|
| | Laser | | Laser | Polyjet Technology | |
| Where | Mech Rapid Prototyping Lab (RPL) | | | | Business department |
| Build Platform Size | 200mm x 250mm 330mm | 406 x 355 x 406 mm (16x14x16in) | 250mm x 250mm x 250mm | 350mm x 350mm x 200mm | 246 L x 152 W x 155 H mm |
| Layer thickness | PA 2200 is now also available in 0.06 and 0,12 mm layer thicknesses, as well as 0.1 mm | 0.330mm | Minimum — 0.02 mm (0.001 in); Typical — 0.10 mm (0.004 in) | 16 micron | 100 micron |
| Material | PA 2200, PA 2201, PA 3200 GF, PrimeCast 101, PA 2105 and various other materials in planning (plastic) | Thermoplastic / Polycarbon | ProtoGen O-XT 18420 (ABS-like photopolymer) WaterClear Ultra 10122 ( optically clear resin with ABS-like properties ) | FullCure 720 Transparent , Vero Materials, Tango Materials | PLA / ABS |
| Price | $0.37/g | $0.33/g | $0.38/g | $0.34/g | |

Table 2-1: Various 3D printers available at UIUC, their specifications, and the cost for printing. The red highlighted printer is the one that will be used for further studies.

Besides 3D printed plastics, we will also test using mylar and kapton as replacements for the glass. Mylar and kapton have very different resistivities of $10^{19}$ and $10^{16}$ Ω-cm, compared to float glass ($10^{13}$ Ω-cm), but this should be partly compensated by the fact that mylar and kapton are available in much thinner sheets than glass (by over an order of magnitude). The key technical challenge is to be able to keep the stacked sheets flat over a relatively large area of about 20x20 $cm^2$, and keeping a gas gap of ~100 um between each sheet. We believe this should be possible by attaching the sheets to 100 um shims, which have a thickness tolerance of 5%, and then tensioning the sheets. Additionally, the usual carefully placed fishing line that is used for glass mRPCs will counter the sag that would occur in the middle of the mylar or kapton sheets.

Another possibility for improving the performance of the mRPC might be to identify a gas which can produce more initial ionization electrons, since these are one of the main contributions to the resolution. In table 2-2 we have listed the properties of some gases, where $n_p$ is the number of primary ionization electrons [3]. These initial electrons may have enough energy before acceleration by the electric field to create more electron-ion pairs. The total of the $n_p$ and secondary electron creation is $n_t$. Here one can see why i-C4H10 is used in mRPCs. Just for illustration, one can see that a possible alternative, better gas for timing applications is Xe, since it has a large number of initial electrons created. However, Xenon is expensive, so as part of our R&D we will research other possible gases to find one that is a good combination of cost and performance. We will also consider other parameters, such as pressure (as suggested by

the committee), which may also help to increase performance in a way that is possible to implement at the EIC.

| Gas | Z | A | Density $10^{-3}$ ($g/cm^3$) | $E_x$ (eV) | $E_i$ (eV) | $w_i$ (eV) | $[dE/dx]_{mip}$ ($keV\ cm^{-1}$) | $n_p$ ($cm^{-1}$) N.T.P | $n_t$ ($cm^{-1}$) N.T.P. | Radiation Length (m) |
|---|---|---|---|---|---|---|---|---|---|---|
| He | 2 | 2 | 0.178 | 19.8 | 24.5 | 41 | 0.32 | 4.2 | 8 | 745 |
| Ar | 18 | 39.9 | 1.782 | 11.6 | 15.7 | 26 | 2.44 | 23 | 94 | 110 |
| Ne | 10 | 20.2 | 0.90 | 16.6 7 | 21.56 | 36.3 | 1.56 | 12 | 43 | 345 |
| Xe | 54 | 131.3 | 5.86 | 8.4 | 12.1 | 22 | 6.76 | 44 | 307 | 15 |
| $CF_4$ | 42 | 88 | 3.93 | 12.5 | 15.9 | 54 | 7 | 51 | 100 | 92.4 |
| DME | 26 | 46 | 2.2 | 6.4 | 10.0 | 23.9 | 3.9 | 55 | 160 | 222 |
| $CO_2$ | 22 | 44 | 1.98 | 5.2 | 13.7 | 33 | 3.01 | 35.5 | 91 | 183 |
| $CH_4$ | 10 | 16 | 0.71 | 9.8 | 15.2 | 28 | 1.48 | 25 | 53 | 646 |
| $C_2H_6$ | 18 | 30 | 1.34 | 8.7 | 11.7 | 27 | 1.15 | 41 | 111 | 340 |
| i-$C_4H_{10}$ | 34 | 58 | 2.59 | 6.5 | 10.6 | 23 | 5.93 | 84 | 195 | 169 |

Table 2-2: Physical properties of gases at 20° C and 760 Torr.

Since the parameter space is very large, a full simulation of the physical process of avalanche creation in small gas gaps is needed in order to guide our R&D. The processes are well understood, and there are a few simulations that have been done before, but to our knowledge no one has undertaken a systematic study to determine the best combination of factors that will improve the timing resolution. We are building on the pre-existing work [4], and over the next year will hopefully identify a configuration in the parameter space that maximizes the timing resolution. The code is currently about halfway done, is open source and available at

https://www.github.com/EIC-eRD10/mrpc_garfield

A master's student at Howard University has been identified who will complete the studies, under the tutelage of Marcus Alfred. These studies, once completed, will help us to optimize some of the other design decisions with regard to choosing the properties, such as the resistivity and flatness requirement of the materials we would like to use to replace the float glass that is currently the standard.

## 2.2 LAPPD MCP-PMT based TOF R&D

An extremely high performing TOF can be made using MCP-PMT's, as shown in figure 2-4. A thick glass (or fused silica) plate of about 1 cm thickness is used as the front window of the MCP-PMT. When a charged particle goes through the window, it radiates Cerenkov photons. These Cerenkov photons hit the bottom side at about the same time (since they form a wavefront) and generate photoelectrons from the photocathode almost simultaneously. Thus,

the time measurement will be approximately TTS/√N.P.E., where TTS = transit time spread. Since the TTS spread of the MCP-PMT is about 50 ps, one can achieve timing resolutions of much less than 10 ps if one generates enough Cerenkov light.

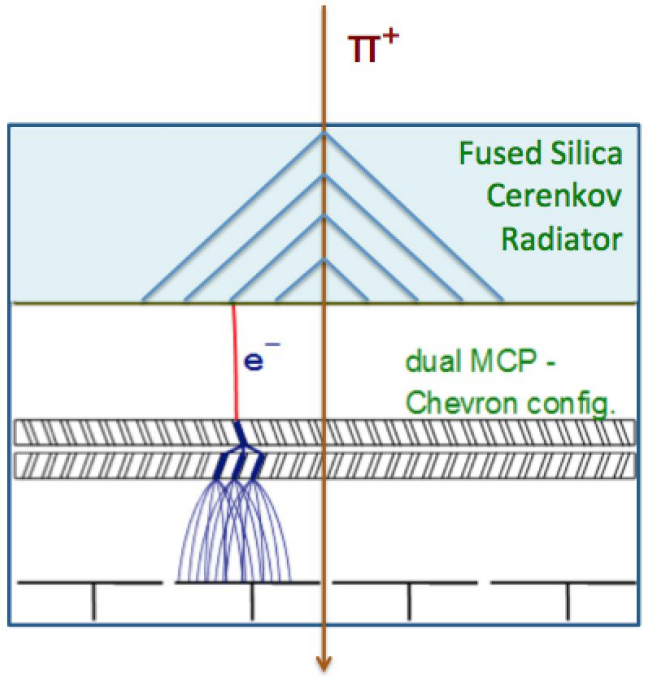


**Figure 2.4:** Schematic drawing of the signal development in a MCP-PMT.

In table 2-3, we have calculated the theoretical maximum for the N.P.E. and the resulting theoretical best resolution for the timing resolution. These calculations assume a TTS of 50 ps for the MCP-PMT, and uses the photocathode QE curves from figure 5-2 (as well as a QE curve from John Smedley for $K_2CsSb$).

| RadiatorWindow | Thickness (cm) | Photocathode | N.P.E. | $\sigma_t$ (ps) TTS=50 ps |
|---|---|---|---|---|
| Borosilicate Glass | 1 cm | $K_2CsSb$ | 70 | 6 |
| Borosilicate Glass | 1 cm | $CsNa_2kSb$ | 100 | 5 |
| Fused Silica | 1 cm | $K_2CsSb$ | 127 | 4.4 |
| Fused Silica | 1 cm | $CsNa_2kSb$ | 250 | 3.2 |

| | | | | |
|---|---|---|---|---|
| MgF2 | 1 cm | $CsNa_2kSb$ | 335 | 2.7 |
| MgF2 | 1 cm | CsI | 316 | 2.8 |
| CF4 | 100 cm | $CsNa_2kSb$ | 72 | n/a |
| CF4 | 100 cm | CsI | 92 | n/a |

Table 2-3: The estimated theoretical maximum number of photoelectrons for various Cerenkov Radiator and Photocathode combinations, and the resulting theoretically best possible $s_t$. The values for CF4 are for a windowless configuration, where the photocathode is deposited on the top MCP.

The LAPPD cathode is $K_2CsSb$, so by changing the window and photocathode it should be possible to improve the timing resolution by a factor of 2, possibly to an amazing 3 ps. In chapter 5 the LAPPD group has proposed a plan for FY16 where they will try changing the normal boro33 glass window to fused silica, and possibly also change the photocathode to $Na_2KSb$. We will test and compare these modules to see if their timing performance really is as good as we hope.

## 2.3 Fast Electronics

For this early R&D phase, we have been able to identify a very cost effective setup for the mRPC readout, despite the challenges in being able to measure at better than 10 picoseconds. Remarkably, whereas just 5 years ago one probably needed $50K for a 10 GHz scope and $1K/ch for GHz amplifiers, we have been able to do our R&D for just $150/ch for the amplifiers and $300/ch for the digitizer.

While we had previously identified a waveform digitizer, the DRS4, we had not identified a good amplifier option. Over the past year several new high bandwidth amplifiers with relatively low power requirements have become available from Texas Instruments. We have been evaluating several different versions of these TI amplifiers: the LMH6554, LMH6881, and the LMH5401. They have gain bandwidth products of 2.8 GHz, 2.4 GHz, and 8.0 GHz respectively, with extremely good slew rates. The LMH5401 for instance has a slew rate of 17,500 V/$\mu$s. The typical power draw for the preamps is about 50 mW/channel, which is quite reasonable. They are fully differential, which is essential in order to reduce noise from the + and - pickup cathodes on the mRPC. To couple to the 50 ohm single-ended DRS4 input, we have found adequate wideband baluns such as the TC1-1-13MA+.

Over the past year we have also successfully tested DRS4 based boards to have a resolution of just 2 ps/sample. This is a major improvement over the 8 ps/sample that we had previously achieved, and is due to a change in the time calibration procedure so that each channel is separately calibrated via a generated sine waveform [5]. Note that no amplifier is necessarily needed for the MCP-PMT readout, since that device is capable of gains of $10^6$, and can thus be

read out directly with the DRS4.

Currently we are optimizing the coupling of the preamps to the detector impedance, and also investigating different transient voltage suppressors to protect the preamps from voltage surges. Once that testing is done, BNL will layout and produce a preamp board that contains the LV power distribution, the protection system, the preamp, and the balun for further testing.

While our electronics setup works well for our current R&D which requires only a few channels of readout (~10), we ultimately require a readout that will be capable of being scaled to thousands of channels at a cost of ~$100/ch, and which can also work in a collider environment. The best options are based around the proposed PSEC5 and DRS5 chips, which are waveform sampling switched capacitor array (SCA) based ASICs. These are based upon the PSEC4 and DRS4 ASICs, which are 1-20 and 0.5-5 GHz SCA waveform samplers, respectively, with roughly 30 MHz digitization rates. The PSEC4 and DRS4 cannot be used since they have only very short arrays of 256 and 1024 cells. For such short buffers, by the time the trigger decision reaches the ASIC the information is gone. At colliders one usually needs at least 3 μs of buffering for this “trigger latency.”

The PSEC5 and DRS5 are both envisioned to have enough cells to cover the trigger latency. Since it is impossible to digitize at the full multi-GHz rate, a windowed digitization scheme will need to be implemented where one digitizes only a triggered window. Neither are funded and would require O($1M) to proceed. Other groups are also interested in developing these ASICs, and we expect we might be able to contribute to this funding if TOF construction is ever approved.

# Schedule

## FY16

1. Ihnjea Choi and students at UIUC will develop a prototype aiming for sub-10ps resolution using 3D printed gaps (or whatever is deemed to work best).
2. BNL group will develop kapton and mylar mRPCs at BNL and test them
3. ACU group will help do studies over the summer at BNL
4. The studies will include systematically understanding the performance of the device with respect to different gas mixtures, voltages, different design decisions (gap sizes, number of gaps, type of dielectric, etc).
5. Howard will work on Garfield++ simulations of the mRPC designs to guide above experimental studies
6. UIUC will continue MC simulations (Geant4 based) with a fully integrated PID system using TOF + RICH + DIRC so that we can help to determine the best PID configuration for an EIC detector, and make sure that our most important physics goal are achievable.
7. BNL, along with UIUC, will make initial studies of more UV sensitive LAPPD MCP-PMT's from Argonne to evaluate them for TOF purposes.

## FY17

1. All the involved groups will collaborate to produce several full scale prototypes using the best technology we will have developed during FY16, and comparatively test them in the test beam. Full scale means that one module would be the typical module size we expect at an EIC detector, perhaps 20x20 $cm^2$. The optimum module size will be determined based on simulations and occupancy considerations, as well as the necessities of the detector properties.
2. MC simulations will continue at UIUC
3. LAPPD MCP-PMT evaluation will continue. Potentially, evaluation large area (20x20 $cm^2$) LAPPD MCP-PMT's produced commercially at Incom will be available for evaluation as well.

## FY18

1. MC simulations will continue at UIUC.
2. We hope our mRPC R&D will be relatively completely by FY18, and expect more of our effort to gravitate toward LAPPD based TOF development. Thus, this work plan will evolve (as well as our budget request) as we learn more about how LAPPD development is going.

# Budget Request

| mRPC | FY16 | FY17 | FY18 | Total |
|---|---|---|---|---|
| UIUC Postdoc (0.5FTE/yr) | $60,000 | $0 | $0 | $60,000 |
| Travel | $3,000 | $6,000 | $3,000 | $12,000 |
| mRPC Subtotal | $63,000 | $6,000 | $3,000 | $72,000 |

The budget requested includes costs for a postdoc (Ihnjea Choi) in FY16 that is cost-shared between the EIC R&D program and UIUC. Ihnjea has been supported by a total of $120K over FY14 and FY15, amounting to 1 FTE's worth of funding, most of which was received in FY15. We believe Ihnjea has done an extraordinary job, and we strongly urge the committee to support one more 0.5 FTE of funding for him to complete his research over the next 6 months. Without that funding the R&D on 3D printed mRPC's will be seriously delayed. Travel funding is also requested for trips to EIC meetings twice a year and for a test-beam in FY17.

No materials costs are requested for FY16 as these can be covered by UIUC and their NSF base grant, as well as Mickey's PECASE funding from BNL. The materials cost has totaled about $30K so far. Travel costs over the past year for Ihnjea were funded through UIUC (he made a trip to CERN to learn from Crispin Williams, and to assist with a project there to build large area mRPC's). UIUC also has and will provide funding for an undergraduate student to do simulation studies of physics observables using PID via a TOF and RICH detectors in a realistic EIC geometry. In FY15 this was done by Chong Han who has recently graduated. Another UIUC student will be identified for FY16.

Howard University will provide a Master's Student, Majed Awadi, to work on the mRPC Garfield simulations. Majed is funded for the next two years by a Saudi Arabia fellowship, and can work at the 0.3 FTE/year level. He is expected to start in June 2015 and work through the summers, and in his spare time during the school year while he is taking classes.

Abilene Christian University is funded through a DOE grant to work on PHENIX Spin during the summers at BNL, and will begin to transition their program toward EIC topics. They will provide students to help with building prototypes, setting up the lab, running some prototype tests and analyzing the data.

# References


[1] S. An, et. al., “A 20-ps timing device: A Multigap Resistive Plate Chamber with 24 gas gaps”, Nucl.Instrum.Meth. **A594** (2008) 39-43. We also note that in a private communication to us, Crispin says that he achieved 16 ps as the best result, and he expected from simulation that 8 ps resolution is achievable.

[2] K. Doroud, et. al., “Performance of Multigap Resistive Plate Chambers with pure Freon 134A”, Nucl.Instrum.Meth. **A629** (2011) 106-110

[3] Archana Sharma, “Properties of some gas mixtures used in tracking detectors”, SLAC-JOURNAL-ICFA-16-3, 1998.

[4] K. Doroud, et. al., “Recombination: An important effect in multigap resistive plate chambers”, Nucl.Instrum.Meth. **A610** (2009) 649-653

[5] D. Stricker-Shaver, S. Ritt, B.J. Pichler, “Novel Calibration Method for Switched Capacitor Arrays Enables Time Measurements with Sub-Picosecond Resolution”, http://arxiv.org/pdf/1405.4975.pdf

# 3. RICH - Ring Imaging Cherenkov Counter

Contact/Coordinator Email: hubert@lanl.gov

F.Barbosa[e], W.Brooks[i], M.Contalbrigo[d], A.Datta[h], M.Demarteau[a], C.L. da Silva[f],J. M. Durham[f], D.Fields[h], X.He[c], H. van Hecke[f,*](co-PI, contact), J.Huang[b], M.Liu[f], J.McKisson[e], P.Rossi[e], Yi Qiang[e], M.Sarsour[c], R.Wagner[a], W.Xi[e], L.Xue[c], Z.Zhao(co-PI)[g], Carl Zorn[e], B. Zihlmann[e] (co-PI.)

a. Argonne National Lab, Argonne, IL 60439
b. Brookhaven National Lab, Riverhead, NY 11901
c. Georgia State University, Atlanta, GA 30303
d. INFN, Sezione di Ferrara, 44100 Ferrara, Italy
e. Jefferson Lab, Newport News, VA 23606
f. Los Alamos National Lab, Los Alamos, NM 87545
g. Duke University, Durham, NC 27708
h. The University of New Mexico, Albuquerque, NM 87131
i. Universidad Tecnica Federico Santa Maria, Valparaiso, Chile

## Abstract

An R&D program is proposed to investigate the technology used for a Ring Imaging Cherenkov (RICH) detector for the hadron particle identification in the forward region of the future Electron-Ion Collider (EIC). Both the dual-radiator RICH option and a modular RICH concept will be investigated and the associated special optics design will be carried out. In particular, a newly developed Large-Area Picosecond Photo-Detector (LAPPD) using innovative Micro-Channel Plate (MCP) technology may become available for the readout of the RICH detector. If feasible, the excellent timing resolution provided by this new readout will greatly improve the PID capability of the RICH detector. A GEM-based readout option will be investigated as well. At the end, the project will be able to determine the best detector technology under four concurrent EIC detector designs and provide optimized conceptual designs of the RICH detector for EIC. This is an update based on original proposal eRD11.

## 3.1 Dual-Radiator Concepts

When compared with two separate Cherenkov detectors, a dual-radiator RICH detector has the advantage of a more compact size and lower cost by using a shared readout, Figure 3.1.1 and 3.1.3 shows three options for dual-radiator RICH detectors for the EIC: lens focused, approximate focused and mirror focused designs.

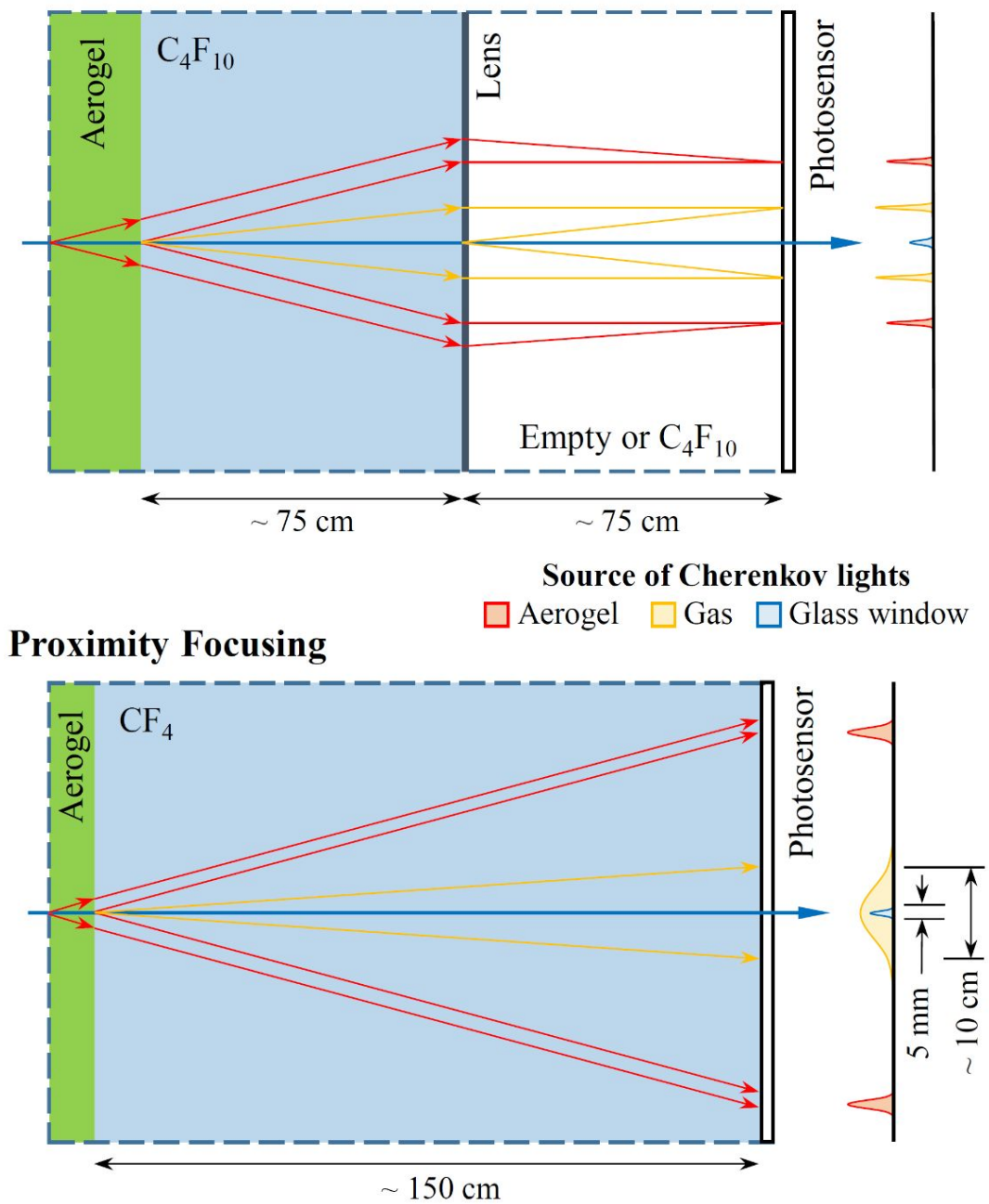


**Figure 3.1.1:** Options for a dual-radiator RICH detector for the EIC. Top: a concept with focusing using a Fresnel lens; Bottom: a concept using proximity focusing.

The length of both devices is chosen to be about 150 cm, given the space available in the MEIC design.

The first concept shown on top is a focusing RICH detector. In this concept, an aerogel radiator is put in the front to cover the 3–10 GeV momentum range. Following the aerogel is a 75 cm long gas radiator volume containing $C_4F_{10}$ to cover the 10–15 GeV range. The Cherenkov photons generated in each of the radiators are then focused by a Fresnel lens with a focal length of 75 cm. A super ultraviolet transmitting (SUVT) acrylic lens may be used to allow transmission of Cherenkov photons with wavelengths longer than 280 nm, as shown in Fig. 3.1.2. With about 10–20 photoelectrons per Cherenkov ring, the required position resolution of the readout is a few millimeters in order to reach 4$\sigma$ kaon/pion separation. Furthermore, because of the spatial resolution of the readout device, the photosensors don't need to be placed at the focal plane of the lens, but can be moved closer to reduce the total length of the detector.

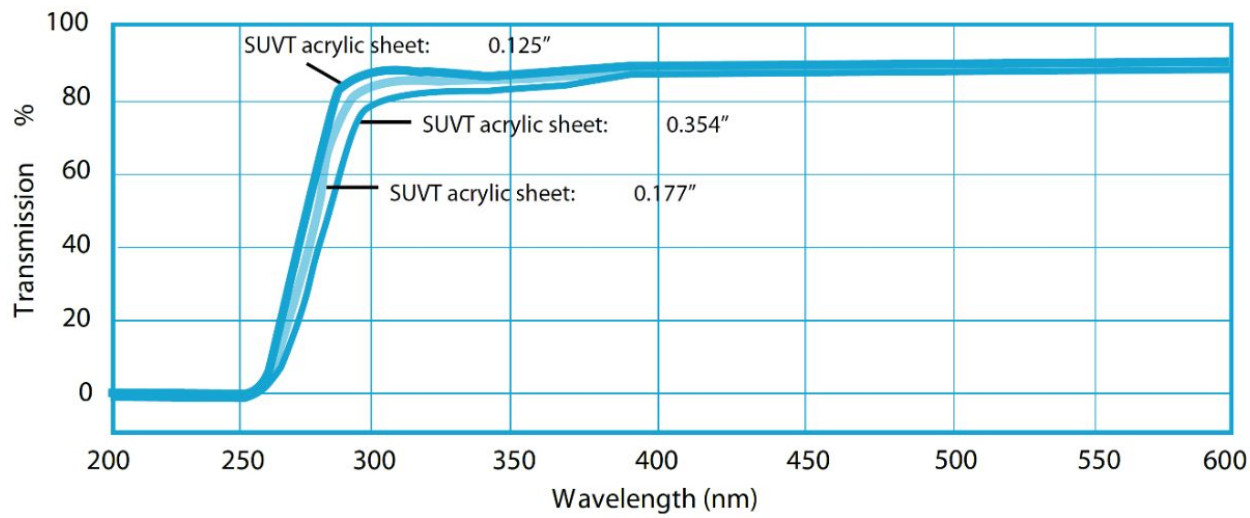


**Figure 3.1.2:** Transmittance of super ultraviolet transmitting (SUVT) acrylic sheet [13].

The second concept is a proximity focusing RICH detector. The first radiator is still aerogel. In order to achieve a reasonable angular reconstruction with proximity focusing, the thickness of the aerogel has to be limited to a few centimeters and the readout needs to be far away. Hence a 150-cm long volume is left between aerogel and readout. This volume will be filled with $CF_4$ gas and serves as a threshold Cherenkov detector to veto pions up to 17 GeV. In the high momentum range (10–15 GeV), the separation of kaons and protons will still rely on aerogel. Although the proximity design seems much simpler in terms of optics design and mechanical construction, one big challenge will come from the Cherenkov radiation in the glass window of the readout sensors. Because of the photocathode coating, Cherenkov photons will exit the window and produce photoelectrons in the photocathode, instead of being trapped inside the

window due to internal reflection. The hits generated by these photoelectrons will be concentric with the Cherenkov hits originated from $CF_4$. The coverage and amplitude of such a background signal depend on the window thickness. A 2 mm window typically generates about 10 photoelectrons with a spread of 5 mm. With a 2-dimensional readout, these signals from glass window can be removed by applying geometric cuts. Nevertheless, thinner windows will clearly help suppress this kind of background. Both concepts shown here are still in a very preliminary stage. More effort will definitely be needed to identify the best option with optimal optical design and an appropriate combination of radiators. These efforts are part of this proposed project.

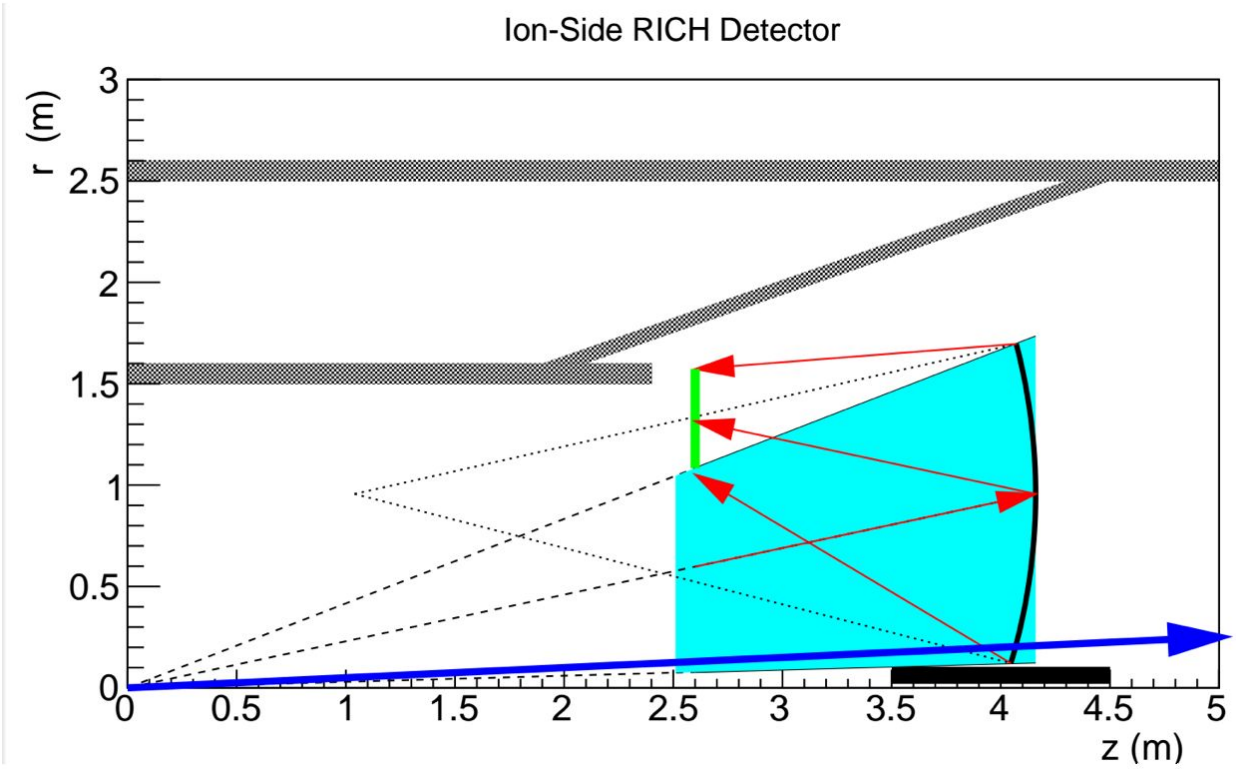


**Figure 3.1.3:** A mirror-based design, with compact readout outside of the radiator volume. The detector plane (green) can be placed such that it is shadowed by the barrel calorimeter.

In the third concept, mirror-based designs will also be explored. An LHCb-style layout, with the readout placed to the sides, can be adapted to fit into an EIC detector, such as shown in Figure 3.1.3. The readout area in such a design can be more compact, and can be placed in the shadow of a barrel calorimeter. Since the readout is placed outside the radiator acceptance, the total thickness of this arrangement can be very small.

## 3.2. Modular Concepts

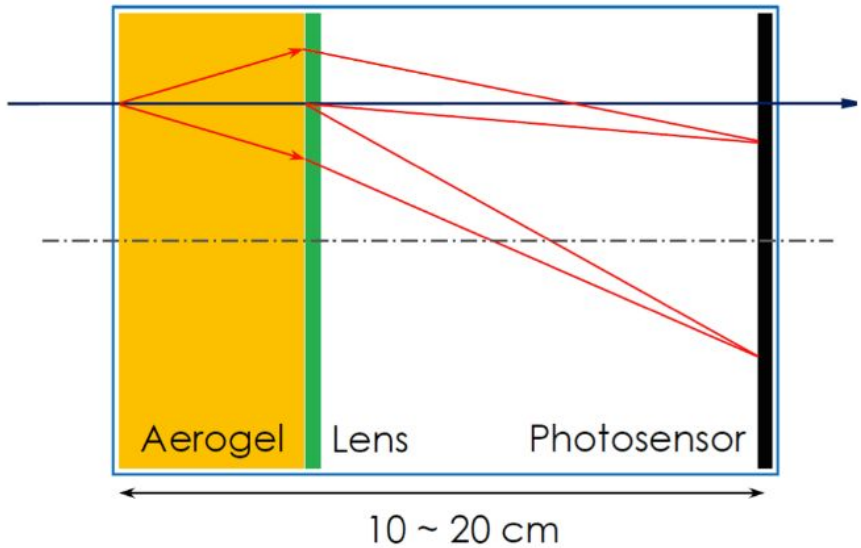


**Figure 3.2.1:** Diagram of a modular imaging aerogel detector, which consists of an aerogel radiator (orange), a Fresnel lens (green) and a photon detector (black). Although not shown, a proximity focusing design will also be explored. A module would be 10-20 cm across.

In this scheme, a large detector would be built up out of small, independent aerogel-based RICH units. A schematic of one unit is shown in Fig. 3.2.1. Each unit would contain a Cherenkov radiator, in this case aerogel (orange), followed by an acrylic Fresnel lens (green), which focuses the Cherenkov photons onto a photon detector (black). In addition, the acrylic lens functions as a filter blocking scattered, short-wavelength photons. An alternative option that will be examined will be proximity focusing design using a stack of aerogel blocks of varying indices of refraction, as proposed for the Belle-II detector.

The scale of this unit would be determined by the size of the aerogel tiles used (assuming a single tile per unit), or by the size limitations of available Fresnel lenses or readout systems, but is expected to be of scale 10-20 cm. For particles that are incident parallel to the axis of the unit, Cherenkov rings would be centered in the unit's axis. The lens' focal length should be chosen such that the ring is smaller than the unit's diameter. Off-axis incident tracks result in rings offset from the center, but if the off-axis angular distribution is limited, the diameter of the sensitive area could be smaller than the size of the unit. The spatial resolution of the photon detector will be determined by the requirement that kaons and pions be distinguished at the upper end of the momentum range. Since the ring size in the modular design is expected to be of order ~10 cm, the pixel size will likely need to be small, one-to-few mm.

Full simulation of these units in the experimental environment will determine the parameters of this scheme, such as the necessary resolution of the photon detector, the focal length *etc*. When more than one charged particle traverses a given module, position and momentum information available from other detectors will be used in combination with the ring-hit distributions to determine the particle identities. Detailed algorithms will be developed based on full simulations.

Comparing with the dual-radiator concept, the modular aerogel RICH require additional detector to cover to larger momentum end. One excellent match would be the HBD-based gas RICH prototype as developed by Dehmelt, Hemmick et al., now eRD6, in the 2012 proposal 'Proposal for detector R&D towards an EIC detector'.

## 3.3. LAPPD Readout

One possible choice for position-sensitive detection of Cherenkov photons is LAPPDs, large-area picosecond photon detector. These devices will be studied by eRD10, the TOF group of this consortium.

## 3.4. GEM-Based Readout

GEMs with a reflective photocathode film deposited on the uppermost surface have recently emerged as an attractive photon detection technology [21], see Figure 3.4.1. Since the amplification structure is effectively decoupled from the charge collection plane, the geometry of the readout pattern can be optimized for the desired resolution with a minimal channel count. GEMs are available in various sizes from a range of foreign and domestic manufacturers. GEMs function well in magnetic fields. They have also been shown to operate in a variety of gases that are transparent in the wavelength range of interest, which minimizes Cherenkov photon losses.
In the wavelength range of interest for unscattered Cherenkov photons produced in aerogel, ~300–500 nm, bialkali crystals such as Sb-Cs-K have the necessary quantum efficiency (QE) to function as photocathodes as shown in Figure 3.4.2. Early studies by Breskin *et al.* [22] have shown a reasonable QE when deposited onto GEM foils. However, the effective QE is also strongly dependent on the choice of gas, which affects photoelectron scattering back into the photocathode.
Part of this research will therefore be to find the appropriate gas or mixture of gases to maximize the collected photoelectron yield in the 300-500nm range. Bialkali photocathodes are notoriously reactive with oxygen, and therefore the detector must be assembled without exposure to oxygen. However, the relatively small size and modular nature of the design considerably simplifies this task. In addition, the design of the detector greatly simplifies maintenance during operation and allows for straightforward replacement of individual modules, if necessary.

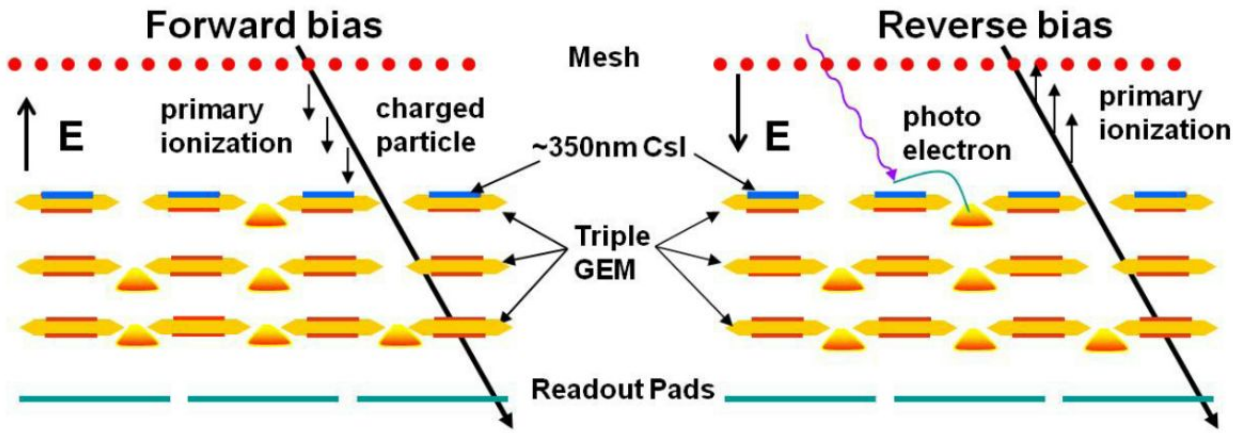


**Figure 3.4.1:** Triple GEM stack operated in the standard forward bias mode (left) and in the hadron-blind reverse bias mode (right) [21].

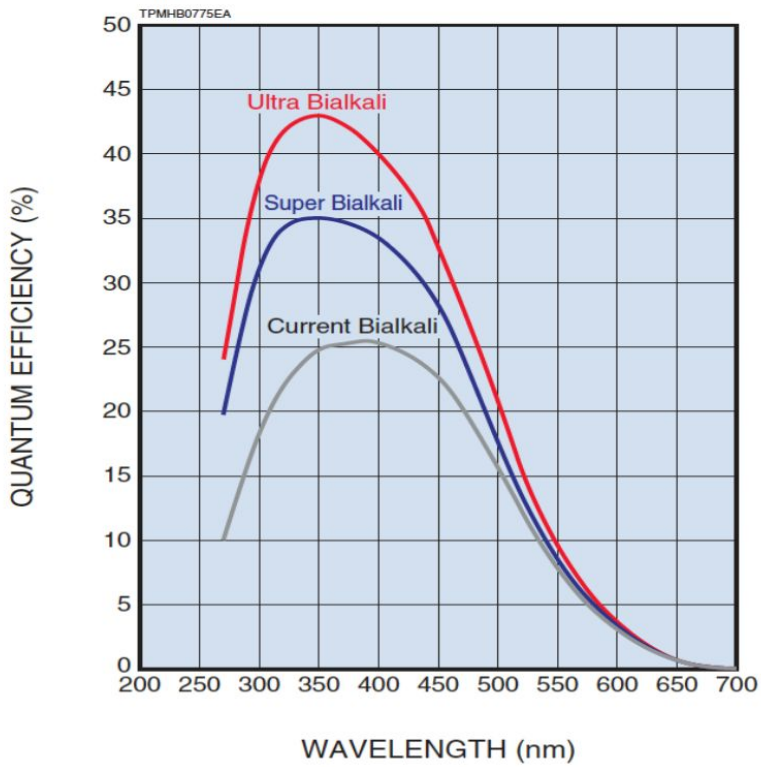


**Figure 3.4.2:** Typical quantum efficiency curves for bialkali photocathodes from Hamamatsu Photonics Corporation.

# 3.5. Goals and R&D Activities

The goal of the project is to determine the detector technology and provide a set of conceptual designs of the RICH detectors, available to be used in various full EIC detector designs. This project span over a course of three years.

We will carry out feasibility studies in various aspects toward a conceptual design:

- Provide a set of conceptual designs, compare their performance in an generic EIC environment. Depending on the final full EIC detector designs, the future EIC experimental collaboration can use the performance specifications to choose one or a combination of RICH designs and apply them to the final full EIC detector.
- Simulation to quantify the performance of above designs in Geant4. Construct generic analysis package for EIC RICH-based PID analysis.
- Large area visible light sensor development. Besides the LAPPD R&D as discussed in Chapter 5, we also study of a GEM-based photodetector in the 300-600nm wavelength range, and compare its performance.
- Test of prototypes, including the construction of a prototype modular Cherenkov detector.

Upon the completion of the project, with a detector technology and the conceptual design chosen for a future EIC detector collaboration, further work is anticipated for continuous development and producing more specific prototypes of such RICH detectors.

## 3.5.1 Further quantification for conceptual designs

Different collision environments and detector topologies require different solutions for hadron particle ID in the forward direction, using the RICH technique, in combination with other techniques as studied in this consortium. Therefore, we plan to study a set of optimized concepts for a generic EIC environment:

- Aerogel-only detector. These detectors emphasize kaon-pion separation in the few-GeV range, which is complementary to the HBD-based gas-radiator RICH as developed in eRD6 consortium. Two concepts are being pursued:
    - A novel design of modular RICH using Fresnel lens as focusing element. This work started in FY15 under funding of eRD11. We would like to extend this design work to constructing a prototype in the coming funding cycles as further discussed in the following sections.
    - Proximity focusing RICH using a stack of aerogel blocks of varying indices of refraction, as proposed for the Belle-II detector.
- Aerogel-gas dual radiator detector. The focusing strategy includes proximity focusing, lens-focusing (as discussed in the last section) and a mirror focused detector (as used in for example in LHC-b). This work has just started under project eRD11, under funding from JLab and INFN.

We plan to quantify the performance of each design within at least one of the proposed facility (eRHIC and MEIC) and detector (MEIC-concept, BeAST, ePHENIX and eSTAR) concepts through full Geant4 simulation. The preference of different detector design . The first stage of this work is demonstrated in the next section, since the funding of the eRD11 project since FY15.

## 3.5.2. Detector Simulation

The goal for detector simulation is to obtain the requirements on various components of the RICH detector, aid the development of the conceptual design and justify its performance in full EIC detector and beam environment. After initiation of the project in FY15, an initial standalone GEANT4 implementation of the modular concept was constructed, as shown in Figure 3.5.2.

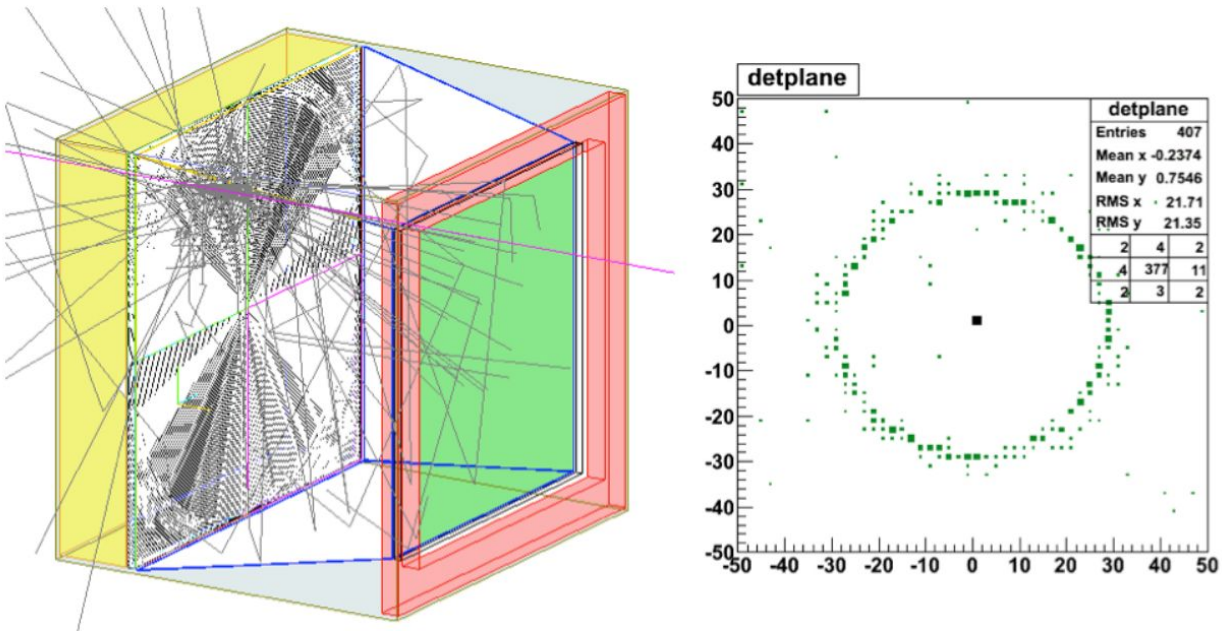


**Figure 3.5.2:** a) Implementation of a modular counter unit in Geant-4. Visible are aerogel(yellow), a Fresnel lens, flat mirrors (blue), photon detector (green), detector readout (red). b) superposition of 10 rings from incident 5 GeV muons.

The major simulation studies are listed:

- Implementation of optical elements
- Study of the requirements on aerogel: refractive index, uniformity, flatness and clarity
- Requirements on the photodetector: rate capability, sensitive wavelength, single photon detection efficiency, position resolution, field sensitivity and radiation tolerance
- Study multiplicity and ambiguity with different readout/charge-collection segmentations - strip and pixels
- Develop a preliminary reconstruction algorithm
- Study the performance of the RICH detector in a generic EIC detector model and in the full EIC collision environment.

The basic simulation framework we choose to use is the GEMC [23] (GEant4 Monte-Carlo)

based MEIC simulation [24] developed by Jefferson Lab. It serves as a C++ wrapper around GEANT4. For detector subsystems, the geometry, material, field, sensitivity are entered as external input to GEMC. MEIC-GEMC has the ability to customize hit processing routine and output according to various detectors. Overall, these features enable simulating individual sub-detectors and the whole detector in the same framework and make it effortless to switch between them. With its modularized design, MEIC-GEMC framework can easily incorporate the proposed RICH detector into the simulation to study its performance and how it can work with other detector systems together to achieve the physics goals. Dr. Zhiwen Zhao, now at Duke University, is one of the authors and the current maintainer of the MEIC-GEMC software. He will continue to provide guidance and support of the simulation. A JLab postdoc together with one student and one postdoc from GSU will conduct the simulation work. Co-PI Hubert van Hecke (Los Alamos) and Dr. Jin Huang (BNL) will coordinate the effort as they are both experienced with designing large scale detector systems such as BNL's PHENIX and sPHENIX [27] spectrometers and an EIC detector built upon BaBar magnet at eRHIC [3].

Over the last year, a considerable amount of progress has been made on some of the goals listed above. For full details, refer to the June 2015 ERD11 progress report, or to the technical note posted at

http://phynp6.phy-astr.gsu.edu/~hexc/EIC/mRICH_note/technote.pdf

In particular, the modular device has been implemented in the GEMC framework, and ring finding algorithms have been developed. In this full simulation, and using the maximum likelihood analysis method for ring pattern recognition, the pi, K, p identification efficiencies can be determined as a function of incident angle and momentum. An example set of efficiencies is shown in Figure 3.5.2 for incident particle angles of $\theta = 5^o$, $\phi = 45^o$ at momenta ranging from 2.5 to 15 GeV/c. There is reasonable separation up to ~7 GeV in the current configuration. This limit can now be studied as a function of aerogel refractive index and other system parameters.

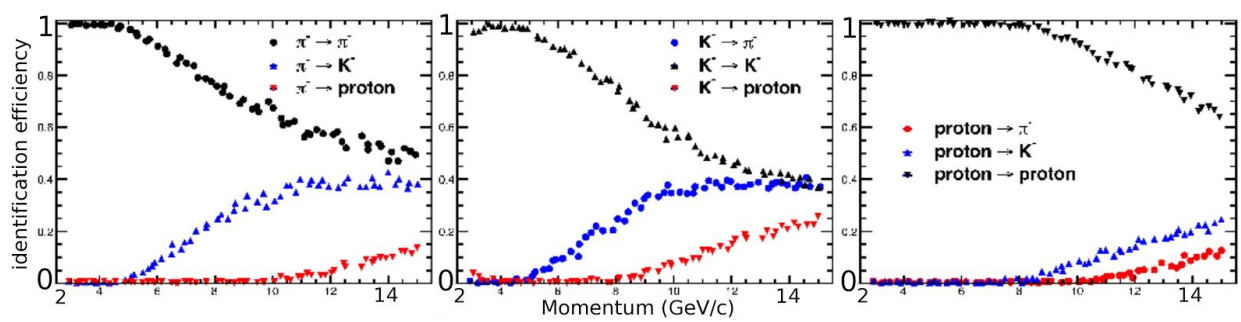


**Figure 3.5.2:** The (mis)identification probabilities plotted versus momentum for pi, K, and p using a maximum likelihood ring-finding method as further described in eRD11 progress report. This set is simulated for particles with incident angles polar angle of $\theta = 5^o$, and azimuthal angle of $\phi = 45^o$

As one example implementation inside a full EIC detector, an array of modules has been constructed in the simulation of an EIC detector and are now being studied.

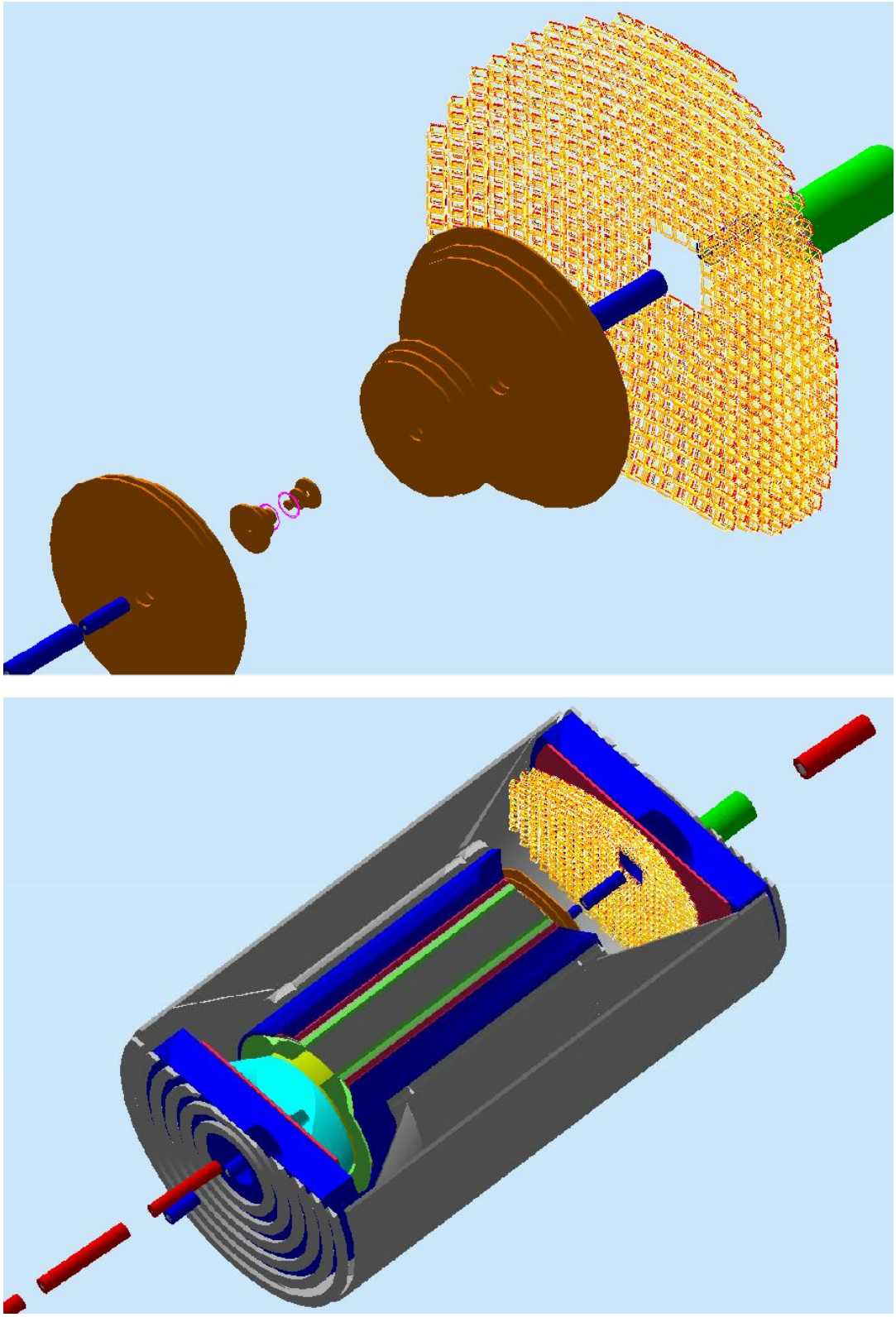

**Figure 3.5.4:** Modular RICH detectors integrated in MEIC.

## 3.5.2. Study of GEM-Based Readout

While GEMs coated with CsI have been used to detect UV photons in previous experiments, the use of a GEM photocathode coating that is sensitive in the wavelength range appropriate for aerogel radiators (~300–500 nm) has not yet been realized on a large scale. The first phase of photosensitive GEM development will focus on optimizing photocathode deposition parameters and operating gases to give the highest possible effective quantum efficiency (QE).
The group of III-V semiconductor materials, such as GaAs, have relatively high quantum efficiencies in the wavelength range of interest to this project. Appropriate photocathodes developed over the course of this research could be used in conjunction with either the LAPPD or GEM readout systems.

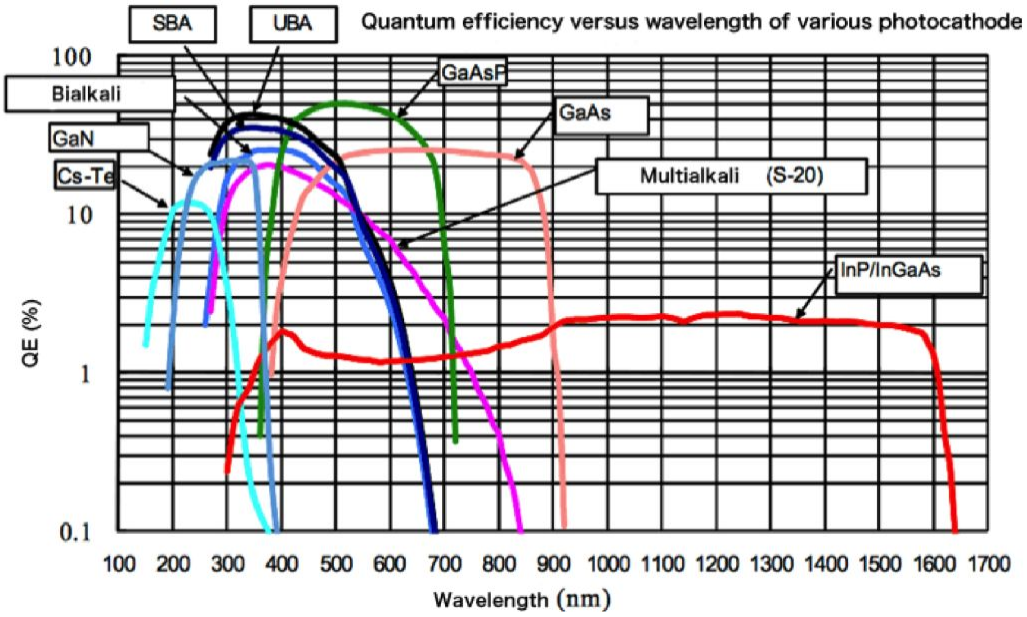


**Figure 3.5.2.1:** Comparison of quantum efficiencies for various photocathode materials, from Hamamatsu Corp.

Development of such photocathodes for high-energy physics experiments has typically been limited by the necessity of using large, expensive, dedicated crystal growth facilities to produce acceptable samples. The University of New Mexico Center for High Technology Materials (CHTM) is such a facility. The CHTM houses two metal-organic chemical vapor deposition reactors, five molecular beam epitaxial growth reactors, and extensive clean rooms for testing and evaluating semiconductor materials.

Photocathode development and characterization will proceed as follows: First, candidate materials will be grown at the UNM CHTM, starting with a simple GaAs crystal fixed to glass.

During the first year, the photocathodes will be tested by exposing them to light from LEDs and collecting the resulting current on a charged plate. Comparisons to a reference phototube of known QE will allow the absolute QE of the GaAs samples to be measured. The effects of the electric field at the surface, photocathode thickness, and activation agents (such as Cs0) on the current extracted into both vacuum (for the LAPPD application) and gas (for coupling to GEMs) will be studied. The QE in both reflective and transmission modes will be measured.

In order to achieve a high total quantum efficiency at the lowest wavelengths of light that will be emitted from the aerogel (~300 nm), gap tuning of the semiconductor materials with the introduction of P into the material will be studied, in parallel with the photoelectron collection tests. Combinations of glasses that are transparent down to the aerogel cutoff and tuned semiconductors will be measured.
The ultimate goal of this phase of the project is the development of a suitable combination of entrance window and photocathode that will produce a high photoelectron yield in the 300-500 nm wavelength range.
We have already begun a discussion with several of the faculty associated with CHTM and have received our first samples (GaAs) from them to characterize at the Medium Energy Physics lab at UNM. A small vacuum chamber for testing the photocathode's quantum efficiency in vacuum has been identified at UNM.
Triple-GEM detector kits, with an x-y strip readout plane and associated electronics, will be purchased from CERN. In such a manner, along with bench measurements of GEM gain in the gas, a suitable operating gas can be chosen. In parallel with these laboratory measurements, a suitable readout pattern will be developed in simulation, which can maximize ring resolution while minimizing channel count. This readout pattern will then be tested on the bench

### 3.5.3. Construction of a prototype

While photon detectors are being developed, a prototype modular detector can be constructed to test other aspects of the design. This prototype would have a block of aerogel, an acrylic Fresnel lens, a housing with mirrored interior surfaces. The photon detector will use a multi-anode PMT (Hamamatsu H12700A selected) or a SiPM array (Hamamatsu S13361 considered).
With this prototype many aspects of the proposed detector can be studied, such as the optical properties of the aerogel, transmission efficiency and focusing ability of the fresnel lens. Using a silicon telescope to define the trajectory of incoming particles, these tests can be done using cosmic rays, and in a test beam at Fermilab, in conjunction with test being planned for other devices in the Spring of 2016.

## 3.6. Budget

The budget needed to complete the proposed project is listed in Table 2 and Table 3.
Table 2. Budget breakdown by activities, in k$.

| Item | Time (FTE)/Cost | | | Remarks |
|---|---|---|---|---|
| | FY16 | FY17 | FY18 | |
| | **Simulation** | | | |
| Equipment | $0 | $0 | $0 | Computers |
| Staff & Professor | 0.3/$0 | 0.3/$0 | 0.3/$0 | Free research: 0.1 JLab + 0.1 BNL + 0.1 LANL |
| Postdoc | 0.5/$40<br>1.0/$46 | 0.5/$40<br>1.0/$55 | 0.5/$40<br>1.0/$55 | 0.5 GSU<br>1.0 JLab/INFN |
| Student | 0.5/$10 | 0.5/$10 | 0.5/$10 | GSU |
| Travel | $6 | $6 | $6 | GSU, BNL, Duke |
| **Sub-total** | **$102** | **$111** | **$111** | |
| | **GEM** | | | |
| Material | $10 | $10 | | |
| Equipment | $7 | $3 | $1 | Vacuum pump, vac components |
| Staff & Professor | 0.3/$12 | 0.3/$12 | 0.3/$12 | 0.2 of LANL (free research) + 0.1 UNM |
| Postdoc | 0.5/$25 | 0.5/$25 | 0.5/$25 | UNM |
| Student | 0.5/$15 | 0.5/$15 | 0.5/$15 | UNM |
| **Sub-total** | **$69** | **$65** | **$53** | |
| | **Prototype** | | | |
| Material | $5 | $5 | $5 | Lens, enclosure, electronics /GSU |
| Equipment | $30 | $0 | $0 | spectro-photometer /GSU |
| Staff & | 0.2/$0 | 0.2/$0 | 0.2/$0 | Free research |

| | | | | |
|---|---|---|---|---|
| Professor | | | | GSU/LANL |
| Travel | $20 | $20 | $20 | FNAL beamtest for GSU, LANL,BNL |
| **Sub-total** | **$55** | **$25** | **$25** | |
| **Grand Total** | **$226** | **$201** | **$189** | |

Table 3. Budget breakdown by institution, in k$.

| **Item** | **Time (FTE)/Cost** | | | **Remarks** |
|---|---|---|---|---|
| | **FY16** | **FY17** | **FY18** | |
| **INFN Frascati / JLab** | | | | |
| Staff | 0.1/$0 | 0.1/$0 | 0.1/$0 | Simulation |
| Postdoc | 1.0/$46 | 1.0/$55 | 1.0/$55 | INFN/JLab |
| **Sub-total** | **$46** | **$55** | **$55** | |
| **UNM** | | | | |
| Material | $10 | $10 | | GEM |
| Equipment | $7 | $3 | $1 | GEM |
| Professor | 0.3/$12 | 0.3/$12 | 0.3/$12 | 1 month summer sal. |
| Postdoc | 0.5/$25 | 0.5/$25 | 0.5/$25 | |
| Student | 0.5/$15 | 0.5/$15 | 0.5/$15 | |
| **Sub-total** | **$69** | **$65** | **$53** | |
| | | | | |
| **BNL** | | | | |
| Staff & Professor | 0.1/$0 | 0.1/$0 | 0.1/$0 | Free research, Simulation |
| Travel | $6 | $6 | $6 | Simulation(2)/beam test(4) |

| | | | | |
|---|---|---|---|---|
| **Sub-total** | **$6** | **$6** | **$6** | |
| **Duke** | | | | |
| Equipment | 0.1/$0 | 0.1/$0 | 0.1/$0 | Simulation |
| Travel | $2 | $2 | $2 | Free research, Simulation |
| **Sub-total** | **$2** | **$2** | **$2** | |
| **LANL** | | | | |
| Staff | 2x0.1/$0 | | 2x0.1/$0 | Test beam travel |
| Travel | $4 | $4 | $4 | |
| **Sub-total** | **$4** | **$4** | **$4** | |
| **GSU** | | | | |
| Material | $5 | $5 | $5 | Lens, enclosure, electronics/GSU |
| Equipment | $30 | $0 | $0 | Spectrophotometer |
| Staff/professor | 0.2/$0 | 0.2/$0 | 0.2/$0 | |
| Student | 0.5/$10 | 0.5/$10 | 0.5/$10 | Simulation/beam test |
| Postdoc | 0.5/$40 | 0.5/$40 | 0.5/$40 | Simulation/beam test |
| Travel | $14 | $14 | $14 | Simulation(2)/beam test(12) |
| **Sub-total** | **$99** | **$69** | **$69** | |
| **Grand Total** | **$226** | **$201** | **$189** | |

## 3.7. Further Work

With the completion of this proposed project, we expect to continue the project in a second phase to develop and fabricate a proof-of-principle prototype. With the chosen detector technology including radiators and readout, the collaboration will join the effort on prototyping

such a detector. Depending on the conceptual design provided by this project, the approach of future prototyping will vary. Also R&D on some particular detector components may be needed to meet the final requirements.

By the end of the second phase, we will conduct necessary beam tests to demonstrate that the detector's performance will satisfy the EIC's needs on particle identification. As Jefferson Lab will soon have 12 GeV electron beams available in Hall-D, the swept electrons in Hall-D's tagger hall will be an ideal source for these tests. Signal from the tagger hodoscope can be used as a trigger. Various electron rates can be chosen by putting the detector at different locations.

# 3.8. Summary

An R&D program is proposed to investigate the technology used for a Ring Imaging Cherenkov (RICH) detector for the hadron identification in the forward region of the future Electron-Ion Collider (EIC). Both the dual-radiator RICH option and a modular RICH concept will be investigated and the associated special optics design will be carried out. In particular, a newly developed Large-Area Picoseconds Photo-Detector (LAPPD) using renovated Micro-Channel Plate (MCP) technology will be carefully evaluated as the readout of the RICH detector. If feasible, the excellent timing resolution provided by this new readout will greatly improve the PID capability of the RICH detector. In parallel, a GEM-based readout option will be investigated as well. At the end, the project will be able to select the best detector technology and provide a conceptual design of the RICH detector for the EIC.

## References


[1] *EIC Proposal RD6: Letter of Intent for Detector R&D towards an EIC detector*, K. Dehmelt *et al*.

[2] *Progress in gaseous photomultipliers for the visible spectral range*, Breskin *et al.*, Nucl. Instr. and Meth. **A623** (2010) 318

[3] *GEant4 Mont-Carlo*, https://gemc.jlab.org/gemc/Home.html

[4] *EIC Detector Software Simulation*, https://eic.jlab.org/wiki/index.php/EIC_Detector_Software_Simulation

[5] *A Study of Meson and Baryon Decays to Strange Final States with GlueX in Hall D*, the GlueX Collaboration, proposal to JLab PAC 39 (2012), http://www.jlab.org/exp_prog/proposals/12/PR12-12-002.pdf

[6] Mapping the Spectrum of Light Quark Mesons and Gluonic Exceitations withLinearly Polarized Photons, the GlueX Collaboration, proposal to JLab PAC 30 (2006), http://www.jlab.org/exp_prog/proposals/06/PR12_06-102.pdf

[7] *Concept for and Electron Ion Collider (EIC) detector built around the BaBar solenoid*, PHENIX Collaboration, arXiv:1402.1170

# 4. DIRC-based PID for the EIC Central Detector and Photosensor Testing in High Magnetic Fields

L. Allison[1], T. Cao[2], R. Dzhygadlo[3], T. Horn[4] (co-PI), C. Hyde[1] (co-PI), Y. Ilieva[2,**] (co-PI), G. Kalicy[1], P. Nadel-Turonski[5,*] (co-PI), K. Park[1], K. Peters[3], C. Schwarz[3], J. Schwiening[3] (co-PI), J. Stevens[5], W. Xi[5], and C. Zorn[5].

[1)] Old Dominion University, Norfolk, VA 23529
[2)] University of South Carolina, Columbia, SC 29208
[3)] GSI Helmholtzzentrum für Schwerionenforschung GmbH, 64291 Darmstadt, Germany
[4)] The Catholic University of America, Washington, DC 20064
[5)] Thomas Jefferson National Accelerator Facility, Newport News, VA 23606
[*)] turonski@jlab.org, [**)] jordanka@jlab.org

## Abstract

An essential requirement for the central detector of an Electron-Ion Collider (EIC) is a radially-compact subsystem providing particle identification (e/π, π/K, K/p) over a wide momentum range. To this end, the electromagnetic calorimeter needs to be complemented by one or more Cherenkov detectors. With a radial size of only a few cm, a Detector of Internally Reflected Cherenkov light (DIRC) is a very attractive option. Currently, R&D is being undertaken for several DIRC projects around the world (Belle-II, PANDA, LHCb). A future EIC DIRC can benefit from many aspects of these efforts, but it also provides its own unique set of requirements, such as somewhat higher hadron momenta than in the $e^+e^-$ colliders of the b-factories and a need for a hermetic endcap, which needs to be integrated with the readout of the DIRC bars.

The initial goal of the DIRC R&D (eRD4) undertaken as part of the Generic R&D for an EIC program was to demonstrate the feasibility of building a high-performance DIRC that would extend the momentum coverage by up to 50% beyond state-of-the-art. Through a combination of simulations and prototype studies we now consider this goal to be achieved using an approach an approach with BaBar-like boxes with narrow bars, each coupled to an advanced spherical three-layer lens, and a common, compact (30 cm deep) expansion volume of fused silica. Some work is still ongoing to evaluate the performance of the final lens prototype (such as the determination of the photon yield in CERN test beam data from the spring/summer of 2015), but we expect most of this to be completed in FY15. This was, on one hand, made possible by the high performance of the advanced three-layer spherical lens over the full range of polar angles (in terms of achieved single-photon $\theta_c$ resolution and photon yield) that was designed in FY13 and procured in FY14, and on the other by the flatness of its focal plane, which allowed us to save a substantial amount of funds by not having to build and test a new expansion volume designed specifically to match the lens properties.

An aspect of eRD4 that has greatly expanded during the course of the R&D effort (even though the total budget remained flat – in part due to contributions from the participating groups), has been the studies of component performance in the environment of an EIC detector. The flagship project was the development of the high-B sensor test facility, which was commissioned in FY14 and started taking production data in FY15. The initial results for MCP-PMTs with small pore size are intriguing, as they suggest that on one hand this type of sensor could provide a low-noise sensor solution for single-photon measurements (required for Cherenkov applications) in fields of 1–3 T, but also that the performance of the MCP-PMTs is strongly dependent on the angle with respect to the local B-field, and is significantly affected by the details of the design. The latter suggests that the effort could eventually move beyond the characterization of different sensors and, together with sensor manufacturers, develop sensors optimized for the magnetic environment of an EIC detector. As such, the high-B test facility not only provides synergies with the other PID-related activities, but also is an important resource for all EIC detector R&Ds. Over time the photosensor work could become an independent effort within the consortium, but for now we chose, for continuity, to keep it in the DIRC chapter.

Following the suggestions from the committee, the main goal of the DIRC R&D proposed as part of the PID consortium proposal will now be aimed developing a specific, cost-performance optimized DIRC

solution for the EIC detector(s). This will involve several steps.

In order to establish a baseline solution, we will address the radiation hardness of the high-performance DIRC lenses already developed. The lens prototype that was procured for the optics tests used radiation hard fused silica as well as NLaK33 glass. Destructive radiation tests are under way with one such lens, but for the longer term we will try to build another prototype using either $PbF_2$ or a radiation hard glass (the latter would somewhat reduce the photon yield due to absorption of shorter wavelengths). Due to the lead content, making such lenses will first require us to find an appropriate manufacturer (planned for FY16).

In addition, two other solution will be investigated. The first will focus on potential cost savings by replacing the narrow BaBar-like bars with wider plates. Since the radiator fabrication cost is driven mostly by the number of pieces, the cost of wider plates is dramatically lower than the cost of narrow bars. Furthermore, since the number internal reflections between the faces and sides is smaller, the fabrication tolerances on the radiator squareness can be relaxed, which makes the production less demanding and less expensive. With good timing resolution (~100 ps), it becomes possible to use the photon propagation time as an important input into the particle identification algorithm. However, in contrast to Belle II TOP counter, which will rely primarily on the time information, we would like to pursue a full 3D (x, y, t) capability. To do so will require developing appropriate optics (*e.g.*, advanced cylindrical lenses) and new reconstruction algorithms (with possible synergies with the proposed RICH effort). As previously, there will be large synergies with the PANDA DIRC group. This work can start right away in FY16.

The other solution will focus on an FDIRC-like readout for BaBar-like bar boxes, using SLAC experience and synergies with the GlueX DIRC project, which aims at producing such a solution over the next three years for four of the actual BaBar boxes. Based on this work, we will investigate the possible performance improvements by coupling the bars directly to a compact expansion volume (without the performance-limiting wedges used in the BaBar DIRC) and by using smaller pixels. However, in order to fully benefit from the synergies with GlueX, the bulk of this work will be done in FY17 and FY18. This will also have the advantage that later on, an investigation can be made of the suitability of an FDIRC-like readout for plate radiators and a comparison made with cylindrical lenses.

We feel that this plan addresses the suggestions of the committee to continue the high-B sensor program, pursue the development of radiation hard lenses, and make a comparative cost-performance study of the different configurations possible for a specific EIC DIRC application.

# Table of Contents


- 4.1. Introduction
- 4.2. A DIRC for the EIC Central Detector
  - 4.2.1 General layout of the EIC central detector
  - 4.2.2 Integration of DIRC readout “camera” with the detector solenoid and endcap
  - 4.2.3 Impact of the magnetic field on photosensors
  - 4.2.4 Impact of radiation and backgrounds
- 4.3. DIRC detectors
  - 4.3.1 Principle
  - 4.3.2 Contributions to the Cherenkov angle (θc) resolution
  - 4.3.3 Adaptation to EIC requirements
- 4.4. Proposed DIRC R&D
  - 4.4.1 Progress and R&D Goals
  - 4.4.2 Simulation and reconstruction
    - 4.4.2.1 Simulations of the lens-based high-perfomance DIRC
    - 4.4.2.2 Simulation and reconstruction using plate radiators
    - 4.4.2.3 Simulations of FDIRC-like, mirror-based expansion volumes
  - 4.4.3 Optics development and testing
    - 4.4.3.1 Compact expansion volume
    - 4.4.3.2 Development of an advanced lens with high refractive index
    - 4.4.3.3 Mapping the lens focal planes in test bench measurements
    - 4.4.3.4 Large prototype setup for in-beam tests
    - 4.4.3.5 Validation of simulations with test beams at CERN and GSI
- 4.5. Proposed photosensor R&D
  - 4.5.1 Gain studies at High-B Field Test Facility at JLab
    - 4.5.1.1 Progress and current status
    - 4.5.1.2 Planned Tests and Procedures
  - 4.5.2 Timing studies at GSI
  - 4.5.3 Radiation hardness
- 4.6. R&D Timeline and Deliverables
  - 4.6.1 Timeline
    - 4.6.1.1 FY16
    - 4.6.1.2 FY17
    - 4.6.1.3 FY18
  - 4.6.2 Deliverables
    - 4.6.2.1 FY16
    - 4.6.2.2 FY17
    - 4.6.2.3 FY18
- 4.7. Management Plan
  - 4.7.1 Funding Request and Budget
  - 4.7.2 Manpower
  - 4.7.3 Travel
  - 4.7.4 Procurement
  - 4.7.5 Responsibilities

## 4.1. Introduction

The layout of this chapter generally follows that of the earlier eRD4 proposal. The main changes are that the physics motivations have been merged into one common for the consortium, and that the high-B measurements are a separate section. This would make it easier to make it a separate chapter next year, as was done for the LAPPDs, or to merge it with the latter into a sensor chapter. However, while that perhaps would be a more elegant long-term solution, for this year we opted to keep the DIRC and the high-B parts together. The reasons were primarily to show continuity in the combined FY16 budget, which remains the same as in eRD4 (at $115k), and due to the broad overlap in terms of personnel efforts. For instance, the primary responsibility of the ODU postdoc (G. Kalicy) is simulation, but he is also heavily involved in the sensor program. Regardless of the chapter structure, though, we foresee a high level of collaboration between the high-B effort and the LAPPD work. To emphasize the importance of the high-B sensor part of the proposal, the title of this chapter now explicitly includes the sensor work and Y. Ilieva has been added as a second contact.

As described in the abstract, the DIRC R&D has completed a major milestone by presenting a design for a lens-based high-performance DIRC, and is now moving to the next phase according to the guidelines provided by the R&D committee. Given the limitation in the amount of available R&D funding, a key consideration throughout the project has been to maximize cooperation and reduce costs. So far we have been able to benefit from very significant synergies with the PANDA DIRC development, which allowed us to develop the lens-based high-performance DIRC concept and to validate the performance of the optics in test beams at CERN and GSI. The other major activity of the DIRC R&D, the sensor gain evaluation in high magnetic field, lead to the establishment of a dedicated facility at JLab, which became operational in 2014. This effort has been strongly supported by JLab, which made large in-kind contributions including a 5-T superconducting magnet, infrastructure required for setup and operations, and personnel for cryogenic operations and data acquisition implementation. As this effort develops further, the R&D will see closer cooperation with the LAPPD project. In the future, we hope to also have considerable synergies with the GlueX DIRC effort.

The synergies with the PANDA DIRC R&D go beyond the value of the hardware that was made available. The know-how, simulation tools, and expertise provided to all aspects of the past, ongoing, and planned activities have been key to the success of the EIC DIRC R&D. In terms of hardware contributions, the PANDA group essentially made available an entire prototype setup, including several radiator bars (and plates) of fused silica with the required optical quality ($30-60k each), two fused-silica expansion volumes ($20k each), electronics, and mechanical infrastructure, as well as transportation for the latter to the test beams. This has allowed the EIC DIRC R&D to purchase only a few key components – most importantly the prototype of the advanced spherical three-layer lens – in order to carry out the prototyping, and to only provide travel for the ODU postdoc to the test beams at CERN and GSI (where the system based on the new lens was tested to obtain the data needed for analysis). In the future, the same general setup could be used for further tests involving a plate radiator – possibly with different optics (*e.g.*, an advanced three-layer cylindrical lens, or mirror-based configurations). For GlueX, the plan is to start a production effort in FY16. While this will be a dedicated effort, it should provide ample opportunity to gain experience. Tests carried out during this process should provide important

benchmarking for future simulations (and perhaps prototyping) for a mirror-based readout "camera" option for an EIC DIRC. With this in mind, J. Stevens, who is the JLab Hall-D person responsible for the GlueX DIRC, has joined the proposal this year, and although the bulk of the DIRC effort related to a mirror-based readout is scheduled for FY17–18, this will allow for effective coordination to begin already in FY16.

## 4.2. A DIRC for the EIC Central Detector

### 4.2.1 General layout of the EIC central detector

Although there are some differences between the various EIC detector concepts being developed at JLab and BNL, all share the same general solution for the PID in the central region: an electromagnetic calorimeter for e/π identification, and a DIRC detector for hadron (π/K, K/p) and supplementary low-momentum (< 1 GeV) electron ID. Additional low-momentum hadron ID in the barrel could be provided by a high-resolution TOF detector or *dE/dx* (in, for instance, a TPC). Although the limited flight path in the barrel would restrict the maximum momentum, an independent time measurement would help the event reconstruction in the DIRC.

In contrast, many possible solutions have been considered for the central tracker. One option would be a TPC (of relatively small size compared to the solenoid volume), perhaps augmented by inner and outer layers of micromegas detectors. A non-TPC solution, allowing for a larger radius, could also be interesting. The main options here would be either pure micromegas solution or a He-filled, low-mass, cluster-counting drift chamber (such as the one proposed for the ILC 4th concept detector) – or a combination of the two. From the DIRC point of view, the most important characteristic of the tracker is the angular resolution, which must be comparable to (or preferably better than) the Cherenkov angle resolution that the DIRC aims for. For this R&D, we have assumed that all of the possible solutions will be able to reach resolutions of 1 mrad or better. However, as we will see in section 4.4, the impact of better tracker resolution is quite significant, making it an important consideration for that part of the R&D effort.

### 4.2.2 Integration of DIRC readout "camera" with the detector solenoid and endcap

The EIC is unusual among colliders in that much of the relevant physics processes produce particles in the detector endcaps and near the beamline. In contrast to BaBar, where the DIRC readout volume essentially occupied an entire endcap, in an EIC the readout has to be much more compact. However, as shown in Fig. 4.2.1, the compact readout "camera" that was designed as part of this R&D project is relatively straightforward to integrate with the other subsystems. At the same time, it is also possible, with only minor adjustments (or even none at all), to extend the bars and locate the readout outside of the endcap in an area of lower magnetic field and where the geometric constraints on the expansion would be small. Thus, the detector integration constraints are not as significant as we originally thought, and one can adopt the best DIRC layout depending on the bar and readout camera design that one decides to adopt.

For instance, a larger, FDIRC-like, mirror-based expansion volume could be placed outside of the endcap, while a smaller PANDA-like, lens-based expansion volume could be placed inside the detector volume. Unless one opts for a large gas-RICH on the side of the outgoing electrons as well as on the hadron side, the location of the expansion volume will thus not be the determining factor, but investigation of mirror-based expansion volumes will tend to favor placement outside of the endcap.

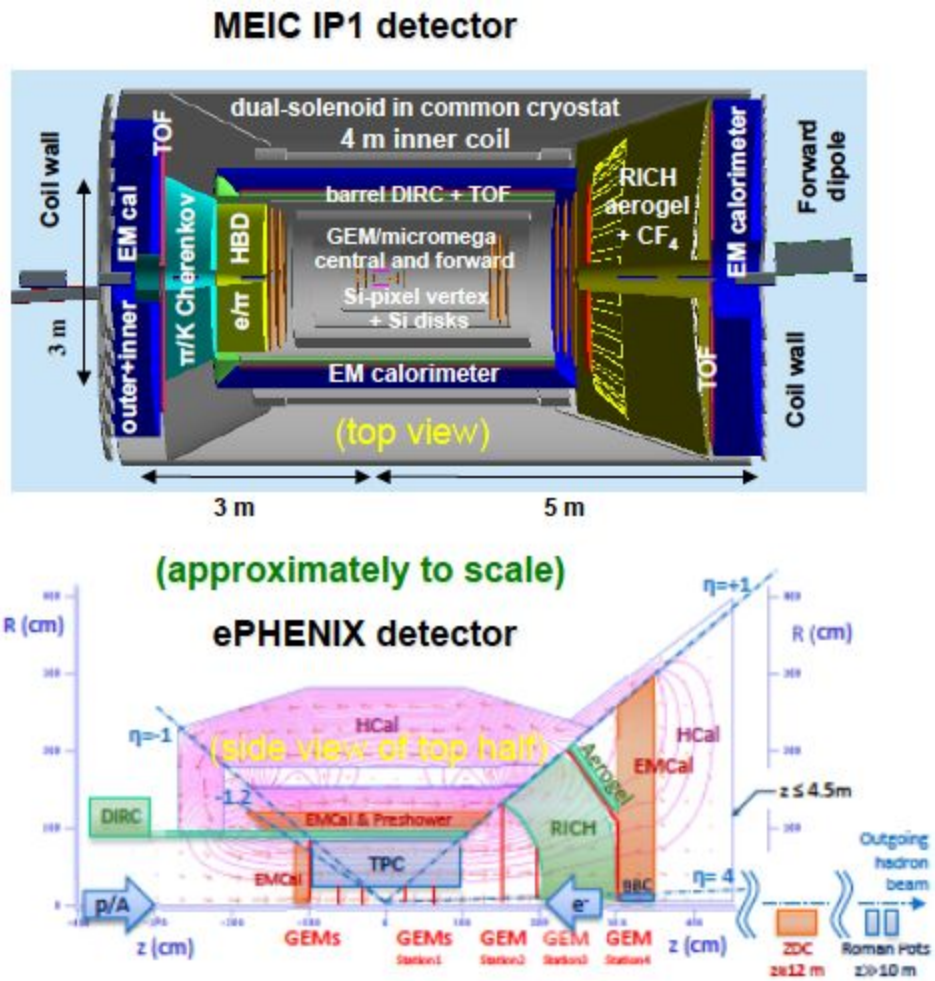


**Figure 4.2.1:** The MEIC IP1 (top) and ePHENIX (bottom) detectors. The former could be based on a 3-T dual solenoid (shown), or the 1.5-T CLEO solenoid intended for the SoLID detector. Both of these, as well as the BaBar solenoid used for the PHENIX upgrade, have the same coil dimensions (4 m length, 3 m diameter). The PID in the central detector includes an EM calorimeter (e/π) and a DIRC (K/p, π/K, and also low momentum e/π). In addition, an independent time measurement by a high-resolution TOF detector not only provides low-momentum hadron ID, but also could improve the event reconstruction in the DIRC detector. In the top figure, the triangular expansion volumes (light green) for the high-performance DIRC (narrow bars with spherical lenses) are shown to scale. In the lower figure, a larger external expansion volume is shown, which could be replaced by an FDIRC-like option. Both endcap layouts are, relatively easy to adapt for either an internal or external expansion volume.

However, the need to use longer bars would favor a solution based on wider bars known as plates (20–40 cm *vs.* 3–4 cm for bars) since the cost of a long-bar solution with narrow bars could be excessive. The wider plates will require a different PID approach, which makes maximum use of precision photon timing. Such an approach has been pursued by the Belle-II TOP, but for the EIC DIRC one would combine the time-of-propagation with good spatial resolution. On the other hand, due to lower tolerances and cost, plates may be an attractive alternative for shorter radiators. But regardless of length, they also reduce the azimuthal segmentation, potentially leading to more sensitivity to event background, the

impact of which will require further studies.

### 4.2.3 Impact of the magnetic field on photosensors

The solenoids considered for the EIC would have on-axis fields between 1.5 T (existing BaBar and CLEO magnets), and up to 3 T for a new magnet. However, in the vicinity of the coil the field can reach higher values, and can locally have a significant angle with respect to the solenoid axis. It is thus important to find a suitable low-noise sensor solution, suitable for DIRC (and RICH) detectors. At the moment, SiPMs offer the required high-B capabilities, but have too high noise levels. On the other hand, the square MCP-PMTs currently on the market have not been optimized for operations in high magnetic fields. The high-B sensor testing program could, in collaboration with manufacturers, lead to a new generation of sensors that would combine the best features (such as pore size, pore angle, L/D ratio, voltage distribution, *etc.*). In the future, SiPMs (aka Geiger-mode Avalanche Photodiodes, G-APDs) could also become a viable photosensor solution for the EIC, but while they are potentially less sensitive to magnetic fields, their high dark count rate (~1 MHz/cm$^2$ at room temperature) will make single-photon measurements difficult with the time gates needed for a barrel DIRC, and any such application would likely require cooling to reach the desired performance. To support the EIC sensor effort, a dedicated test facility was set up at JLab as part of this project. A description of the facility and test plans can be found in section 4.5. In addition to addressing key R&D issues, the expanded sensor program has also brought additional collaborators to this proposal.

In parallel with this effort, we are also looking at reducing the impact of the magnetic field by optimizing the sensor location and orientation. The new generation of three-layer lenses allows the creation of a flat focal plane. For prototyping we chose this plane to be vertical. However, our studies show that one can have a flat, but tilted plane. An expansion-volume prism with such a configuration would allow an optimization of the local angle between sensor and field to optimize performance, and is an illustration of the synergies between the different R&D activities.

### 4.2.4 Impact of radiation and backgrounds

Radiation hardness is an important consideration for any detector system for the EIC. However, due to the crossing angle between the beams, allowing the electron beam to go straight through the detector solenoid, it is possible to minimize both direct effects of synchrotron radiation, as well as indirect ones. The latter include outgassing that, in HERA, led to poor vacuum, which in turn created backgrounds from interaction of the ion beam with the residual gas, which was the largest source of background at HERA. In an e-p (A) collider there is also, for instance, no Bhabha contribution, which was an issue for BaBar. And initial studies presented at an EIC simulation workshop in 2012 suggest moderate levels of radiation – in particular for systems located far away from the beamline. While more detailed information about accelerator conditions may eventually be presented by both labs (JLab and BNL), there is no reason to believe that these backgrounds would be particularly challenging. For the DIRC, which will have its readout in the quietest part of the detector, any radiation related issues may be further reduced. It is, nevertheless good to investigate the radiation hardness of key components as the committee suggested, in particular evaluating the options for the new, advanced lenses.

Another important aspect that needs to be studied is the multiplicity of particles hitting each bar. But the subset of relevant events is somewhat different from the general DIS event (or photoproduction if low-$Q^2$ is included). What we really need to know is the multiplicity of particles hitting the same bar as, for instance, a kaon in the momentum range (and angle) covered by the DIRC. This subset of events can then be further refined to study a few specific benchmark processes with the typical cuts that are imposed in analysis. A single, high-$z$ kaon in semi-inclusive (or exclusive) meson production may, for instance, have a different number of close neighbors (in angular space) than a generic current jet containing a kaon. Such a study is already under way using Pythia by an ODU postdoc (not funded through the R&D). It will be important for checking the impact of the polar and azimuthal segmentation (*i.e.*, length and width of the radiator bars). The latter is, of course, of particular relevance for selecting the best plate geometry.

## 4.3. DIRC detectors

### 4.3.1 Principle

DIRC detectors are inherently 3D devices, measuring the image on the detector surface (*x, y*) and the time of arrival of each photon (*t*). If the distance to the detector surface is large compared with the bar size, as was the case in BaBar, no additional focusing is needed. Bringing the detector surface closer requires sensors with smaller pixels and some focusing optics. Fig. 4.3.1 shows a typical configuration where the focusing can be done using lenses or mirrors.

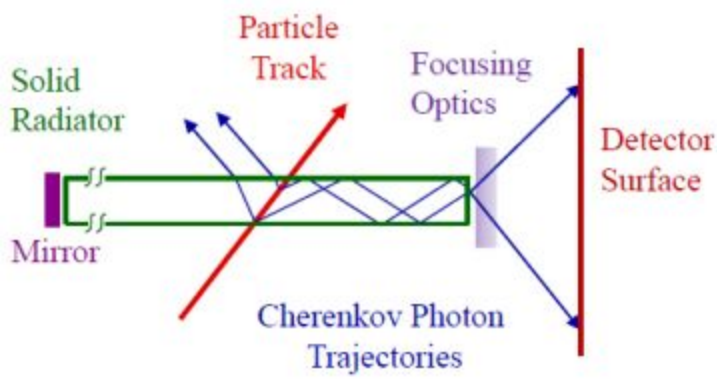


**Figure 4.3.1:** Conceptual drawing of a DIRC with focusing optics.

Event reconstruction and particle identification for actual experiments can be done in different ways, but in general they involve probabilistic approaches finding the maximum likelihood for a given hypothesis. However, from a design point of view it is extremely useful to reconstruct and use the Cherenkov angle *($\theta_c$)* resolution and the photon yield, which can then serve as figures of merit of the design that can be verified in test experiments with particle beams.

### 4.3.2 Contributions to the Cherenkov angle ($\theta_c$) resolution

The expected PID performance of the DIRC is determined by the resolution in $\theta_c$, the polar opening angle of Cherenkov light emitted from the particle traversing the detector. The angle $\theta_c$ is defined as $\cos\theta_c = 1/(n(\lambda)\beta)$, where $\beta = v/c$, $v$ is the particle velocity and $n(\lambda)$ is the index of refraction of the material. In a dispersive medium, the latter is a function of $\lambda$, the wavelength of the Cherenkov photon.
The uncertainty of the Cherenkov angle for a particle track, $\sigma_c^{track}$ , behaves as

$$(\sigma_c^{track})^2 = (\sigma_c^{photon}/\sqrt{N_{p.e.}})^2 + (\sigma^{track})^2 ,$$

where $N_{p.e.}$ is the number of detected photoelectrons and $\sigma_c^{photon}$ is the single-photon Cherenkov angle resolution. The last term, $\sigma^{track}$, is the uncertainty of the track direction in the DIRC, dominated by multiple scattering and the resolution of the tracking detectors.

The single-photon Cherenkov angle resolution $\sigma_c^{photon}$ can be estimated as

$$\sigma_c^{photon} = \sqrt{(\sigma_c^{2\,pixel} + \sigma_c^{2\,bar} + \sigma_c^{2\,imperfections} + \sigma_c^{2\,chromatic})}$$

where $\sigma_c^{pixel}$ is the contribution from the detector pixel size, $\sigma_c^{bar}$ is the uncertainty due to optical aberration and imaging errors, $\sigma_c^{imperfections}$ is the uncertainty due to bar imperfections (such as non-squareness), and $\sigma_c^{chromatic}$ is the uncertainty in the photon production angle due to the dispersion n(λ) of the fused silica material.

The readout "camera" consists of an expansion volume (EV) with attached sensors. The purpose of the expansion volume is to project a spatial image of the Cherenkov light from the DIRC bar onto the sensors. Using sensors with a small pixel size makes it possible to reduce the size of the expansion volume, or to improve the spatial resolution of the image. The size of the expansion volume can also be reduced by introducing active focusing elements (lenses or mirrors), although careful design and testing is required to minimize photon losses.

In order to reduce the EV size and to simplify operations, the water used in BaBar can be replaced with mineral oil or fused silica. The latter would be the preferred choice for the EIC. The depth of the fused-silica expansion volume planned for the PANDA barrel DIRC is 30 cm (the height is comparable but could be somewhat smaller), while the FDIRC that was planned for SuperB had a radial height of 56 cm and a depth of 22 cm. Since an important goal of this R&D is to improve the DIRC performance beyond state-of-the-art, and there is a tradeoff between size and resolution, we expect the EIC expansion volume to be comparable to, or only a little smaller than, the one planned for PANDA.

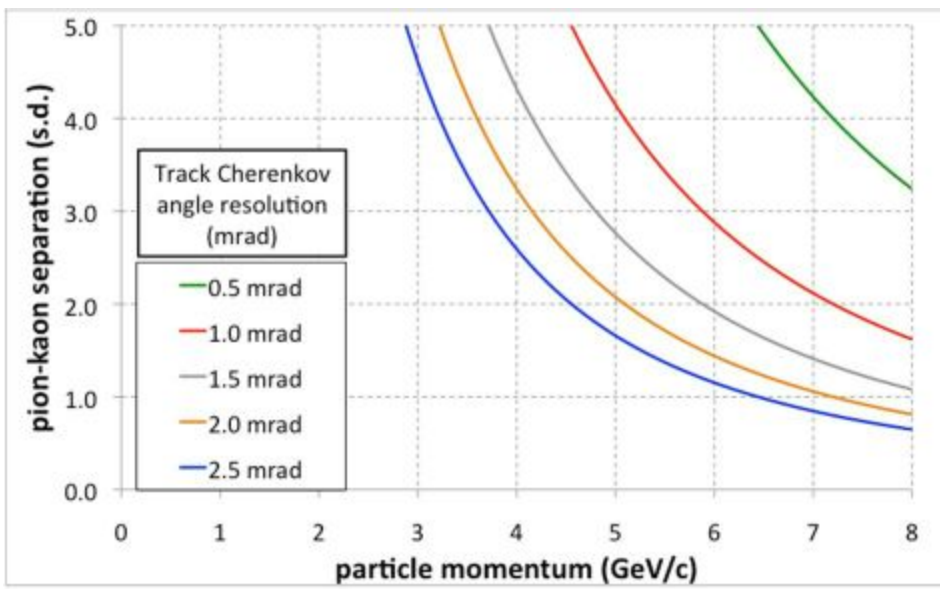


**Figure 4.3.2:** In order to have 3σ π/K separation at 6 GeV/$c$ one needs to reach a $\theta_c$ resolution of 1 mrad.

### 4.3.3 Adaptation to EIC requirements

The primary goal of developing a high-performance "Super-DIRC" is to have a compact device that can satisfy the PID requirements of the EIC without the need for a supplementary gas Cherenkov detector. Figure 4.3.2 shows how an increased momentum range for $\pi$/K separation translates into Cherenkov angle resolution. In an EIC, the pion background for kaons varies with reaction channel and kinematics, but is typically about 3:1. The usual $3\sigma$ criterion thus seems relevant. Achieving $3\sigma$ separation using radiator bars of fused silica would require a Cherenkov angle resolution of 1.3 mrad at 5 GeV/*c* and 1.0 mrad at 6 GeV/*c*. Achieving this resolution assumes that the central tracker will be able to provide an angular resolution at the sub-mrad level (*i.e.*, comparable to or slightly better than the CLAS12 forward detector). As suggested by the equations above, there are five ways to improve the Cherenkov angle resolution:

1. Reducing the size of the image from the DIRC bar using focusing optics.
2. Reducing the pixel size of the readout to better resolve the image.
3. Improving the photon yield and collection (other than increasing the 0.2 *r.l.* bar thickness).
4. Reducing the effect of chromaticity ($n = n(\lambda)$) through precise timing (< 100 ps) or wavelength filters (also an intrinsic feature of most radiation hard glasses).
5. Reducing the effect of the correlated term, the uncertainty of the track direction, by improving the measurement of the track direction from the DIRC data in a fit to the ring center.

The proposed R&D will address all five.

## 4.4. Proposed DIRC R&D

### 4.4.1 Progress and R&D Goals

The proposed R&D follows up on the work done as part of the eRD4 (formerly known as RD2011-3) project. The initial goals were the following.

1. To investigate the possibility of building a high-performance DIRC for use in a future EIC detector, pushing state-of-the-art (BaBar) for resolution (momentum coverage) by up to 50%.
2. To develop a compact readout "camera" and study its integration with the EIC detector.
3. To study the performance of photosensors in high magnetic fields.

All three have reached critical milestones. In particular, we have developed a new type of spherical, three-layer lens with high index of refraction (no air gap between lens and expansion volume), which provides excellent single-photon resolution, a good photon yield – even at 90° where traditional air-gap lenses have no transmission, and a flat focal plane (which can either be vertical or angled, making it possible to align the sensors to the magnetic field). As shown in Fig. 4.4.1, each lens would cover one bar in the bar box.

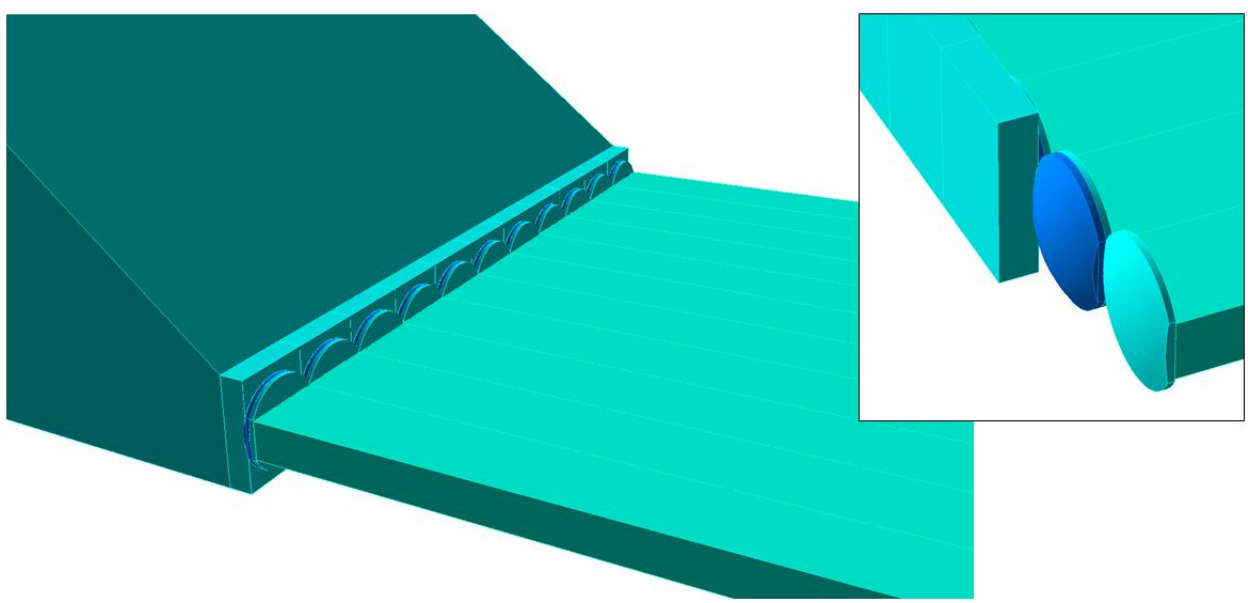

**Figure 4.4.1:** Geant4 geometry for the simulation of the high-performance DIRC. On the left we see the common expansion volume of fused silica, a row of spherical three-layer lenses with high index of refraction (no air gaps) and the radiator bars.The insert shows the individual lenses and layers of the spherical lens system.

The lenses were attached to a common expansion volume (matching the width of a bar box). The depth of the prism was chosen to be 30 cm, which provides a good match with the layout of the EIC detectors shown in Fig. 4.2.1, making integration very straightforward. With this configuration it was possible to show a simulated $\theta_c$ resolution better than 1 mrad, or 6 GeV/$c$ for a 3σ π/K separation when using

photosensors with 2-mm pixel size, as shown in Fig. 4.4.2.

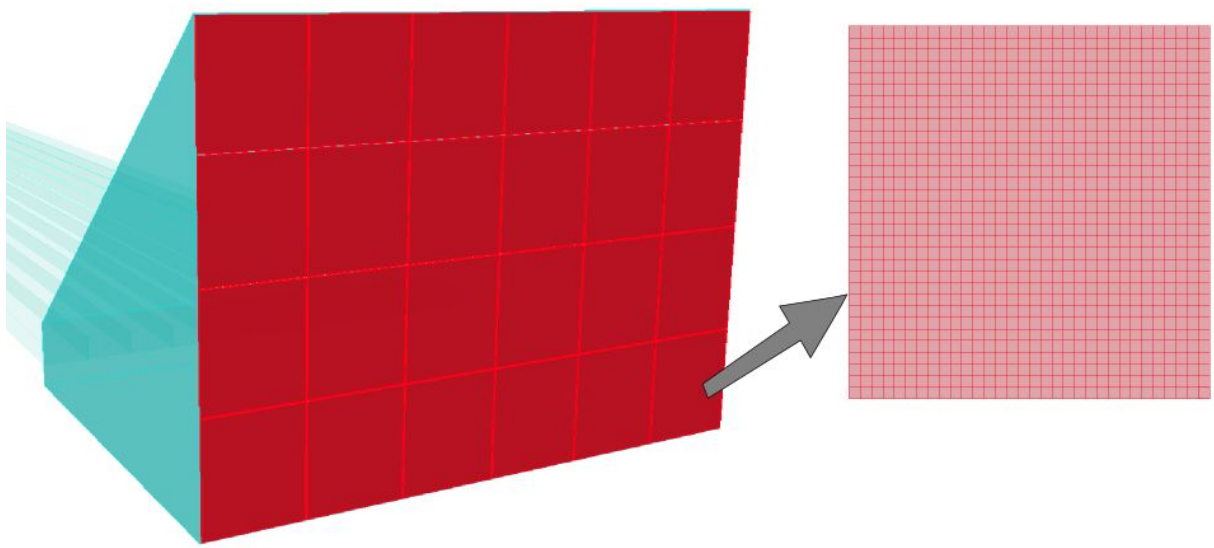

**Figure 4.4.2:** Geant4 geometry of the high-performance DIRC with fine-grained pixel coverage of the detector plane. The zoom shows one sensor with 32x32 pixels, each with a size of 2 mm.

The performance of the new lens was tested during two test beams. The first one (a proof-of-principle test) was carried out in the summer of 2014 at GSI, and the second one (to measure the resolution and photon yield) was done at CERN in May 2015, with an additional run coming up in July 2015. In these tests Planacon photosensors with a pixel size of 6 mm were used, *i.e.*, twice the size of the ones proposed for the EIC high-performance DIRC, and a narrower expansion volume (17cm width, made out of fused silica) coupled to one bar. To verify the simulation results for the EIC, simulations were also undertaken with a narrow expansion volume and 6-mm pixels and the actual sensor spacing matching the test beam setup. The participation in the beam tests and analysis of the data by G. Kalicy were a crucial step in validating the simulation results.

The new results for the high-performance DIRC were better than previously shown since 1) the actual three-layer lens was improved compared with the initial simulations (and slightly improved since), and 2) the larger expansion volume helps to reduce the number of ambiguities creating a combinatoric background, thereby improving the quality of the reconstruction.

The simulations were performed both using the DrcProp ray-tracing software, the results from which had been shown before, as well as in Geant4, which provides a more detailed model of the interactions of the photons as well as interaction of the particle with the materials. The final results can be seen in Fig. 4.4.3.

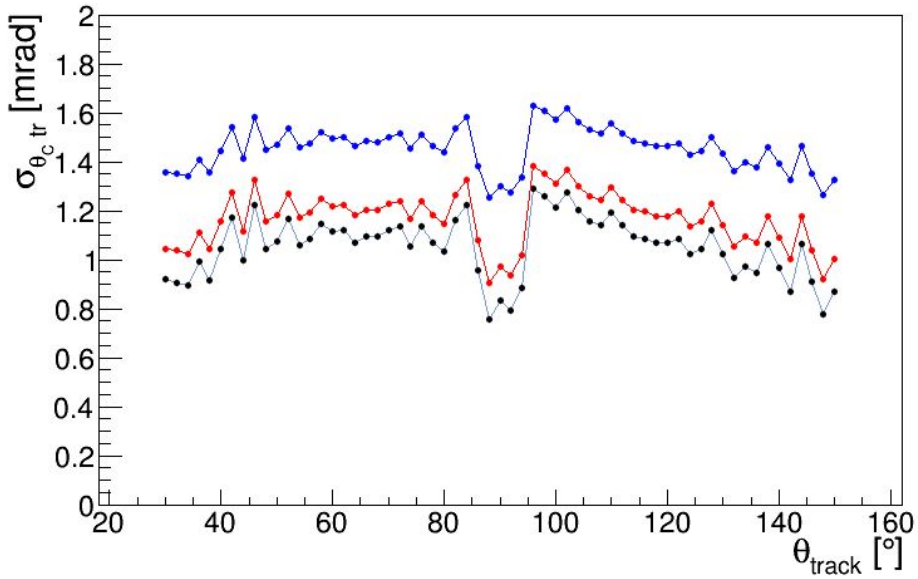


**Figure 4.4.3:** Geant4 results for the track resolution of the high-performance EIC DIRC assuming three different angular resolutions for the central tracker: 0 mrad (black), 0.5 mrad (red), and 1 mrad (blue). The simulation shows how critical the tracker is for achieving optimal PID performance. Assuming that this could approach 0.5 mrad, a high-performance EIC DIRC should be able to reach a $\theta_c$ resolution of 1 mrad, or a 3σ π/K separation up to 6 GeV/*c*, and an e/π separation up to 1 GeV/*c*.

These results show that the R&D has achieved its two major milestones: it has produced a design for a high-performance DIRC, the key new components of which have been tested in beam, and this has been done so using a compact readout "camera" compatible with an EIC detector. Furthermore, the flatness of the focal plane even when it is not perpendicular to the radiator bar, ensures that it can be matched to any desired expansion volume geometry. We would, thus, take full advantage of the synergies with the PANDA DIRC R&D, for which two fused silica prisms with a vertical back plane had already been procured and would not need to build an expensive expansion volume matching the focal plane of the lens. The possibility to choose the angle of the sensor plane at the back of the expansion volume also means that it can be optimized to the local field. Guidance will be provided by the high-B sensor tests described in section 4.5.

Following guidance from the advisory committee, the R&D proposed for FY16–18 will move its focus from demonstrating the feasibility of building a high-performance DIRC for the EIC, to the study of alternative solutions aimed at producing a cost-performance optimized solution. The R&D will, therefore, focus on three areas.

The first will be, in addition to finishing the analysis of the 2015 test beam data, to follow up with the study of the lens-based high-performance DIRC by looking into the radiation hardness of the lens optics. The main component of the three-layer lens is radiation hard fused silica, but the middle layer needs to have a different index of refraction, as shown in Fig. 4.4.4. A limited number of optical materials with the required refraction index are available, some of which are not known to be radiation hard.

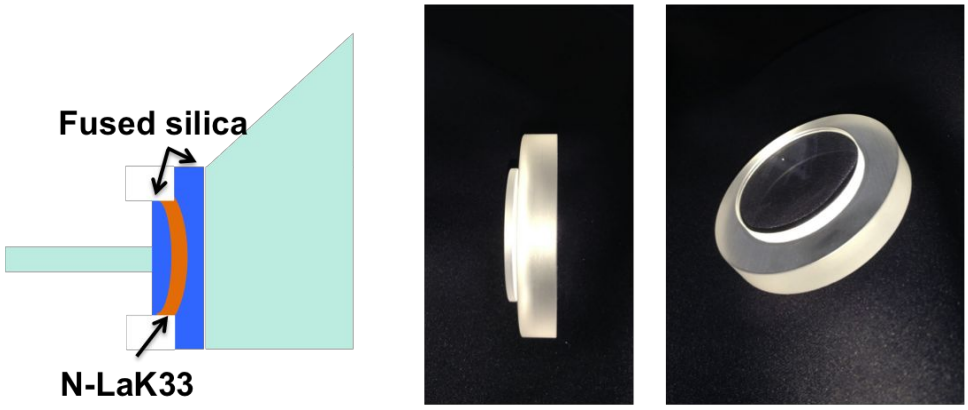


**Figure 4.4.4:** Schematic diagram and two photos of the prototype three-layer spherical lens.

For the prototype lens, the main goal was to perform a verification of the simulated optics on a test bench and in beam. The NLaK33 glass, which only has limited radiation hardness but good transmission over a wide range of wavelengths, was thus a natural choice. In a final application, the accumulated dose rate could, however, eventually be an issue. Therefore, we are going to first perform a potentially destructive test with a prototype lens at the end of FY15 to see what dose it can withstand before its optical properties are degraded. In the upcoming R&D period we will then investigate the possibilities to replace the NLaK33 material with either a radiation hard glass or lead fluoride, $PbF_2$. The latter would offer good optical properties, but be a greater manufacturing challenge, making it difficult to find a vendor[1]. The former should be somewhat easier to produce, but would have a cutoff in the transmitted wavelengths in the UV range, resulting in a reduction of the photon yield (and hence resolution). On the other hand, the narrower band of photons would suffer less chromatic effects, and the photon loss could be, at least partially, offset by a new generation of MCP-PMTs that promise to have a higher photon detection efficiency. During FY16, design and simulations will be performed for lenses with both materials, and vendors will be identified. An order will then be placed for a radiation-hard lens in FY17. Optical and radiation hardness tests will then be carried out with the lens during FY18.

The second new effort will be directed towards studying the feasibility of using wide radiator bars known as plates. In this configuration, the many bars in the box shown in Fig. 4.4.1 would be replaced by only one or two plates, which in turn would either be connected directly to the expansion volume (possibly using a small focusing mirror on the opposite end of the plate as in Belle II), or through a cylindrical lens. In a wide plate the number of bounces on the side walls is much smaller, which has two consequences. First and foremost, the manufacturing tolerances, as well as the cost, can be greatly reduced, making the cost profile of a DIRC more similar to gas and aerogel RICH detectors, where the bulk of the cost is in the photosensor array rather than the radiator. In turn, this would make it possible to use DIRC detectors in more than one EIC detector regardless of whether it would be possible to reuse the radiator bars from BaBar (which, due to an unfortunate arrangement of prisms are not well suited for use in a

[1] Most optical companies that would be able to produce a three-layer lens are not willing to introduce lead into the production environment. The company Korth Kristalle GmbH (www.korth.de) has experience with lenses and the tooling of $PbF_2$ and could try the production of a lens from this material.

high-performance DIRC without some level of disassembly). Since the EIC will support more than one interaction region, it is likely that more than one detector will eventually be built, making it imperative to investigate this cost-effective radiator configuration as part of the EIC DIRC R&D.

On a technical side, the wider bars require a departure from the basic assumption of the BaBar-DIRC geometric reconstruction: that the photons are in good approximation emitted from the center of the radiator bar. This approximation is still valid in the vertical (thickness) dimension but fails in the horizontal (width) dimension. Therefore, a different reconstruction approach, referred to as time-based reconstruction, will have to be used. While all DIRCs are 3D imaging devices ($x$, $y$, $t$), actual implementations have focused on either the spatial (BaBar) or time (Belle II) parts, although the latter has moved toward expanding its spatial imaging capabilities (which are limited by the space available in the detector). For EIC applications, where particles reach higher momenta, it would be interesting to pursue development of new, fully 3D reconstruction algorithms for a plate geometry with a "camera" instrumented for full 3D imaging. Of course, one possible outcome could be that for various kinematics, either time or spatial imaging could become dominant, and some simplified approach could be developed. However, not making such an assumption a priori but pursuing reconstruction and "camera" development in parallel could lead to a very cost-effective, high-performance DIRC. The study of algorithms for plates offers many synergies with the PANDA DIRC R&D, which also pursues this avenue of potential cost optimization.

The development of such a time-based reconstruction algorithm for both the narrow bars and the wide plates is one of the main goals of the reconstruction effort in FY16. Initial studies, performed as part of a Ph.D. thesis on the PANDA Barrel DIRC, suggest that the $\pi$/K separation obtained using a time-based algorithm is superior to the result of the geometric reconstruction, arguably due to the optimum use of all observables. The approach is based on the Belle II TOP software design and calculates probability density functions (pdf) for the photon propagation time in each X/Y pixel for each particle type and momentum vector. These pdfs can be calculated either in simulation or analytically and the PANDA DIRC Ph.D. project, to be completed in the fall of 2015, will inform the initial approach to the reconstruction for the EIC DIRC.

Another possible approach to improving the DIRC performance in software is based on an idea also pursued for the BaBar DIRC: although the reconstruction requires the track momentum vector as input, it may be possible to include the track direction as a free parameter in a fit to the Cherenkov ring center. The initial momentum vector from the central tracker could therefore be improved to better match the observed hit pattern. This is a standard approach for RICH counters with a more ring-shaped image but is difficult in DIRC counters due to the disjunct hit patterns. Any ring-fit has to be performed after a conformal transformation, for example into Cherenkov azimuth *vs*. polar angle space, and still suffers from large gaps in the occupancy across the ring circumference. Although this technique ultimately did not succeed in the BaBar DIRC, it is expected that the smaller pixels and better resolution of an EIC DIRC may result in successful fits and be able to mitigate the influence of the tracking resolution on the overall DIRC resolution. A study of this approach will start in FY16.

An additional constraint to using plates is the hit multiplicity for events of interest. These can be defined as broadly as any event where a kaon in the momentum range covered by the DIRC hits a radiator plate, or be very specifically associated with one particular channel. While it may be possible to reconstruct two simultaneous hits, large multiplicities in each plate would pose a limit on, in particular, the width (*i.e.*, azimuthal angle covered by each plate). Studies of hit multiplicities are currently under way, and are

expected to be completed in FY17.

The third major effort, also suggested by the advisory committee, is to make a comparison of different readout "camera" designs – and in particular that of the lens-based high-performance DIRC with an FDIRC-like, mirror-based option. The latter would be looked at in two configurations, both using the smaller pixel size (2–3 mm) of the lens-based option. The first would match the existing BaBar bars (with the additional prisms), and the second would have the bars attached directly to the expansion volume. Since the original FDIRC was developed for the first configuration, the first step could essentially only be a study of the impact of pixel size. However, since the GlueX experiment at JLab is currently developing an FDIRC-based readout for a DIRC system using four of the BaBar bar boxes, but reverting to a larger water-based expansion volume. The R&D for the mirrors required in the optical design is currently ongoing at MIT-Bates. The photodetection and readout electronics will follow a scheme developed for the CLAS12 RICH detector using the Hamamatsu H12700 MaPMTs. The ongoing R&D for the GlueX DIRC project is planned to be completed in FY16, with construction beginning thereafter. The GlueX DIRC project is currently planned to be completed by the end of FY18. In case one wanted to re-use the BaBar boxes as is, a GlueX-like readout "camera" could potentially also offer a low-cost (but also low-performance) solution for an EIC detector with a more minimalistic endcap design on the outgoing electron side, as shown in Fig. 4.2.1 for ePHENIX. Thus, it would be natural to take advantage of the synergies with the planned GlueX expansion volume design and construction to fully explore this option. Based on the experience studying an expansion volume matching the existing BaBar bar boxes, we would then, as the committee suggests, explore higher-performance designs using a mirror-based, FDIRC-inspired expansion volume. However, even with the bars attached directly to the expansion volume and a readout with smaller pixels, finding an optimum that would be very different in configuration compared to the FDIRC could require a quite extensive effort as the "phase space" of configurations is quite large. Thus, collaboration with the experts at SLAC and the GlueX group will be important (it is, however, interesting to note that in the preliminary GlueX studies modest variation of parameters did not seem to significantly affect performance).

### 4.4.2 Simulation and reconstruction

#### 4.4.2.1 Simulations of the lens-based high-perfomance DIRC

The simulations of the lens-based, high-performance DIRC were performed using both Geant4 and the DrcProp ray-tracing code, which was written at GSI. The simulations include:

- Primary photo-statistics of the Cherenkov process.
- Chromatic effects on the Cherenkov light propagation and internal reflections in the bars, focussing elements, and expansion volume (EV).
- Quantum efficiency, collection efficiency, and geometric efficiency of the photodetectors.
- Time-of-propagation (TOP) of the Cherenkov photons from the track to the photo-cathode.

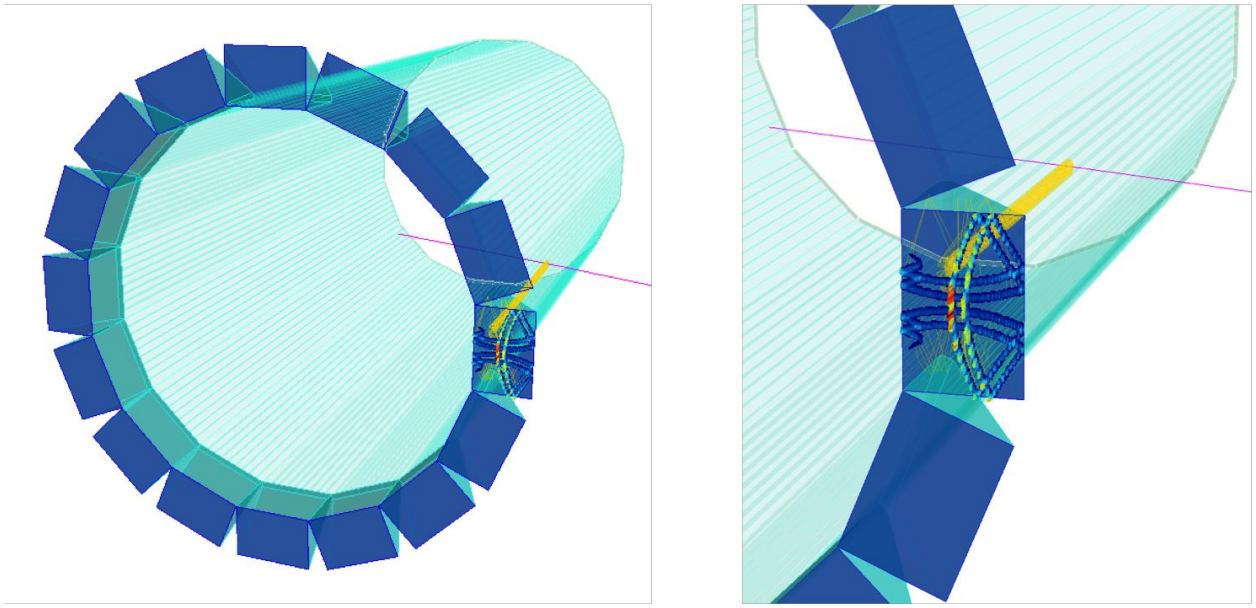

**Figure 4.4.5:** A Geant4 implementation of the tentative geometry of a lens-based, high-performance DIRC for the EIC with narrow bars and a solid fused silica prism. The simulated event shows the primary charged track in magenta, with Cherenkov photons in yellow.

The reconstruction algorithm was based on the approach developed for the PANDA Barrel DIRC. It allowed to quantify the Cherenkov angle resolution for each configuration.
In preparation for this reconstruction algorithm, a bundle of rays is generated in simulation near the end of the DIRC bar. The wave vectors fill the entire angular phase space of total internal reflection in the bar. After propagation of the rays through the lens and expansion volume, a look-up table is created associating each pixel of the photocathode surface with a specific unit wave vector $\hat{k}$ (see Fig. 4.4.6). A separate look-up table is created for photons with a combination of 0, 1, 2, or 3 reflections off the sides, top, and bottom, of the expansion volume (see Fig. 4.4.7). The reconstruction of the detected pattern of Cherenkov photons proceeds as follows:

- For each detected photon, a Cherenkov angle $\theta_c$ is calculated from $cos\theta_C = \hat{k} \bullet \hat{p}$ , where $\hat{p}$ is the track unit vector.
- The value of $\theta_C$ is histogramed, including the 8-fold ambiguity from all possible reflections off the sides, top and bottom, and end of the DIRC bar.
- For each of the 8-fold choices of $\theta_c$ , the Time-of-Propagation (TOP) is calculated and subtracted from the simulated TOP and is histogramed.
- Separate timing and angle histograms are created for each type and possible combination of reflections in the expansion volume (see Fig. 4.4.7).
- An initial cut is placed on the timing histogram. This primarily selects the correct path of either direct propagation from track to EV, or reflection off the downstream end of the DIRC bar. This also helps to remove some of the ambiguity of reflections in the EV.
- A final cut is placed on the $\theta_C$ histogram, and a Gaussian plus polynomial fit is performed. The rms width of the Gaussian fit, divided by the square root of the number of photoelectrons is the

projected DIRC-only per-track resolution. In reconstructing data with a mixture of particles, the final cut position would be repeated for each particle hypothesis (pion, kaon, proton), based on the measured track momentum, and a likelihood assigned based on the number of photon candidates within the cut.

The progress of these studies is presented below.

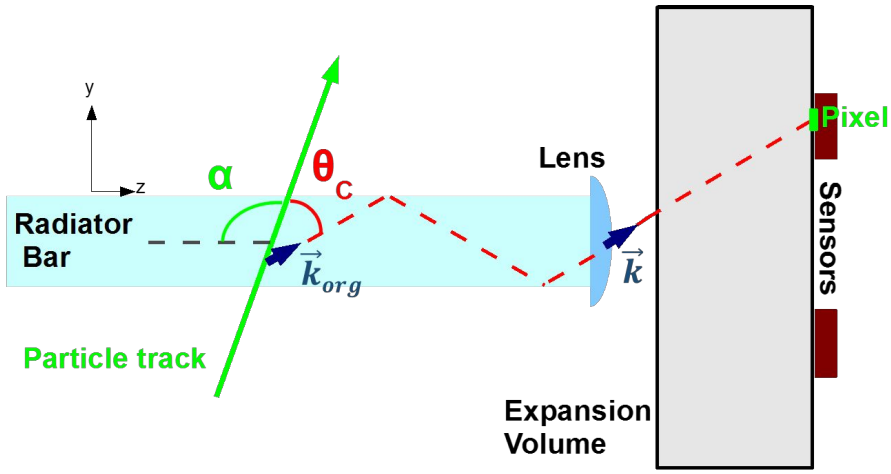


**Figure 4.4.6:** Schematic diagram of the reconstruction concept, with one example photon track emitted from a particle. The direction vector k is an estimator of the origin vector $k_{org}$, and is used to reconstruct $\theta_C$.

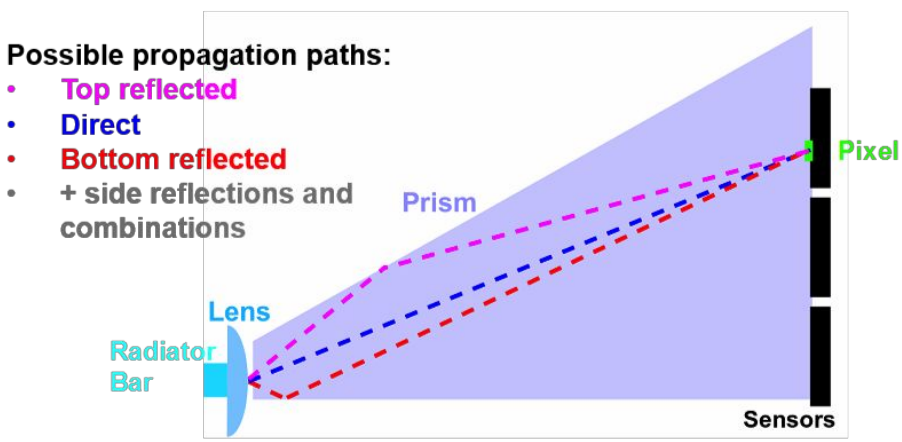


**Figure 4.4.7:** Three examples for possible propagation paths of the photon from the center of the bar end to one of the pixels are shown.

The high-performance DIRC configuration shown in Fig. 4.4.1 uses 35-mm wide and 17-mm high fused-silica radiator bars and a 30-cm-long expansion volume with a 38° opening angle. The three-layer spherical lens is located in between, as shown in Fig. 4.4.4. A flat mirror was mounted opposite to the readout end of the bar. In the DrcProp simulation, the back surface of the prism was covered with 2x2 mm pixels. The results below were obtained from simulations using 6 GeV/*c* pions.

Figure 4.4.8 shows occupancy plots for a few selected track angles. For track angles far from 90° the ring segments are nicely separated, which makes the geometric reconstruction easier. Close to 90°, the middle parts of the ring segments, which contain a major part of the photons, start to overlap. This increases the combinatorial background in the Cherenkov angle reconstruction. This background can be suppressed by using timing information to reject paths that do not match the time of arrival. The result of a time cut using a 2-ns time window is shown in Fig. 4.4.9. The requirement for the timing resolution of DIRC photosensors is 0.1 ns or better.

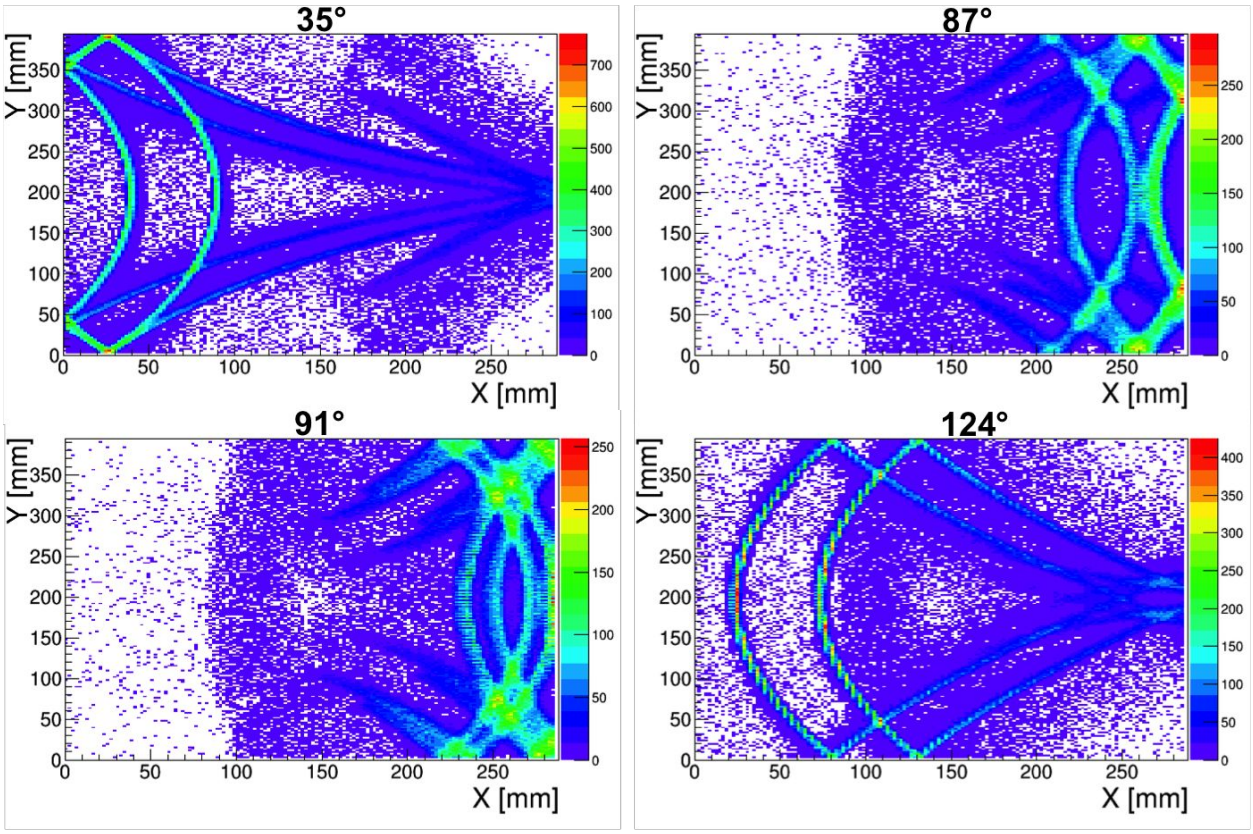


**Figure 4.4.8:** Example hit patterns for different track polar angles simulated with the high-performance EIC DIRC configuration simulated using DrcProp.

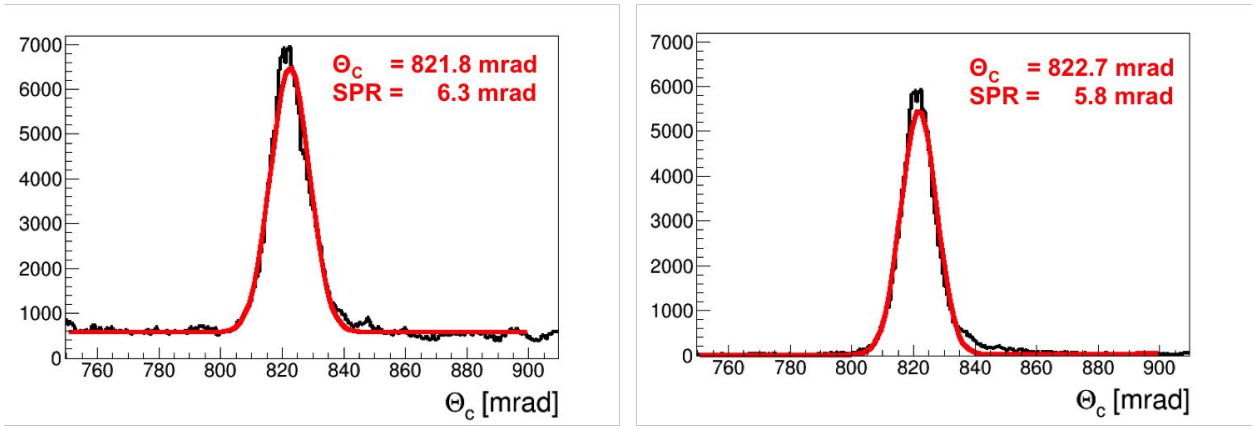


**Figure 4.4.9:** Reconstructed single-photon Cherenkov angle for 124° track angle simulated using DrcProp. Left: without time cut. Right: with 2-ns time cut (measured - expected).

The average number of photoelectrons per track (photon yield) is shown in Fig. 4.4.10 for the Geant4 and DrcProp simulations. Note the large yields around 90° where regular lenses with an air gap would provide almost zero yield. The improvement at forward and backward polar angles mainly reflects the longer path length of the charged particle in the radiator. Standard photocathodes have been assumed. In the future the simulation will be extended to include radiation hard glasses that introduce a cut-off in the transmitted wavelengths. The impact of next-generation photocathodes and microchannel-plates with a larger collection efficiency (for instance, funnel-type MCPs) will also be investigated.

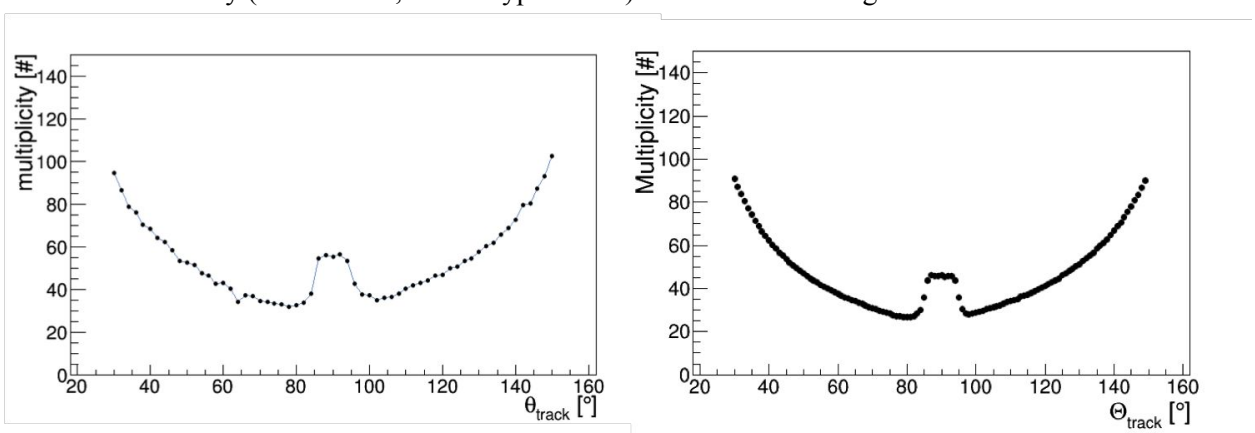


**Figure 4.4.10:** Photon yield for the lens-based high-performance DIRC simulated using Geant4 (left) and DrcProp (right), assuming a sensor packing fraction of 100%.

The reconstructed single-photon Cherenkov angle resolution (SPR), as a function of the polar angle $\theta$ of the incoming track is shown in Fig. 4.4.11. It is consistent with the studies performed using the DrcProp ray-tracing software, with minor differences expected due to the more detailed modelling in Geant4.

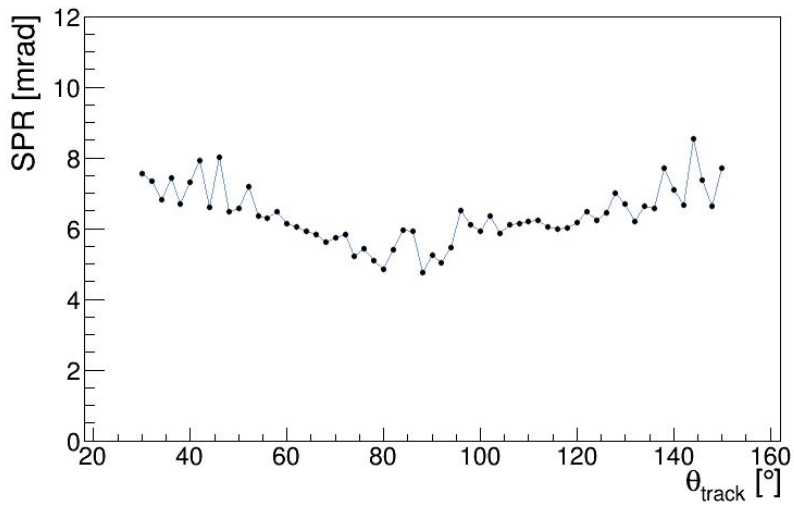


**Figure 4.4.11:** Single-photon Cherenkov angle resolution for the lens-based high-performance DIRC simulated using Geant4 assuming 2-mm photosensor pixels at the end of the 30-cm deep prism.

The resulting resolution per track (see section 4.3.2 for equations) is shown in Fig. 4.4.3 for different angular resolutions of the central tracker, which measures the angle at which the incoming particle enters the radiator bar. The DIRC resolution also depends on the pixel size. In our simulation we assumed pixels less than half the size of the standard square Planacon MCP-PMTs. Reducing the pixel size is not technically challenging for the manufacturers, but it will increase the channel density (and cost). Figure 4.4.12 shows the SPR as a function of the pixel size for four angles of the incoming charged particle track. A pixel size of 2–3 mm would be a good choice for the high-performance DIRC design.

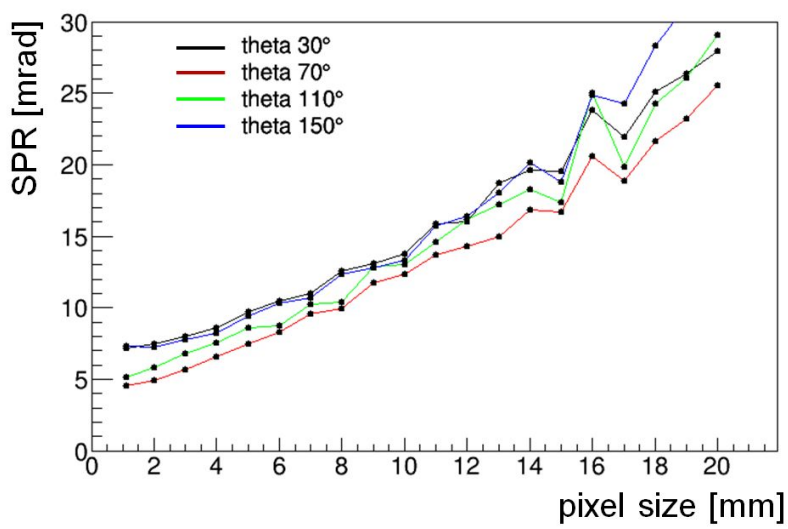


**Figure 4.4.12:** Influence of the pixel size on the single-photon Cherenkov angle resolution for selected track polar angles in Geant4 simulation for a 30-cm-long expansion volume.

### 4.4.2.2 Simulation and reconstruction using plate radiators

As discussed in section 4.4.1, the potential cost savings of using wide radiator bars (plates) can be quite substantial. Thus, simulating such configurations for the EIC DIRC and exploring the performance that can be achieved will be the main simulation effort in FY16, and work on reconstruction and optimization will continue through FY18. As can be seen in Fig. 4.4.13 below, a plate-based geometry has already been implemented in Geant4.

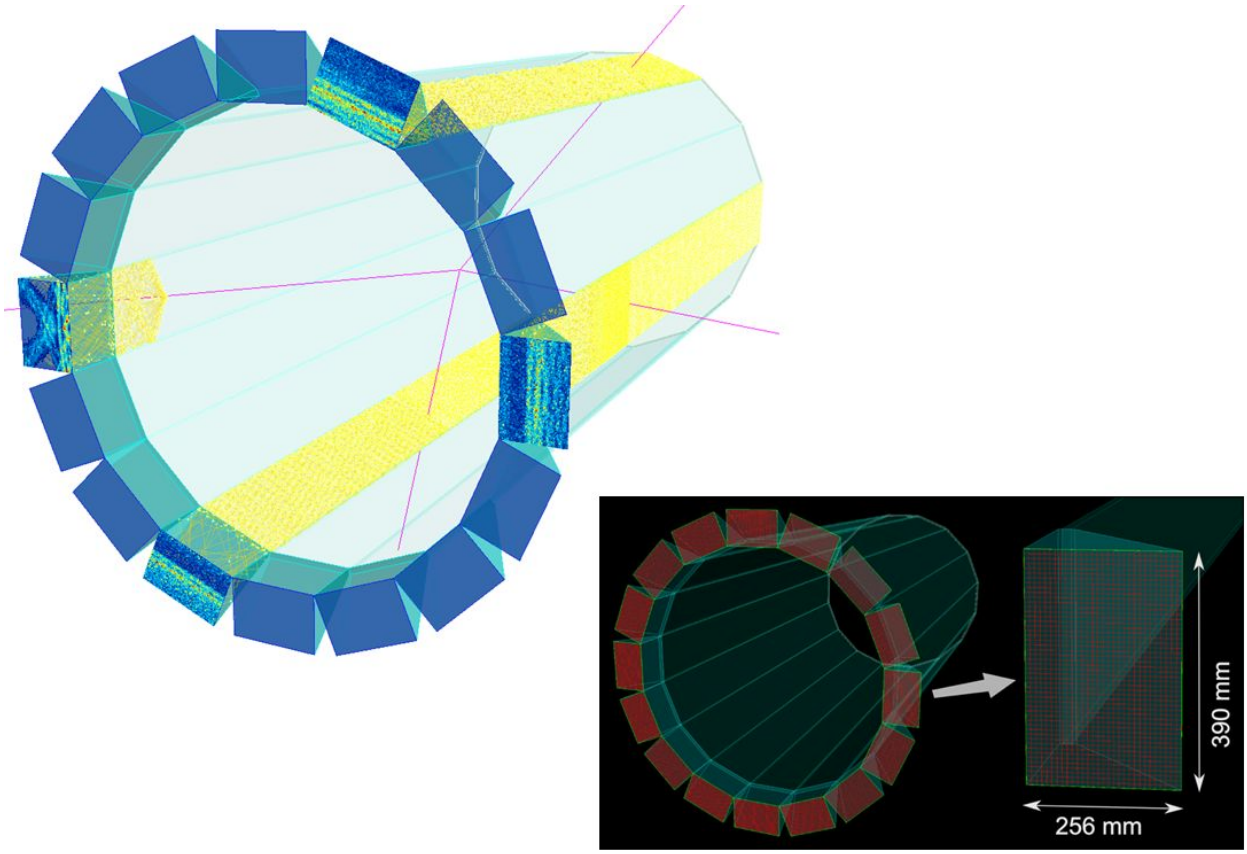


**Figure 4.4.13:** Geant4 simulation of the Barrel DIRC using a geometry with wide plates and a solid fused silica prism. This figure shows a possible configuration where the barrel is formed by 16 modules, each comprising a wide radiator plate in combination with a solid fused silica prism (with an opening angle of 38°) as expansion volume.

### 4.4.2.3 Simulations of FDIRC-like, mirror-based expansion volumes

The second new proposed focus for the simulation effort is to study the performance that can be achieved with mirror-based expansion volumes. A first step has been already taken by incorporating the Focussing DIRC (FDIRC) expansion volume in DrcProp. The image formation of the spherical surface of this design is illustrated in Fig. 4.4.14. In our future work, starting in FY17, we will study reconstruction resolution of this or similar designs.

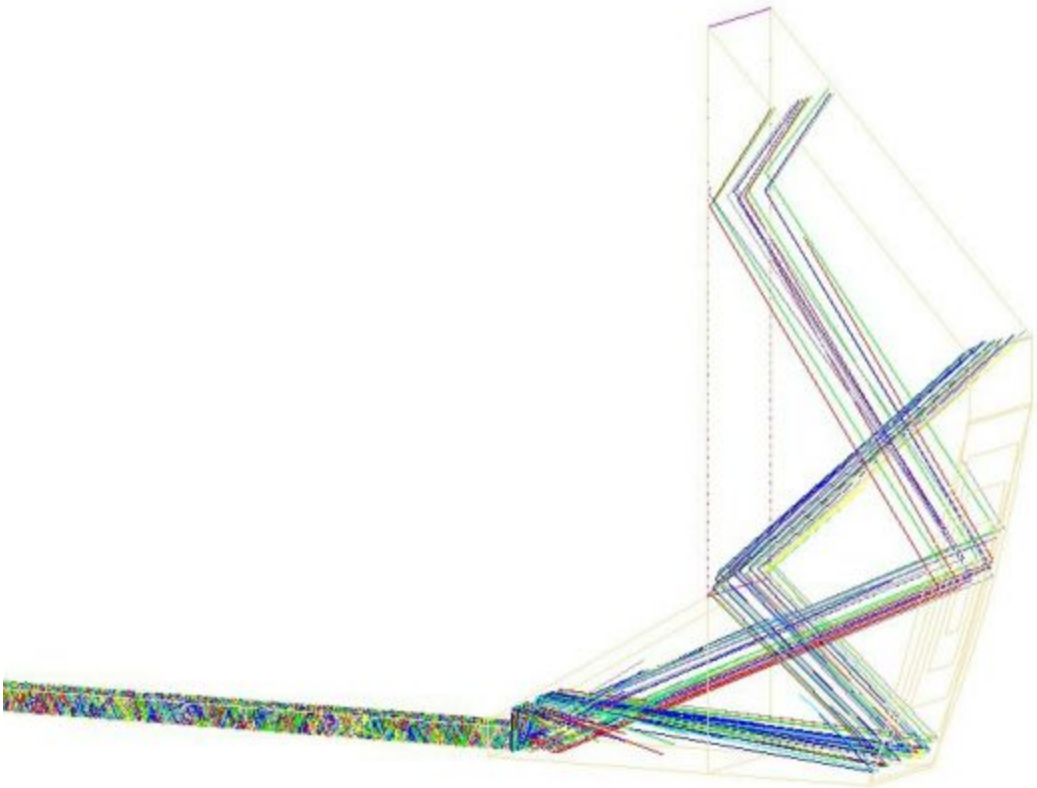

**Figure 4.4.14:** As a reference for simulations with mirror-based focusing and the expansion volume (EV) outside of the magnetic field, the FDIRC EV was implemented in DrcProp. Reflections off the sides of the EV are suppressed in this image. Color coding is based on the number of reflections of the photons inside the DIRC bar (0-9, 10-19,... 90-99).

### 4.4.3 Optics development and testing

The results from simulations described in section 4.4.2 were validated through an extensive series of measurements. To this end, simulations were performed both for the final configuration and the prototype one. The latter was slightly different in that it used only a single radiator bar rather than a full bar box, and sensors with 6-mm rather than 2–3 mm pixels. Through synergies with the PANDA R&D at GSI, which covered most of the costs associated with the prototype development and in-beam tests, this approach allowed to validate the results obtained for a high-performance EIC DIRC while minimizing the R&D costs. Aside from travel and manpower, the EIC R&D funded some small-pixel sensors (for separate tests), DAQ components, and the three-layer spherical lens for the high-performance EIC DIRC (earlier, simpler lenses were purchased with PANDA R&D funds). In the future, we will try to maximize synergies with GlueX R&D (and production) efforts aimed at developing a low-cost,, mirror-based expansion volume – and we will explore if such synergies would also be possible for testing a FDIRC-like expansion volume geared towards higher performance.

#### 4.4.3.1 Compact expansion volume

A compact expansion volume (EV) is an important requirement for any EIC DIRC with the readout

“camera” mounted inside the detector solenoid. In addition to facilitating integration, a small EV reduces backgrounds and maintenance. And while fused silica is an expensive material, a smaller focal plane also reduces sensor cost and the high-quality surfaces provide very well-defined reflection surfaces. However, for prototyping and in-beam tests the cost of a fused silica expansion volume is quite considerable. Fortunately, two prisms were made available by GSI for the EIC DIRC R&D at no cost as a synergy. These prisms, one of them shown in Fig. 4.4.15., have the correct depth of 30 cm, a width of 17 cm, and are available with top angles of 30° and 45°. Based on early lens development, we initially thought that in order to reach optimal performance we would need to develop a special EV with a sensor plane geometry matching that of the lens, but the flat focal plane of the final lens ensures that it can be matched to any standard prism. We are thus able to carry out all tests with the GSI fused silica prisms - a very significant cost saving.

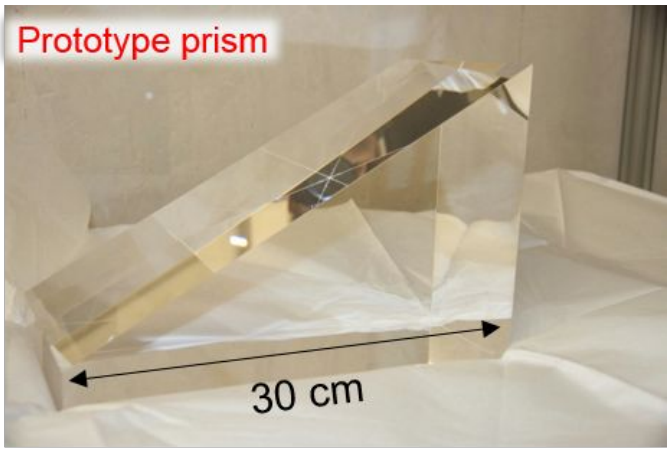


**Figure 4.4.15:** GSI expansion volume prism with a 30° top angle.

### 4.4.3.2 Development of an advanced lens with high refractive index

A simple plano-convex lens, made of fused silica and an air gap between lens and expansion volume, is able to produce a well-focused image of the Cherenkov pattern. However, due to the refractive index jump at the air gap many photons are reflected back due to Fresnel reflection, especially, for large angles between the photon and the surface normal vector. Anti-reflective coating might help and is worthwhile to be studied, but is intrinsically wavelength-dependent and will never be able to fully eliminate the loss from reflections at the air gap. Furthermore, such a single lens unavoidably produces a non-flat focal plane. This effect is shown for an earlier version of the two-layer spherical lens, made of fused silica and NLaK33, in Fig. 4.4.16.

The solution is to eliminate the air gap by using the transitions between fused silica and a higher-refractive index material to create focusing and defocusing surfaces to shape the focal plane. The resulting improvement is shown for a Geant4 simulation of the latest three-layer spherical lens in Fig. 4.4.16 and for a ZEMAX calculation in Fig. 4.4.17.

The combination of a focussing and a defocusing surface produces a flat focal plane up to photon polar angles of 40 degrees or more. Unfortunately, optical glasses with high refractive index, especially

radiation-hard glasses, typically cut off the UV photons at around 400 nm. Lead fluoride, $PbF_2$, has a high refractive index (nd=1.77), is radiation hard, and has a cut off at 300 nm. With this material a flat focal plane at a distance of 300 mm can be achieved. Prototyping a lens from $PbF_2$ will show if this material is mechanically usable for lens production.

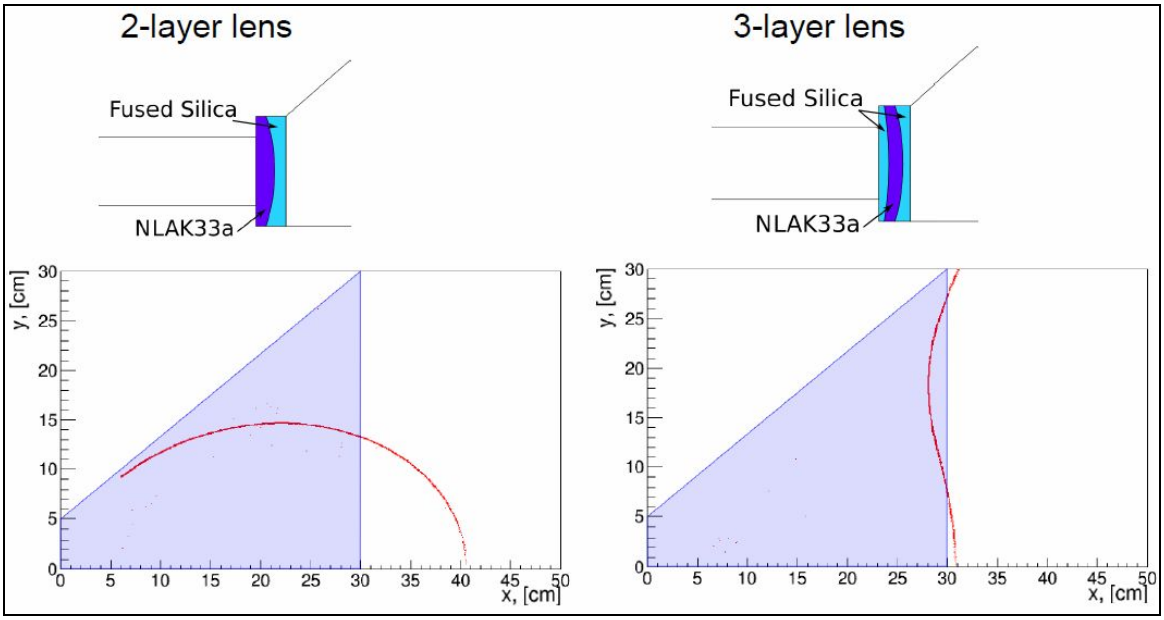


**Figure 4.4.16:** Simulated focal planes for the two-layer lens and the improved three-layer lens in Geant4.

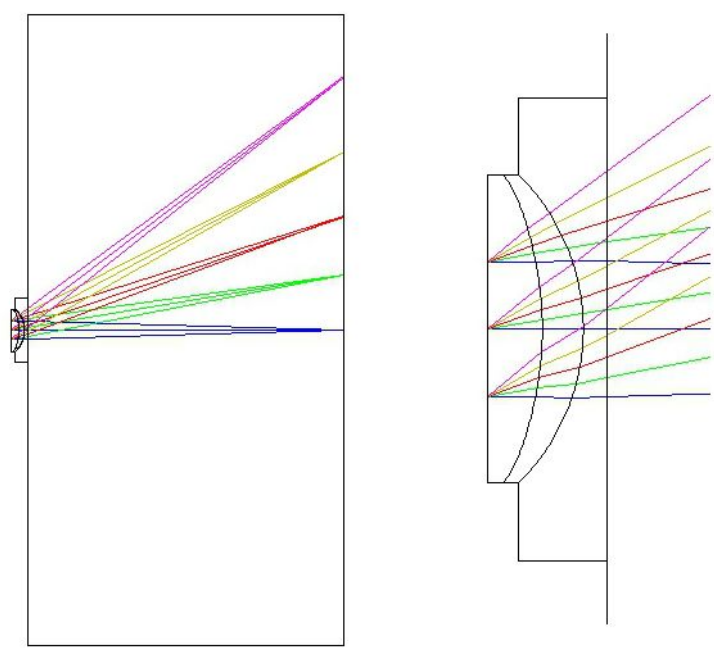

**Figure 4.4.17:** Three-layer-lens spherical designed with the ZEMAX software. The materials used are $SiO_2$-NLaK33-$SiO_2$. The produced lens is shown in Fig. 4.4.4.

## 4.4.3.3 Mapping the lens focal planes in test bench measurements

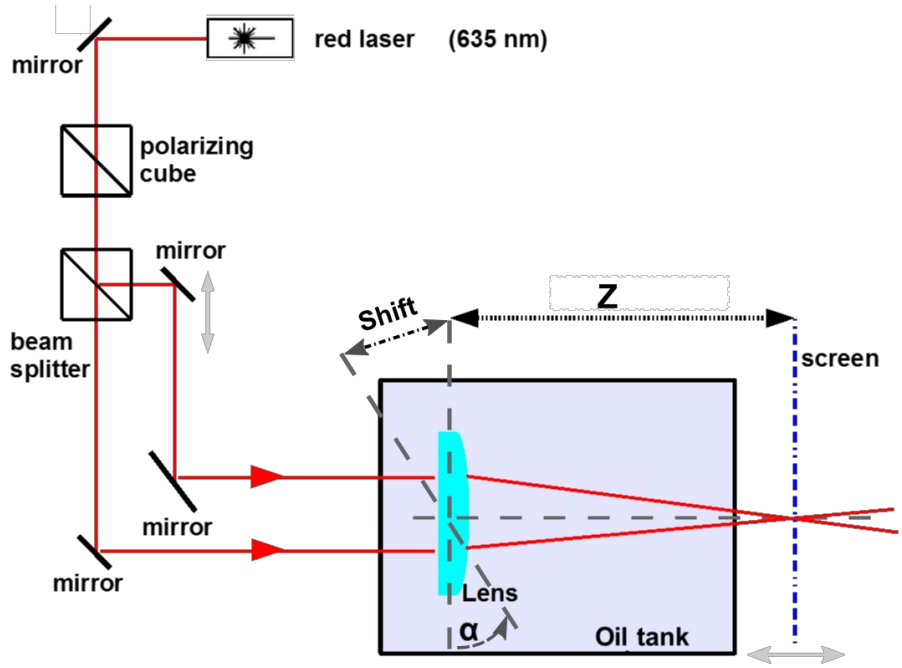


**Figure 4.4.18:** Schematic diagram of the optical setup to measure the focal length Z of the high-refractive lens as a function of angle α. The setup for the standard air gap lens measurements is the same but without the oil tank.

The pixel size and the bar size are important contributions to the Cherenkov angle resolution for a small expansion volume depth, as was discussed in section 4.3.2. The influence of the bar size can be mitigated by a focusing lens. However, the focal plane of a simple lens is not flat but has a parabolic shape described by the Petzval field curvature.

The focal planes of the standard spherical lens and a prototype two-layer high-refractive index spherical lens were studied in Geant4 simulation, as shown in Fig. 4.4.16, and measured in the laboratory to verify the parameters and to evaluate how important the curved surface of the focal plane is for the DIRC resolution. To measure the shape of the focal plane the setup shown in Fig. 4.4.18 was build. The lens was placed on the rotation stage and rotated through two parallel laser beams. The intersection point of two laser beams determines the focal length Z. The two-layer lens was placed inside a 20x20x30 $mm^3$ glass container filled with mineral oil (with a refractive index very close to fused silica) to simulate the focusing behavior for the situation without the air gap. The results are shown in Fig. 4.4.19. The rotation of the lenses is converted to the coordinate system of the prototype to better compare the shape of the focal plane to the back surface of the prism expansion volume. The systematic error of the rotation angle α was 0.1° and 0.1 mm on the Y coordinate. The systematic error of the focal length is estimated from repeated measurements to be 0.5 mm. The obtained shape of the focal plane agrees very well with the results from the Geant4 simulation. The measurements confirmed that the focal plane is strongly curved.

While the current R&D is based on a prism-shaped EV with a flat and perpendicular end surface, it is in principle possible to incline or shape the end of the prism to match the focal plane. Furthermore, an inclined surface may be favored to align the MCP-PMTs with the field lines of the solenoid. We will study these options in the future.

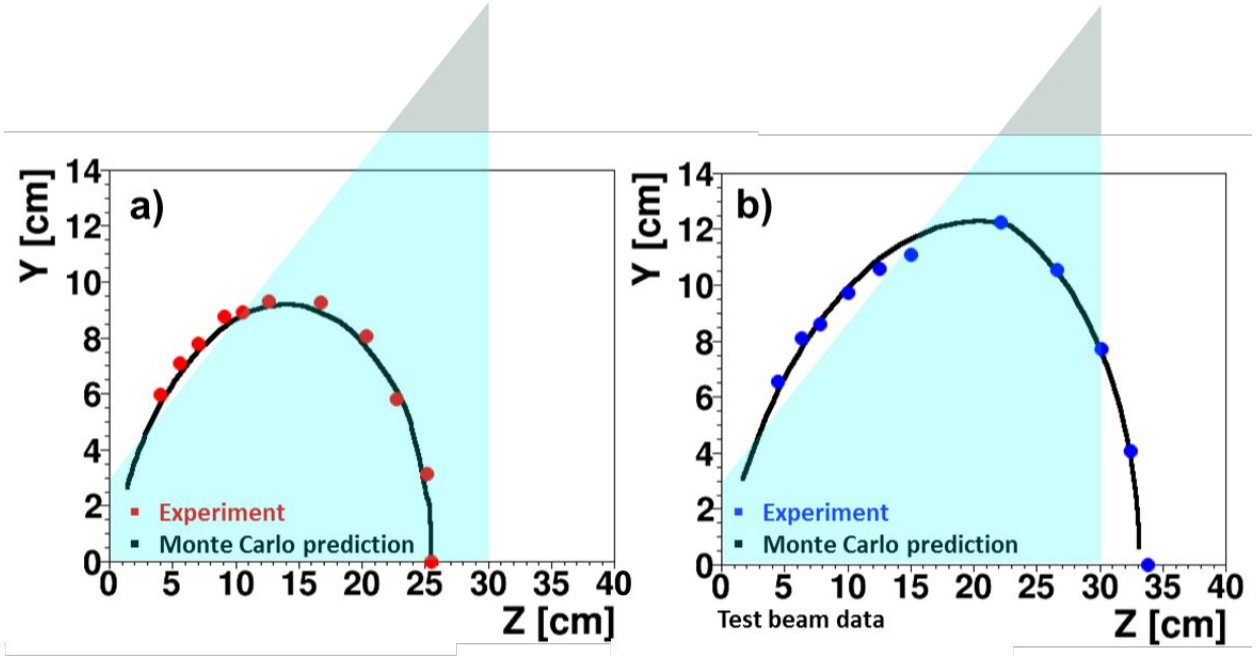


**Figure 4.4.19:** Measurements of the focal length (points) compared to Geant4 simulation (solid line) for two spherical lenses: a standard air gap lens (a) and two-layer high-refractive index lens (b), shown in the detector coordinate system. The cyan shape of the prism is used to illustrate the difference between the shape of the detector plane of the prototype and the shape of the focusing plane of the lenses.

### 4.4.3.4 Large prototype setup for in-beam tests

The prototype for tests in particle beams is based on the PANDA Barrel DIRC prototype built at GSI. The design will be modified to test the specific aspects of this R&D program, such as focusing options and fast timing.

The advantage of the GSI prototype is modularity. Most of the components, such as the support table, radiator and lens holders, as well as the radiators and MCP-PMTs themselves, can be utilized for the EIC R&D. The prototype for the current R&D will modify this prototype by replacing the sensor fixture to allow placement of both MCP-PMTs and MaPMTs on the focal plane to study the focusing quality of different lens designs in detail. The solid fused silica prisms used for the PANDA Barrel DIRC R&D (length 30 cm, width 17 cm, top angle 30º or 45º) can be selected according to the desired top angle. The readout electronics is equally modular and allowed a replacement of the TRB2, used in older beam tests, with the newer TRB3 readout boards procured for this R&D effort.

Additional beam instrumentation, such as trigger counters, hodoscopes, and a time-of-flight system are available in the PANDA group to measure beam properties.

A CAD drawing of the prototype used in 2014 and 2015, and a photo of prototype used in 2012, for a PANDA Barrel DIRC test beam campaign at CERN, are shown in Fig. 4.4.20.
The arrangement of the components that were used in 2015 at CERN are shown in Fig. 4.4.21.

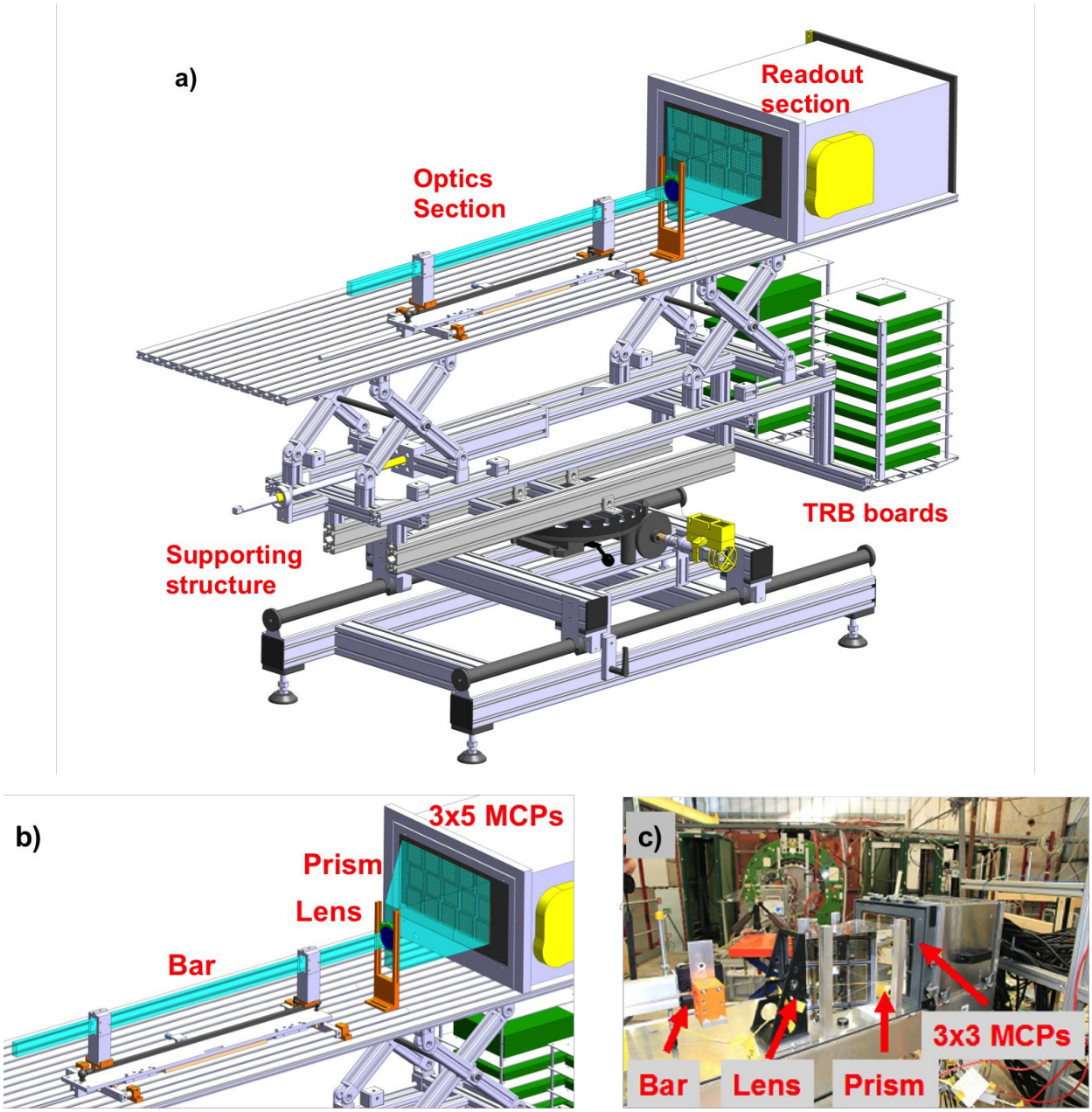


**Figure 4.4.20:** Layout of a the PANDA barrel DIRC prototype from the summer of 2015. Overview of components (a) and close-up of imaging region (b) showing the prism expansion volume, focusing lens, and radiator plate. Photo of the prototype in a beamline at CERN in 2012 (c).

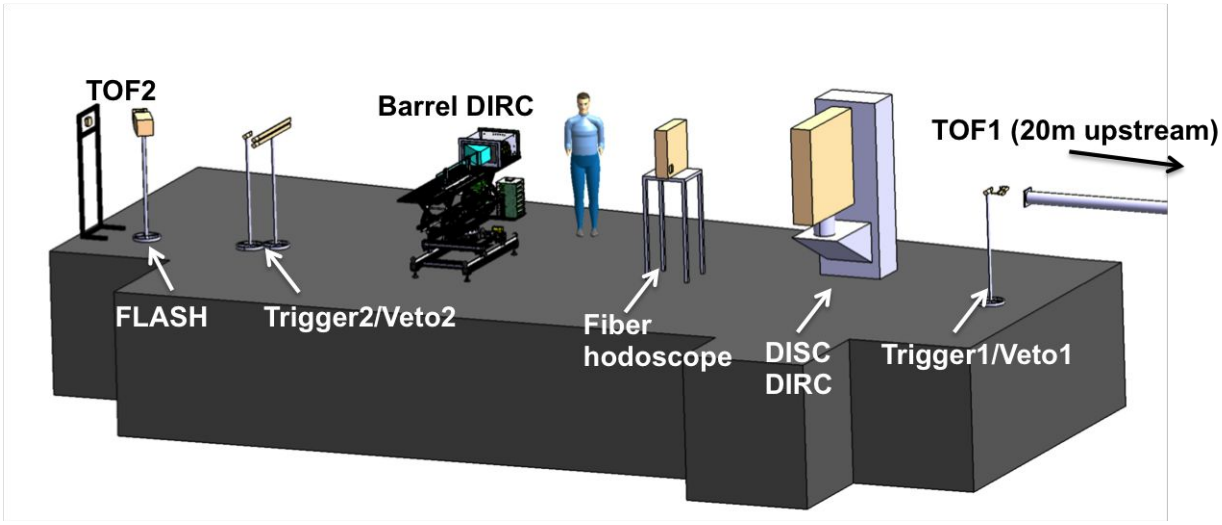


**Figure 4.4.21:** Arrangement of the prototype elements used in the 2015 test beam at CERN.

A height-adjustable table with a precision rotating stage is used to place the prototype into the beamline and to adjust the position and polar angle of the radiator bar or plate relative to the beam. The radiator is placed into a holder on an X/Y stage, which allows precision alignment of the radiator relative to the lens and the expansion volume. A mirror was placed at the opposite end of the bar. A plastic fixture places the sensors into an array structure at the back wall of the expansion volume. The sensors, prism, lens, and radiator are coupled using optical grease. The radiator, lens, expansion volume, and front-end readout electronics are placed in a light-tight box.

The primary goals of the tests of prototypes with particle beams are

- determination of the photon yield per particle;
- determination of the single-photon Cherenkov angle resolution;
- demonstration of the effect of fast timing on the Cherenkov angle reconstruction;
- direct measurement of PID efficiency and mis-identification.

These tests are best performed in a hadron particle beam with momenta between 3 and 8 GeV/*c* to measure the PID performance using pions and kaons or protons. An example of such a beam line is the T9 area at the CERN PS. Successful tests of the PANDA Barrel DIRC prototype were performed there in 2011 and 2012. A low-momentum hadronic beam was available for DIRC tests at GSI in 2011. Due to shutdown plans at CERN and at GSI and DESY, no beam time was available in 2013. In 2014 the 1.7 GeV/*c* pion beam was used for initial tests of the new three-layer lens but the rather large beam divergence and short beam time made most of the quantitative measurements impossible.

An example of the occupancy plot from 2014 for a 124° polar angle is shown in Fig. 4.4.22.a. Although the hit pattern is complicated with overlapping segments due to reflections from the top, bottom, and sides of the prism, these features are in good agreement with the prediction from simulation. The background, visible as violet pixels around main ring segments, comes from processes like δ-electrons, MCP-PMT dark noise, or charge sharing. The corresponding reconstructed Cherenkov angle per photon is shown in Fig. 4.4.22.b.

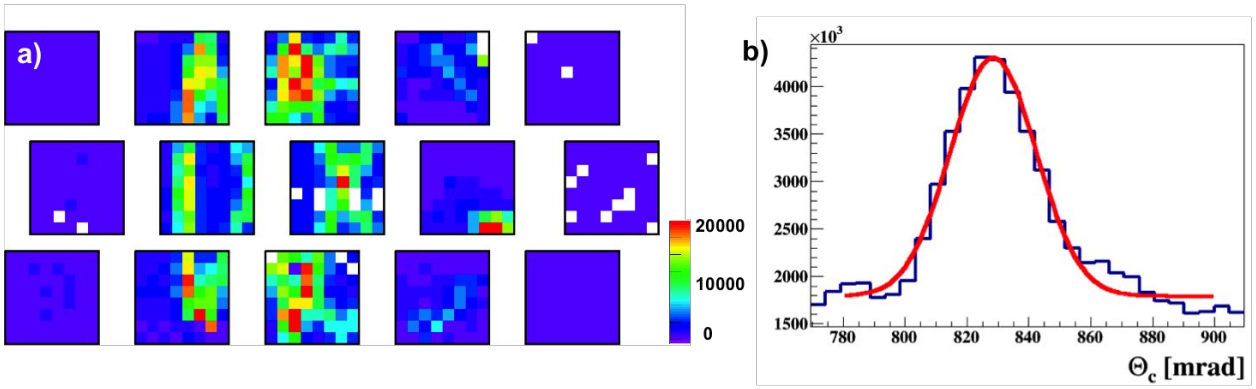


**Figure 4.4.22:** Performance of DIRC prototype with 3 layer lens in experimental data from the 2014 test beam campaign. Distribution of the hits per MCP-PMT (a) and reconstructed Cherenkov angle per photon (b) are shown.

Another test beam campaign was approved for the PANDA DIRC detectors at the CERN PS for the summer of 2015. The EIC DIRC in-beam tests are coordinated with the GSI PANDA DIRC group and performed during May and June/July 2015. Figure 4.4.23 shows photos from the first part of the 2015 campaign. An example occupancy plot for a 124° polar angle is shown in Fig. 4.4.24.

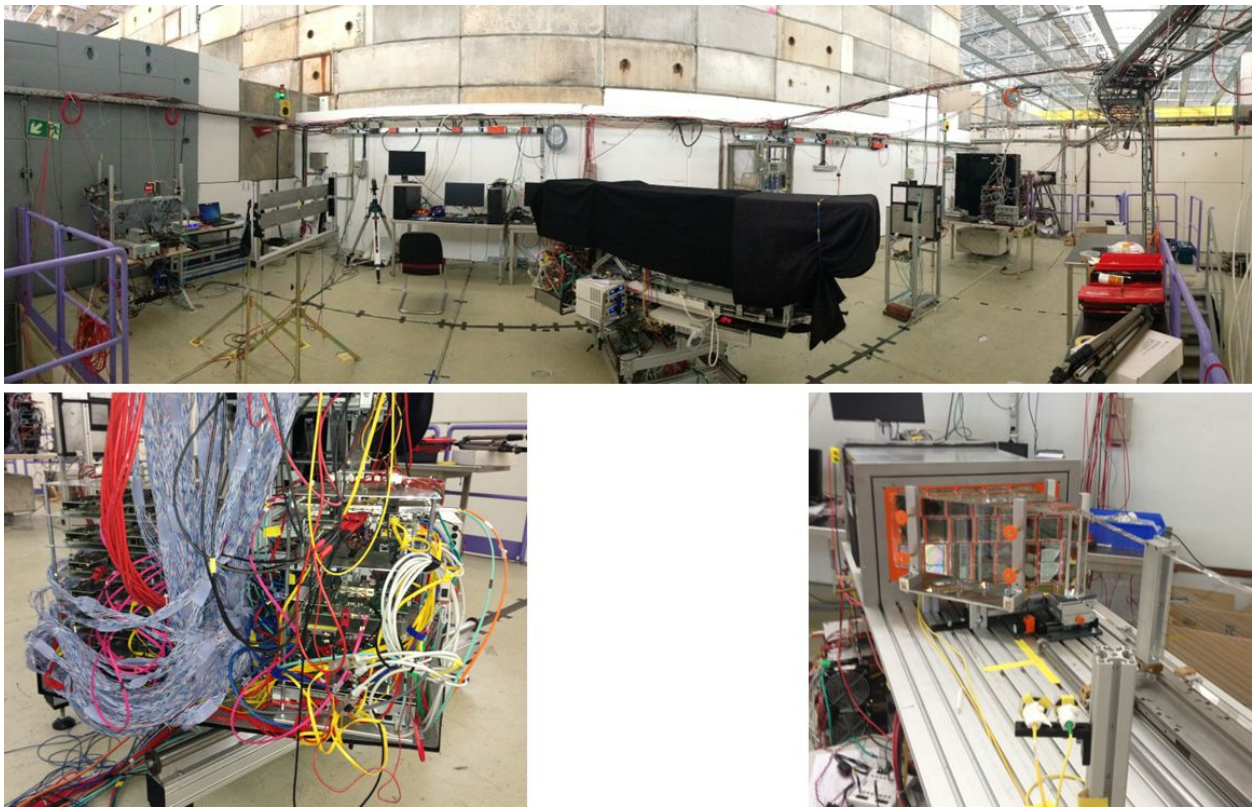

**Figure 4.4.23:** Photos of the PANDA DIRC prototypes in the T9 area of the CERN PS in May 2015. The barrel DIRC prototype, covered in a black cloth, can be seen in the centre of the top image. The stack of TRBs is visible on the lower left. The wide plate, coupled via a two-layer cylindrical lens to the prism EV, with an array of 3x5 Planacon MCP-PMTs placed in the imaging plane, can be seen on the lower right.

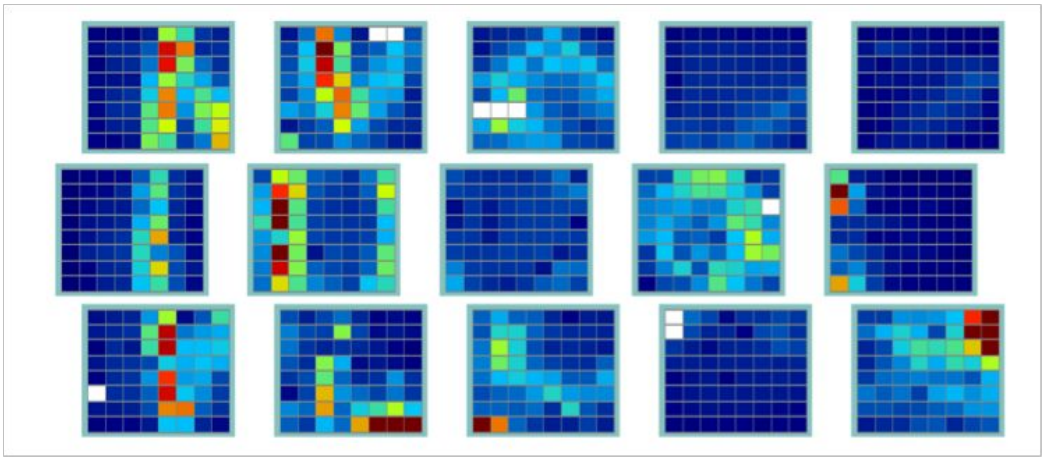

**Figure 4.4.24:** Raw occupancy distribution from the May 2015 data, a 5 GeV/*c* mixed hadron beam at 124° polar angle, for a narrow bar and the three-layer spherical lens. The high quality of the focusing up to large photon angles for several reflections inside the prism EV is seen. The red pixels correspond to a large number of entries, the blue pixels to a small number of entries, while the white pixels correspond to inefficient DAQ channels.

## 4.5. Proposed photosensor R&D

### 4.5.1 Gain studies at the High-B Field Test Facility at JLab

The program for testing photosensors in high magnetic fields has also reached several milestones: the EIC high-B test facility has been commissioned in Summer 2014, and a production run was completed in Fall 2014, with the second one planned for FY15 coming up in July. While the program is only starting, it has already demonstrated that MCP-PMTs with small pore sizes can perform well in magnetic fields up to several Tesla, but that the gain deteriorates (sometimes very rapidly) as a function of the angle between the MCP normal direction and the direction of the magnetic field. Significant variation between sensor types indicates that it would be possible to improve this performance if the optimal parameters were known. We thus ask for funding to continue this exciting R&D, which the committee viewed favorably in its last report, through FY18.

#### 4.5.1.1 Progress and current status

The high-B sensor test facility was installed and commissioned during FY14–15. Jefferson Lab allocated space specifically for this purpose in the new High Bay Test Building. The facility consists of a 5.1-T superconducting solenoid magnet, custom-designed dark test box, and electronics. First measurements of the response of single-anode MCP-PMTs were performed in FY15. Three single-anode small-pore-size sensors were extensively studied not only at various B-field magnitudes, but also for various orientations of the sensors with respect to the B-field direction. Those were, Photek PMT210 (3.2 μm pore size), Photek PMT240 (10 μm pore size), and Photonis PP0635G (6 μm pore size).

For the measurements we used a 470-nm Light-Emitting Diode (LED) driven by a HP8116A Pulse/Function Generator. The generator pulses were delivered with a frequency of 30 kHz. To simulate operation in a single-photon mode, as expected in real experimental conditions, the generator voltage was set such that about 15% of the pulses resulted in a PMT response. The output PMT signals were amplified 200 times by an ORTEC VT120 preamplifier and digitized by Analog-to-Digital Converter fADC250 with a sampling rate of 250 MS/s and a converter bandwidth of 125 MHz.

The design of the dark box allows to rotate the sensors relative to the B-field direction (rotation angle $\theta$) and around their own axis (rotation angle $\varphi$), see Fig. 4.5.1.1. Sensors were tested at two high voltage settings, operating voltage of $0.9\times HV_{ma}$ and a near-the-maximum voltage of $0.99\times HV_{ma}$. The sensor performance was evaluated based on analysis of the recorded output waveform for each setting ($B$, $\theta$, $\varphi$, HV).

More specifically, the sensor performance can be quantified by either estimating the absolute gain from fits to ADC distributions of the total area of the output voltage signal, or by estimating the charge collected on the anode for each pulse after subtracting the pedestal contribution from the total area of the output voltage signal and averaging over all measured pulses. Here we present results using the latter method.

Figure 4.5.1.2 shows the average total charge collected on the anode per pulse for the 3.2-μm and the 6-μm sensors as a function of B-field at $\theta = 0°$ and $\varphi = 0°$. Our results show that generally, smaller pore size MCP-PMTs show better immunity to high magnetic field. Specifically, for the DIRC at EIC application, our measurements suggest that 3.2-μm sensors can be a viable solution as they provide

sufficient gain even at 3 T. 6-µm sensors could be a possible solution if they are operated at maximum high voltage. The 10-µm sensor provided reasonable signal only up to ~2 T, even when operated at maximum HV.

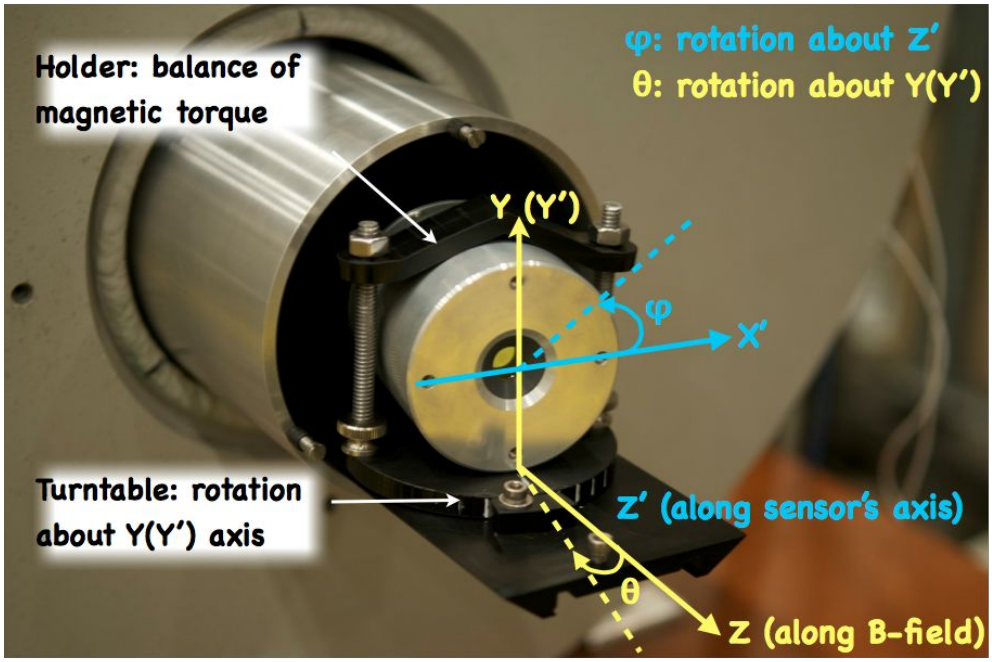


**Figure 4.5.1.1:** Rotation capabilities provided by the design of the dark box. The accessible range in $\theta$ is limited by the length of the sensors and the connectors on its back side and was 0° – 30° for PMT210 and PP0365G. Rotation at 180° – 210° is achieved by rotating the dark box. Full range in $\varphi$ is accessible, although the step size, $\Delta\varphi$, depends on the shape of the sensor.

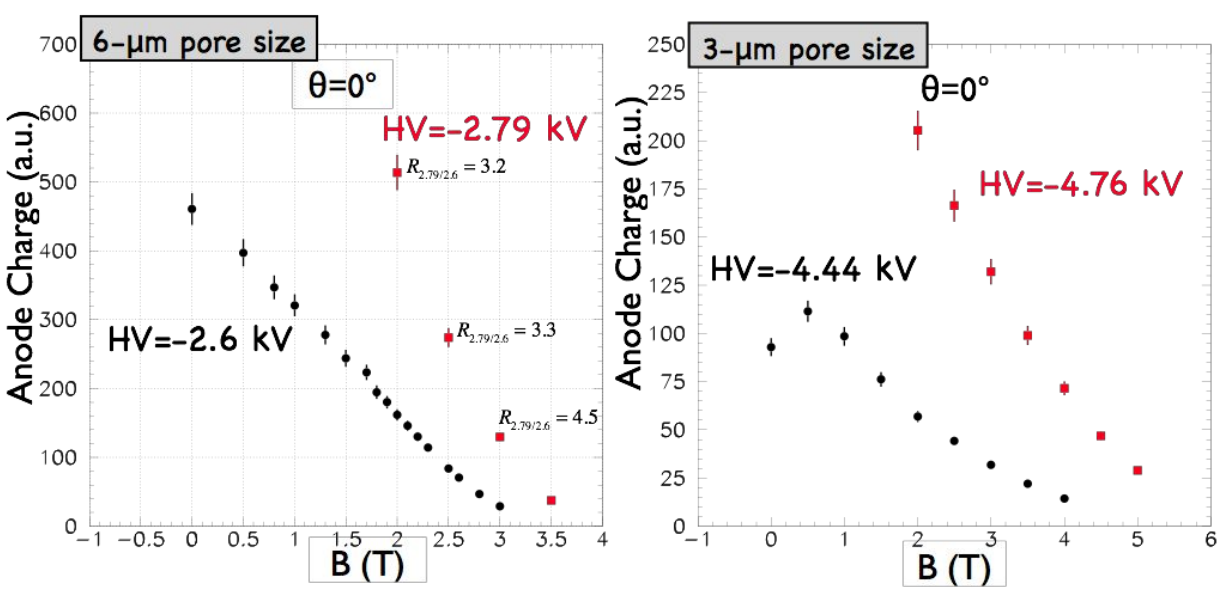


**Figure 4.5.1.2:** Average total collected charge per pulse at the anode for PP0365G (left) and PMT210 (right). Solid circles show results at HV about 90% of the maximum HV. Solid squares show results at near-maximum HV. At $0.9\times HV_{max}$ the collected charge at B = 3 T is about 15 times less than at 0 T for the larger pore-size sensor, while for the smaller pore-size sensor the decrease is about 7 times. Increasing the HV by 10% to $0.99\times HV_{max}$ increases the amount of collected charge by 3 to 5 times depending on the field. This suggests that in a real detector application, increasing the high voltage can be an effective way to mitigate the gain drop due to the presence of a high magnetic field.

The angular dependences of the sensor response are very interesting and can be seen on Fig. 4.5.1.3 and Fig. 4.5.1.4. There is a strong correlation of the average charge collected on the anode with the angle $\theta$, between the sensor and the field axes. The shape of the correlation seems to depend on the internal design of the MCP-PMT as the Photonis sensor shows an improved performance at larger angles and field magnitudes below 1 T, while the Photek sensor shows decreasing gain as the angle increases. In the latter case, the amount of average collected charge on the anode decreases exponentially above 0.5 T even at $\theta = 5°$.

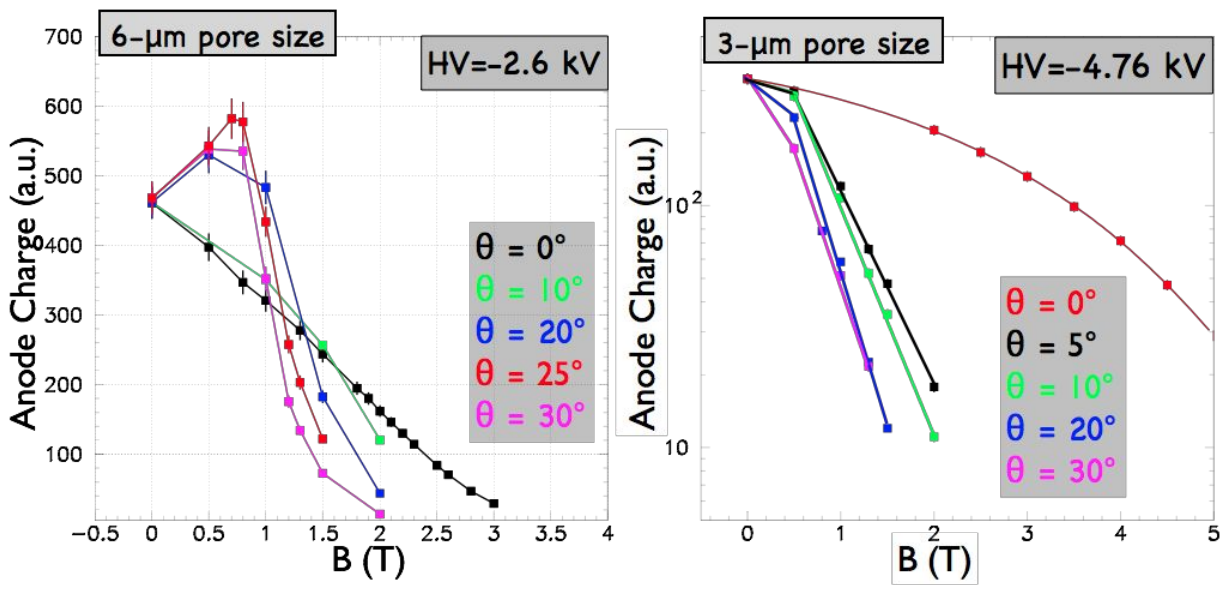


**Figure 4.5.1.3:** MCP-PMT response for various B-fields and rotation angles $\theta$. Left: Photonis PP0365G. Right: Photek PMT210. While it is evident that smaller pore size provides better immunity to magnetic field, it is also apparent that the sensor response varies significantly depending on the relative orientation of the sensor relative to the field direction and that these variations depend on the type of sensor (*i.e.* its internal design). Our efforts in the next years will focus on studies of MCP-PMT design parameters on magnetic-field performance.

Measurements at several $\varphi$ angles show that the amount of the anode charge depends also on that angle with a strong correlation between the $\varphi$ dependence and the $\theta$ angle (see Fig. 4.5.1.4). For fixed $B$, the gain variations with $\varphi$ are significantly larger at $\theta = 20°$ than at $\theta = 10°$, which suggests that for MCP-PMT readout arrangements with large variations of the sensor axis relative to the field direction, special attention needs to be paid to compensate for the gain decrease of sensors located at unfavorable positions.

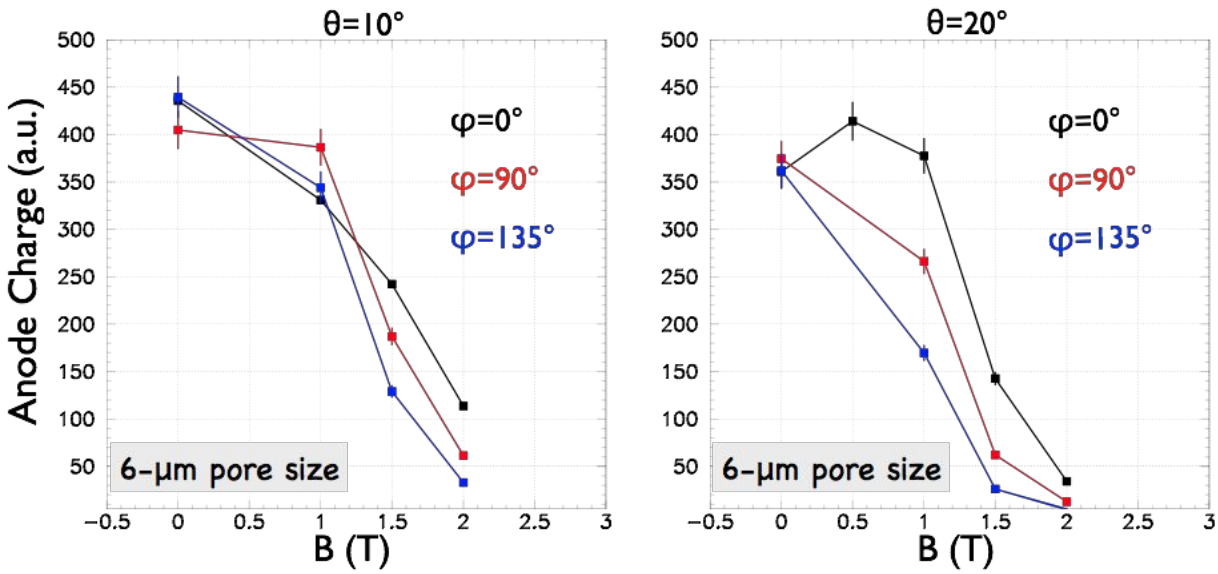


**Figure 4.5.1.4:** A 6-μm-pore-size MCP-PMT response at various B-fields and rotation angles $\theta$ and $\varphi$. For fixed $B$, the gain variations with $\varphi$ are significantly larger at $\theta = 20°$ than at $\theta = 10°$, which suggests that for MCP-PMT arrangements with large variations of the sensor axis relative to the field direction, special attention needs to be paid to compensate for the gain decrease of sensors located at unfavorable positions.

Overall, the 3.2-μm pore-size sensor seems a very promising solution for operations in magnetic fields up to 5 T. However, the current sensor design limits the best performance to $\theta = 0°$. 6-μm pore-size sensors may be appropriate for operation in fields around 3 T, or even larger, after optimization of their design. To allow for a reasonable response at varying orientations between the sensor and the magnetic field direction, as expected in an actual EIC-DIRC implementation, the sensor design needs to be optimized. Further investigation planned for FY16–18 will show the limits of sensor performance in fields of 2 – 5 T that can be achieved with targeted design optimization. The fact that the observed decrease of collected anode charge for various settings was of up to an order of magnitude indicates that the optimizations may not have to be revolutionary and should be attainable within the time frame of the EIC. In any case the sensors must have a gain of $x10^6$ or larger in zero field so that overall no MCP-PMT experiences a gain below $10^5$.

It must be noted that during the FY14–15 measurements, two of the PMTs that were tested experienced damage to the photocathode, evidenced by a decrease in quantum efficiency (QE). A gain deterioration was also observed but to a lesser extent. Notably, there was a 30% QE decrease for the Photonis sensor and about a factor of 5–10 (depending on wavelength) for the Photek 3.2-μm sensor. The larger pore-size Photek sensor was tested only at $\theta = 0°$ and $\varphi = 0°$ and only up to 2 T, and no damage was reported. While, standard causes as malfunctioning modules such as a HV unit or severe instability of the pulser driving the LED causing a large light illumination, may explain the damage, one should not exclude the possibility for the damage to be caused by a substantially increased ion feedback at some ($B$, $\theta$, $\varphi$) coupled with the fact that the sensors were operated at HV of 90% and higher of the maximum voltage. A literature search showed at least one report of observed photocathode damage to a curved-channel MCP PMT when operated in transverse fields below 0.2 T[2]. This suggests that such a possibility should not be overlooked. To minimize the risk of sensor damage caused by malfunctioning electronic modules we are

[2] C.C. Lo, P. Lecomte, and B. Leskovar, IEEE Trans. Nucl. Sci. **24**, 302 (1977).

incorporating a continuous monitoring of the anode current, a reference PMT for continuous light-intensity monitoring, and a HV unit allowing for programmable current limitation. The amount of ion feedback on the photocathode for various ($B$, $\theta$, $\varphi$) will be studied in a Geant4 simulation of MCP-PMT, which will begin in FY17. If indeed, a specific combination of ($B$, $\theta$, $\varphi$, HV) causes a significant ion feedback, which decreases substantially the QE and lifetime of the MPT photocathode, this effect needs to be seriously considered for the in-magnetic-field readout solution of an EIC DIRC. We will also continue to collaborate with the MCP-PMT manufacturers to investigate this problem.

While measurements of single-anode MCP-PMTs provide valuable information about the effect of various parameters, such as pore size, internal design parameters, and orientation on the PMT performance in magnetic fields, multi-anode sensors are of primary interest given their advantage in actual detector implementation. We will study the performance of currently available 10-μm multi-anode MCP-PMTs for various ($B$, $\theta$, $\varphi$, HV). One such sensor is already available at JLab and another one will be provided to us on loan.

Given the large gain variations with ($B$, $\theta$, $\varphi$) observed in our measurements during FY14–15, and the solenoid field non-uniformity in the area where the installation of the EIC-DIRC readout is considered, it is clear that the gain across the readout will not be uniform. Since the timing resolution of an MCP-PMT depends strongly on the amplitude of the output signal, *i.e.* the sensor's gain, the evolution of the sensors timing response with ($B$, $\theta$, $\varphi$, HV) needs to be considered. A theoretical model of the electron avalanche development in the MCP suggests that the transit time spread (TTS) of a straight-channel MCP should not depend on the component of the field parallel to the channel axis[3]. No theoretical input exists regarding the effect of transverse fields. Actual timing measurements of chevron-stacked MCPs exist only for magnetic fields up to 2 T. The study done for the development of the BELL II TOP counter evaluated the timing resolution of a multi-anode Hamamatsu sensor up to 1.5 T for a fixed orientation of the sensor axis relative to the field and found no significant changes[4]. A more comprehensive study was done for the development of the PANDA DIRC as the timing performance was evaluated not only for varying fields but also for varying orientations between the sensor and the field axes[5]. Within the uncertainties of their measurements, the letter study found only a small deterioration of the time resolution towards higher fields. As this study covered a range of fields up to 2 T only, there are no data mapping MCP-PMT timing response above 2 T and it is not known if the observed small deterioration would follow a progressive trend at higher fields. While, based on the published low-field measurements, one expects the timing resolution to deteriorate (if indeed) as the field increases much less than the gain, given the requirement of 100 ps or better timing resolution for the EIC DIRC, it becomes important to evaluate MCP-PMT timing characteristics with ($B$, $\theta$, $\varphi$, HV). Naturally, timing measurements will strongly relate to the gain measurements and will also follow up with sensor design optimization as well as with advancements in performance of timing readout electronics. Extending the functionality of the high-B sensor test facility to allow for precise timing measurements is a natural synergistic activity with the LAPPD project.

Thus, our efforts in the next funding cycle will be focused on (1) Continued tests of single- and multi-anode MCP PMTs in fields up to 5 T, (2) studies of MCP design parameters to help optimizing design for operations in high magnetic fields, and (3) extending the functionality of the high-B test facility to allow for studies of timing properties in high magnetic fields.

---

[3] G.W. Fraser, Nucl. Instr.. Meth. **A 291**, 595 (1990)
[4] S. Hirose, Nucl. Instr. Meth. **A 766**, 163 (2014)
[5] A. Lehmann *et al.*, Nucl. Instr. Meth. **A 595**, 173 (2008)

### 4.5.1.2 Planned Tests and Procedures

We will continue to evaluate the gain performance of manufacturer-available MCP-PMTs up to 5 T. In FY16 and FY17 we will measure two Katod single-anode MCP-PMTs, which were procured in FY14, a multi-anode 10-μm pore size Hamamatsu sensor, which has been already given to JLab on loan by the manufacturer, and a multi-anode 10-μm pore size Planacon, which the manufacturer has agreed to provide on loan. We will map sensor gain for various settings ($B$, $\theta$, $\varphi$, HV).

Part of our efforts will specifically target improving design optimization of MCP-PMTs in high magnetic fields. For this purpose, first measurements will be done in summer of 2015 on the PMT210, which we have already measured in 2014. The manufacturer has refurbished the sensor to allow for independent controls of the high voltages between the photocathode and the first multi-channel plate ($V_{cp}$), across the plates ($V_{pp}$), and between the last plate and the anode ($V_{pa}$). We will study the effect of each one of these voltages on the sensor response. Our aim is to identify if any combination of internal high voltages improves the performance of the sensor at angles $\theta$ larger than 0°. Such measurements will also be performed with the Katod single-anode sensors and with the Planacon and Hamamatsu multi-anode sensors.
In FY17 we will begin to implement the internal structure of a typical MCP-PMT in a Geant4 simulation. Studies of ion feedback, and of the effect of various combinations of internal parameters on the gain and timing performance of a sensor in various fields and for various orientations relative to the field will continue in FY18.

A significant part of our efforts in FY18 will be the installation and commissioning of timing capability of the high-B test facility at JLab. For the timing measurements we will use a pulser-driven LED (the pulser was already procured in FY13). To reduce the timing fluctuations of the pulser signal, the reference START time will be given by a system of two reference PMTs. Together with the LAPPD group (C. Zorn), we are exploring the option of setting the START time by a laser diode, which is already available at Jefferson Lab, but the use of which is very limited due to safety constraints. MCP-PMT signals will be amplified by a fast preamplifier (already procured in FY13), shaped by a constant-fraction discriminator, and digitized by a high-resolution TDC. The timing resolution will be obtained from the width of the difference between the MCP-PMT and the START times. Initial timing-resolution measurements for various settings ($B$, $\theta$, $\varphi$, HV) will be performed with the 3-μm and the 5-μm Katod sensors. During the commissioning of the timing capability we will use a rented fast, high-sampling rate oscilloscope to validate and optimize the timing response of the amplifier–discriminator–TDC branch (which is intended for regular use).

Funding from this project for FY16 is used for Liquid Helium needed to operate the magnet for two sensor-test runs, equipment necessary to set up the cooling system and to do the cool down, such as pipes, valves, protective gear, *etc.*, and for procuring/manufacturing parts to accommodate new sensors in the dark box, such as voltage dividers, sensor holders, connectors, *etc.*

Funding from this project for FY17 is used for Liquid Helium needed to operate the magnet for two sensor-test runs and for procuring/manufacturing parts to accommodate new sensors in the dark box, such as voltage dividers, sensor holders, connectors, *etc.*

Funding from this project for FY18 is used for Liquid Helium needed to operate the magnet for two sensor-test runs of timing properties, for procuring high-resolution fast timing electronics, and for renting fast, high-sampling rate oscilloscope.

## 4.5.2 Timing measurements at GSI

A data acquisition system was set up at GSI for timing studies of MCP-PMTs as part of the prototype configuration, and such measurements can thus be performed both during beam tests and offline. The Trigger and Readout Board 3 (TRB3), shown in Fig. 4.5.2.1, which was designed at GSI, was integrated into the TRB-net to connect the TRB readout boards to a desktop computer.

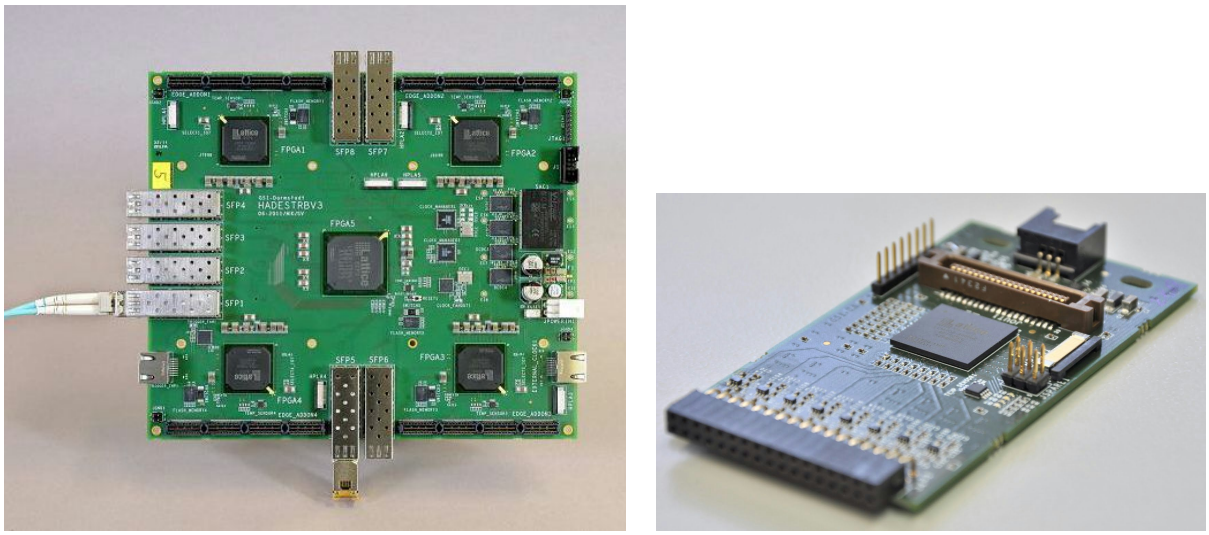


**Figure 4.5.2.1:** Trigger Readout Board 3 (left) with four FPGA holding 256 TDC channels. A fifth FPGA is for communications. PADIWA (PAnda DIrc WAsa) amplifier and discriminator card optimized for single photon detection using MCP-PMTs.

The sensor is connected via an optional adapter board to a compact front-end board, which amplifies and converts the analog signal into a digital signal that is plugged into an add-on card on top of the TRB3. Several choices for the front-end board design exist, including one based on the NINO chip or one using custom ASICs (*e.g.,* the PADIWA chip).

The time resolution for 256 channels of one TRB3 will be better than 20 ps. Together with an existing laser system (PiLas, 405 nm), the time resolution of various MCP-PMTs and MaPMTs can be determined. An example of the Hamamatsu R11265-103-M64 MaPMT, purchased for the EIC DIRC R&D, is shown in Fig. 4.5.2.2 together with the custom adapter board. The Hamamatsu R11265-103-M64 has a size of 26.2 mm × 26.2 mm, a nominal gain of $10^6$, 8×8 anodes, corresponding to a pixel size of about 3 mm, and an active area ratio of 77%. The MaPMTs, socket assembly, adapter boards, TRB3s, and PADIWA cards were part of the procurement in FY14-15.

The measurements will profit from the experience with the TRB2 and TRB3 readout boards and the PADIWA amplifier and discriminator cards gained by the GSI group in the context of the PANDA DIRC R&D. For a test of SiPMs a dark box was prepared and measurements with an existing VME DAQ systems can be started. The capability to cool down the sensors down to temperatures of -20° C will be added in the near future as part of the proposed procurement.

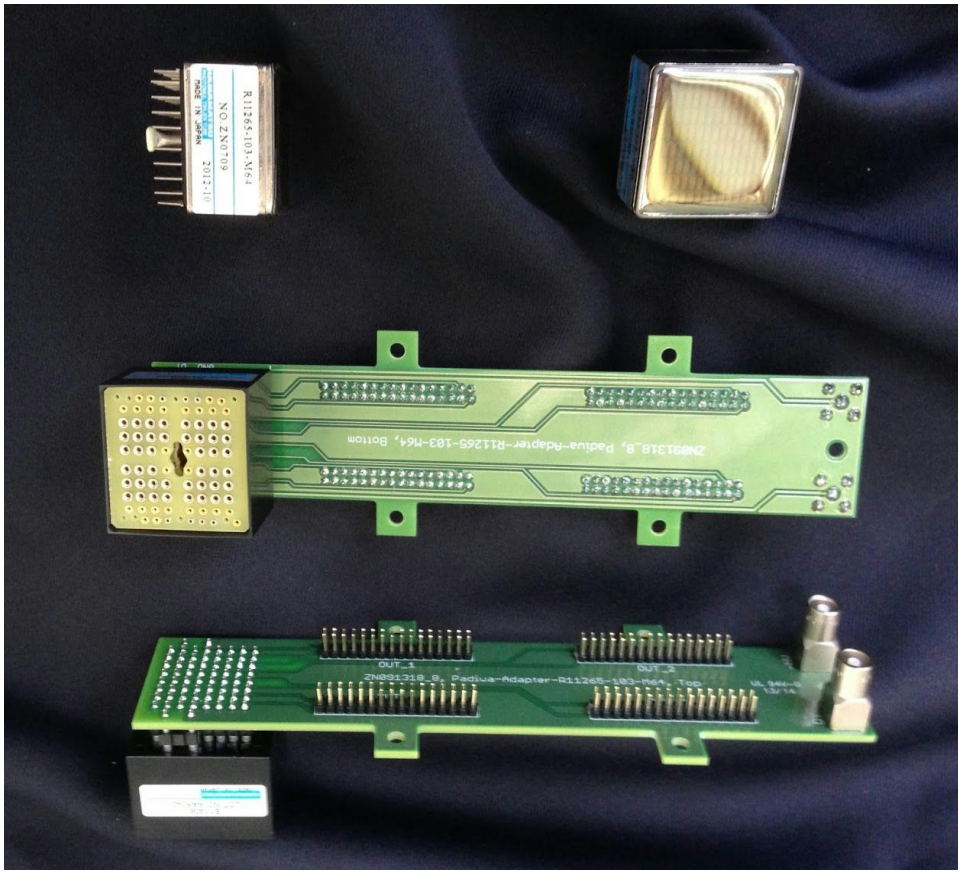


**Figure 4.5.2.2:** Photo of two Hamamatsu R11265-103-M64 MaPMTs together with the socket assembly E11906 and the custom adapter boards, designed and built by Erlangen University, that couple the MaPMTs in their socket assmblies to the high voltage cables and to the PADIWA cards.

## 4.5.3 Radiation hardness studies

The determination of radiation levels and the radiation hardness of material, sensors, and electronic parts is an important issue. FPGA-based TDCs close to the detector and SiPM sensors need special attention. Results of studies made under previous EIC R&D, by C. Zorn *et al.*, have shown that both dark rate and dark current increase linearly as a function of total neutron fluence and the damage does not depend on the temperature or operating voltage. Part of the acute damage can be recovered by increasing the temperature of the damaged unit during non-irradiated periods. There is hope that the new generation of SiPMs with metal resistors are more radiation hard compared to the old generation with poly silicon resistors. The latter are illustrated in Fig. 4.5.3.1. Radiation hardness tests of SiPMs within the PANDA-TOF project, which will take place at PNPI Petersburg, Russia, can be used to measure candidates for the EIC. An independent study of radiation tolerance of SiPMs was also carried out at Jefferson Laboratory by C. Zorn as part of an independent EIC R&D proposal, which was later merged with the DIRC R&D. In the future, we may want to further study the impact of radiation – perhaps in combination with magnetic fields – but this falls outside of the scope of the FY16–18 proposal.

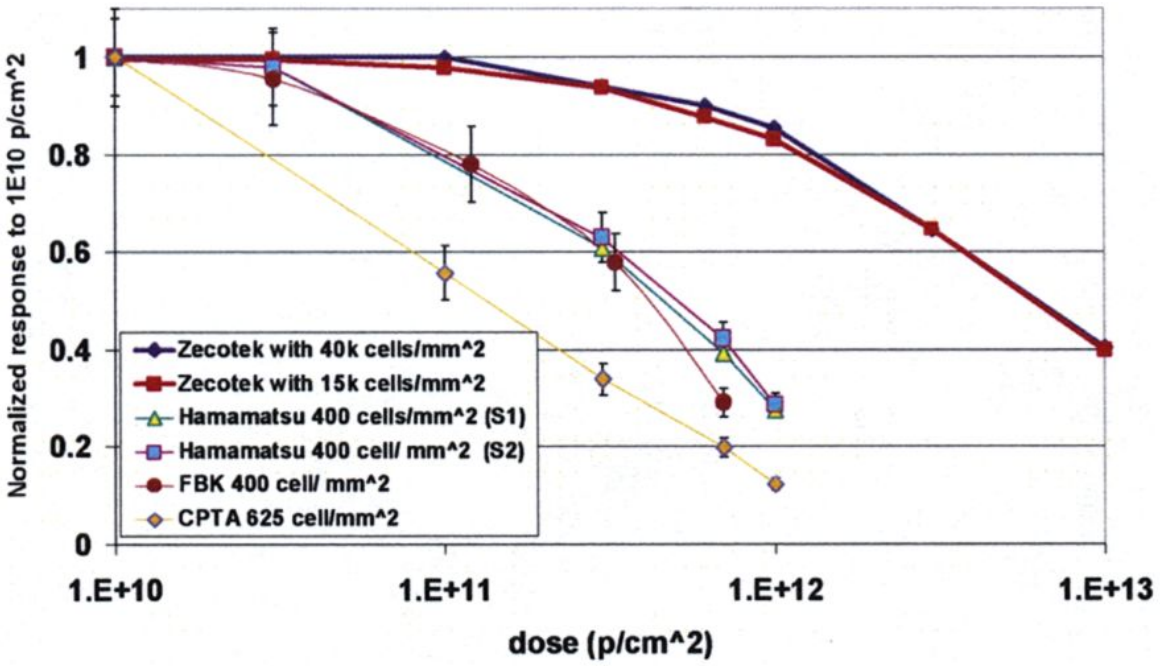


**Figure 4.5.3.1:** Radiation hardness of different SiPMs from Heering *et al.*, IEEE NS SCR 2008 NS-12.

## 4.6. R&D Timeline and Deliverables

### 4.6.1 Timeline

#### 4.6.1.1 FY16

Design and Simulation:

1. Development of a time-based reconstruction algorithm for geometries with narrow bars and spherical lenses as well as for wide plates without focusing and with cylindrical focusing.
2. Add π/K identification efficiency and mis-ID across DIRC phase space as figure of merit for DIRC design evaluation.
3. Add effects of magnetic field simulation to DIRC performance evaluation.
4. Geant4 comparison of high-refractive index materials for radiation hard lens.
5. Design of radiation-hard cylindrical three-layer lens in ZEMAX and Geant4.
6. Investigate fit to ring-center as a way to mitigate effect of insufficient tracking resolution.
7. Investigate opportunities for e/π identification in the central EIC detector using a DIRC.

Hardware:

1. Identify potential manufacturer of radiation-hard cylindrical three-layer lens.
2. Measurement of MCP-PMT gain in magnetic fields up to 5 T.

#### 4.6.1.2 FY17

Design and Simulation:

1. Investigate chromatic dispersion mitigation.
2. Add physics channels to Geant4 simulation for performance evaluation.
3. Study impact of backgrounds on DIRC performance, including accelerator-induced, track-related, and physics background.
4. Start of comparison of DIRC designs, including current lens-based high-performance design with EV inside solenoid, FDIRC design, GlueX design, and other lens- and mirror-based designs with EV outside solenoid.
5. Determining the need for supplementary π/K identification based on estimated DIRC performance.
6. Initial development of Geant4 MCP-PMT sensor simulation to support design optimization for performance in high magnetic fields and study ion feedback.

Hardware:

1. Procurement of radiation-hard cylindrical three-layer lens.
2. Measurement of MCP-PMT gain in magnetic fields up to 5 T.

#### 4.6.1.3 FY18

Design and Simulation:

1. Completion of DIRC design performance comparison.
2. Geant4 implementation of the EIC DIRC in the full EIC detector.

3. Geant4 MCP-PMT sensor simulation studies to support design optimization for performance in high magnetic fields and study of ion feedback.

Hardware:

1. Setup and commissioning of the timing capability of the high-B sensor testing facility at JLab.
2. First measurements of timing performance of MCP-PMTs in magnetic fields up to 5 T.
3. Construction and (in-beam) test of a three-layer lens prototype.

## 4.6.2 Deliverables

### 4.6.2.1 FY16

1. Evaluation of lens-based high-performance design with EV inside solenoid using both geometric reconstruction and time-based reconstruction.
2. $\pi$/K identification efficiency and mis-ID for the lens-based high-performance design with EV inside solenoid as function of particle momentum and polar angle.
3. Performance study of radiation-hard cylindrical three-layer lens in Geant4.
4. Implementation of FDIRC and GlueX designs in Geant4.
5. Gain evaluation of MCP-PMTs (Katod, Photonis) in magnetic fields up to 5 T.

### 4.6.2.2 FY17

1. Implementation of physics- and track-related backgrounds into Geant4 simulation; implementation of accelerator-induced backgrounds (if radiation map for accelerator is available).
2. Evaluation of lens-based high-performance design under different background assumptions.
3. Performance evaluation of lens-based high-performance design with EV outside solenoid using both geometric reconstruction and time-based reconstruction.
4. Comparison of high-performance design designs with EV inside or outside solenoid to FDIRC and GlueX DIRC designs.
5. Initial development of Geant4 MCP-PMT sensor simulation to support design optimization for performance in high magnetic fields and to study ion feedback.
6. Gain evaluation of MCP-PMTs (Photek, Photonis, Hamamatsu) in magnetic fields up to 5 T.
7. Investigation of various combinations of single-anode MCP-PMT internal high voltages for design optimization of sensor performance in magnetic fields up to 5 T.
8. Implementation of MCP-PMT geometry and internal structure in Geant4.

### 4.6.2.3 FY18

1. Construction and test of the initial compound lens prototype with lasers in optical lab and with prototype in particle beams (if available).
2. Comparison of performance of all investigated DIRC designs; selection of prefered design.
3. Initial integration of prefered DIRC design into the EIC detector.
4. Setup and commissioning of the timing capability of the high-B sensor testing facility at JLab.
5. Evaluation of the timing response in magnetic fields up to 5 T of an initial set of MCP-PMTs (Katod, Hamamatsu).

6. Geant4 simulation studies of ion feedback and of MCP-PMT design parameters for optimization of sensor performance in magnetic fields up to 5 T.

## 4.7. Management Plan

### 4.7.1 Funding Request and Budget

The DIRC R&D (proposal eRD4, formerly RD2011-3) was awarded $485k during FY12-15. The detailed budget and procurements for this first phase of the project (i.e., to develop lens-based high-performance DIRC and to start a high-B photosensor program) was presented in the proposal submitted in July 2014. We request an additional $409k for FY16-18, as indicated in the tables below, to continue the high-B sensor program and develop cost-optimized DIRC solution(s) for an EIC detector (including an investigation of radiation-hard lens optics for the high-performance DIRC, wider plate radiators to reduce bar cost, and a performance comparison between readout "cameras" using lens- and mirror-based expansion volumes). The tables below list the budget broken down by category and recipient.

| | FY16 | FY17 | FY18 | *Total* |
|---|---|---|---|---|
| Postdoc (50%) | $55k | $55k | $55k | *$165k* |
| Students | $16k | $24k | $24k | *$64k* |
| Hardware | $20k | $42k | $42k | *$104k* |
| Travel | $24k | $26k | $26k | *$76k* |
| *Total* | *$115k* | *$147k* | *$147k* | *$409k* |

| | FY16 | FY17 | FY18 | Total |
|---|---|---|---|---|
| ODU | $55k | $55k | $55k | *$165k* |
| CUA | $8k | $8k | $8k | *$24k* |
| USC | $16k | $28k | $28k | *$72k* |
| JLab and GSI | $36k | $56k | $56k | *$148k* |
| *Total* | *$115k* | *$147k* | *$147k* | *$409k* |

### Comments

All costs listed include overhead.

### 4.7.2 Manpower

The 50% postdoc at ODU (G. Kalicy) who has been working on the project since early 2014. Funding is also requested for undergraduate student projects at CUA and USC each year to participate in and analyze data from the high-B sensor tests. For FY17−18 we also request funds for a second undergraduate student at USC for sensor simulations. It became clear in FY14−15 that summer undergraduate internships need to be 10-week long rather than the 8 weeks that were budgeted in the DIRC R&.. To compensate for this, additional contributions of $1.5k per year were made by USC to fund the necessary 2-week extension of summer undergraduate participation in the project. The funding levels for FY16−18 should provide for full support of undergraduate internships on the project.

In addition, unfunded efforts will also be provided by:
JLab staff (P. Nadel-Turonski, Carl Zorn)
GSI staff (J. Schwiening, C. Schwarz, postdoc R. Dzhygadlo, and students) - primarily for simulations, test beam data analysis, and prototyping.
USC (prof. Y. Ilieva, and graduate student T. Cao) - primarily for high-B sensor tests
ODU (prof. C. Hyde, postdoc K. Park, and graduate student L. Allison) - primarily for simulations and high-B sensor tests.

### 4.7.3 Travel

The USC travel budget is primarily to support operations of the high-B sensor test facility. The JLab travel budget is primarily to support GSI travel to the annual collaboration meeting, bi-annual presentations to the R&D committee, and postdoc participation in test beams or presentation of results at a conference.
In previous years, the relatively low travel budget has required significant contributions from JLab, USC, and ODU. For instance, in FY15 JLab contributed $8k, ODU contributed $15k, and USC contributed $4.5k for travel related to the DIRC R&D, in addition to the funds provided by the R&D program. The funding levels for FY16−18 should make it possible to reduce these additional contributions somewhat.

### 4.7.4 Procurement

FY16:

1. Liquid Helium, high-B test facility: $12k
2. Cryogenic and protective equipment, high-B test facility: $3k
3. High-B components (sensor holders, dark box cap modifications, *etc.*): $3k
4. Shipping cost of MCP-PMTs on loan: $2k

Total: $20k

FY17:

1. Radiation hard, three-layer lens (for high-performance DIRC): $25k
2. Liquid Helium, high-B test facility:: $12k
3. High-B components (sensor holders, dark box cap modifications, *etc.*): $3k
4. Shipping cost of MCP-PMTs on loan: $2k

Total: $42k

### FY18:

1. Timing upgrade for high-B test facility: $30k
    a. Two 1-month rentals of a fast high-sampling-rate oscilloscope: $9k
    b. High-resolution TDC and Fast Constant Fraction Discriminator: $15k
    c. Reference PMTs: $6k
2. Liquid Helium, high-B test facility: $12k

Total: $42k

### Comments

Listed costs are direct. The cost estimate of the radiation hard lens is based on the previously procured three-layer lens, but could turn out to be different once a manufacturer is found able to produce it.

## 4.7.5 Responsibilities

The proposal is a collaborative effort and most participating institutions will contribute to many aspects of the proposed R&D work. In particular, the postdoc (G. Kalicy) will contribute to all activities, including simulations, test beam data analysis, development of radiation hard lenses, and operations of the high-B sensor test facility. This integration at the level of the participants is also a key reason for maintaining the DIRC R&D and the high-B sensor work as a common chapter. Nevertheless, there are two main areas of responsibility.

1. ODU (G. Kalicy, C. Hyde) and JLab (P. Nadel-Turonski) will have the primary responsibility for simulations, design, and integration of the DIRC into the EIC detector. Although not funded by this proposal, R. Dzhygadlo (GSI) will also spend part of his time working with G. Kalicy on Geant simulations of the DIRC detector.

2. GSI (C. Schwarz and J. Schwiening) will have the primary responsibility for the development and design of the focusing optics, prototyping, and in-beam testing. In FY15, G. Kalicy and L. Allison (ODU) participated in the CERN test beam aimed at establishing the photon yields for the advanced lens that was procured, and will work on the data analysis.

3. The high-B photosensor program is the primary responsibility of USC (Y. Ilieva), which will coordinate the effort, do the data analysis, and assist with maintaining and operating the EIC high-B test facility, which was set up through the EIC detector R&D program (with in-kind contributions from JLab). Local support for the high-B facility is provided by C. Zorn (JLab), G. Kalicy (ODU), and K. Park (ODU). Support for operations is further provided by P. Nadel-Turonski (JLab), L. Allison (ODU), T. Cao (USC), and undergraduate students from USC and CUA. General support is provided by JLab staff (in particular the target group for cryogenics and operation of the superconducting magnet).

# 5. LAPPD MCP-PMT R&D for EIC DETECTORS

Fernando Barbosa[3], William Brooks[5], Mickey Chiu[2] (co-PI), Marcel Demarteau[1], John Harris[6], Matthias Grosse-Perdekamp[4], Richard Majka[6], Rodrigo Mendez[5], Nikolai Smirnov[6], Thomas Tsang[2], Robert Wagner[1], Jingbo Wang[1], Junqi Xie[1], Beni Zihlmann[3], Carl Zorn[3] (co-PI)

*[1)] Argonne National Laboratory*
*[2)] Brookhaven National Laboratory*
*[3)]Jefferson Laboratory*
*[4)]University of Illinois at Urbana-Champaign*
*[5)]Universidad Tecnica Federico Santa Maria, Valparaiso, Chile*
*[6)]Yale University*

The LAPPD Program is a large detector development effort to engineer cost effective microchannel plate PMT's (MCP-PMT) [1]. MCP-PMT's from commercial vendors such as Hamamatsu and Photonis have been shown to have extraordinarily good timing (better than 50 ps TTS) and position resolution, but are generally far too expensive for widespread use, since the current cost is, for instance, about $12K for one 6x6 $cm^2$ MCP-PMT from Photonis. The LAPPD program, funded by DOE High Energy Advanced Detector R&D and Argonne LDRD, aimed to lower the cost of making MCP-PMTs by creating activated micro-channel plates using the atomic layer deposition technique to apply resistive and secondary emissive layers on a glass capillary substrate. Their collaboration has already demonstrated the feasibility of this approach in the laboratory [2], and are now are in the later stages of a SBIR Phase II grant to build a pilot assembly line for initial commercial production at Incom, Inc., a company in Massachusetts. Once this pilot line supported by SBIR II funds demonstrates the commercial viability of producing the LAPPD designed MCP-PMTs, it is believed that by simply scaling up the production to more assembly lines the cost per MCP-PMT will dramatically fall. The hope is that this will give physicists, for the first time ever, the ability to build a detector using high performance photo-sensors over tens of square meters at a reasonable cost. The first 20x20 $cm^2$ MCP-PMTs produced by Incom are expected to be available sometime late this year.

The LAPPD MCP-PMTs would be an ideal photosensor for nearly all of the proposed EIC PID detectors. For the TOF it would allow large area coverage at reasonable cost and unprecedented performance (better than 10 ps resolution). For RICH detectors, that fast timing capability would allow for a dramatic reduction in backgrounds, since one could reject hits that are not highly correlated in time. The single photon timing resolution of the MCP-PMT is expected to be about 50 ps. For DIRC's, the single largest problem is chromatic dispersion, which is the biggest contribution to the DIRC's resolution. A timing resolution of 50 ps would allow for a correction of this chromatic dispersion and vastly improve the DIRC's resolution, as shown in the design of the time-of-propagation DIRC detector being built for Belle-II [3].

While the LAPPD program has been extremely successful (the program won a R&D 100 award in 2012), the program is still in early stages and there are still many possibilities for further improvement in their design, particularly with regard to the PID applications envisioned at the EIC. All the three detector types DIRC/TOP, TOF, RICH rely on Cerenkov light, which is strongly peaked at low wavelengths. Thus, one of the most promising ways to improve their performance for EIC PID detectors is to increase their sensitivity to lower wavelengths, down into the UV region. With the right choice of photocathode and window, it should be possible to measure twice as many photoelectrons as the standard design, while still maintaining affordability.

Another necessary improvement to the LAPPD design for EIC detectors is to develop a pixelated readout of the tiles. So far all of the LAPPD tiles come only with strip-line readout, and no manpower has been allocated within their collaboration for developing a pixelated readout. For both DIRC/TOP and RICH applications, pixelated readout is a necessity since with a strip-line one can have ambiguity problems when multiple photons overlap on the same strip.

As part of the overall LAPPD effort, Argonne has developed a small form factor tile facility to produce MCP-PMT's to give evaluation modules to users. The Argonne facility is ideal for producing regular and also modified R&D versions of the MCP-PMTs. Their MCP-PMT's are 6x6 $cm^2$, which makes it much easier to change some aspect of their design, and the smaller size also makes easier for new users to handle and become familiar with their operation when compared to the 20x20 $cm^2$ ones produced elsewhere (such as at Berkeley's SSL, U. Chicago, or Incom, Inc.). Once these R&D evaluation modules have been produced, the experience can be fed back into the production process for the commercial vendor Incom, Inc., for eventual mass production.

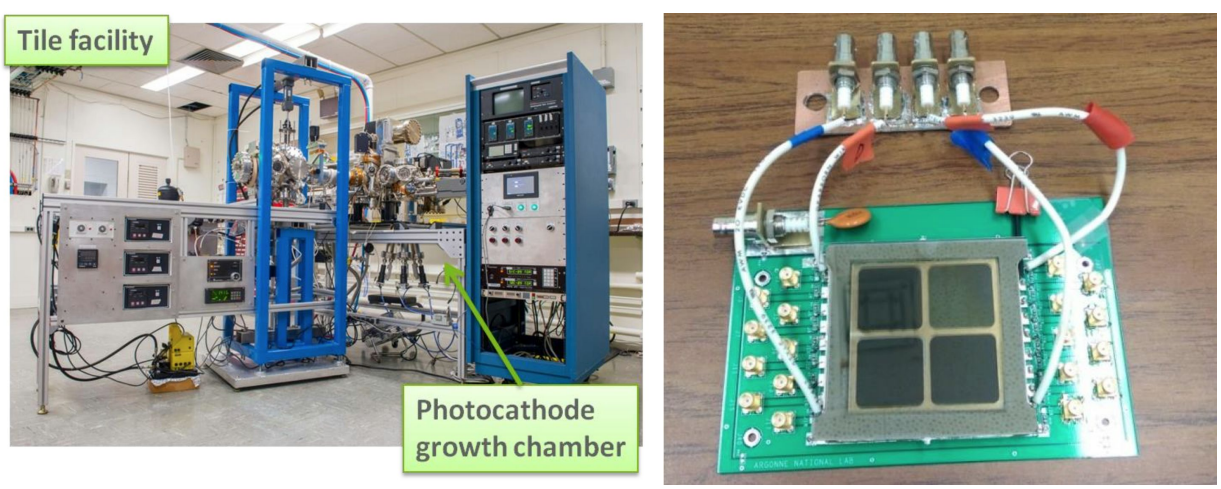


**Figure 5.1:** (left) Argonne small tile facility. (right) A MCP-PMT produced at the Argonne facility with individually biased layers.

First evaluation modules from Argonne have been provided to Carl Zorn at JLab, as reported in the eRD11 progress report. One of the latest modules produced is shown in the right hand side of fig. 5-1. The first modules have been shown to have low and non-uniform quantum efficiency, and an instability in the glass spacer based HV divider chain. These and other quirks are being worked out at Argonne, by either modifying the production process or modifying the design (such as individually biasing each layer as seen in the right hand side of fig. 5-1). Carl and colleagues at JLAB have developed a system that can be used to test the MCP-PMTs in a high-field test facility and will complete their studies of the Argonne evaluation modules once they become available later in the summer of 2015. As shown in the progress report, gain measurements derived from single photoelectron spectra can be done for a limited range of high voltages (2.75-2.85kV) for the first JLAB sample (#28). This will allow some initial magnetic field tests to be performed. It is also planned that this sample will be the first to be used in neutron irradiation tests.

# Improving MCP-PMTs for EIC PID Applications

The number of photoelectrons generated from Cerenkov light is a major determining factor in the performance of all 3 proposed EIC PID detector types. The standard LAPPD MCP-PMTs use a borosilicate glass window with a $K_2CsSb$ photocathode. While the performance is already pretty good with this standard design, one can readily improve the performance by going to windows and photocathodes which will be sensitive to more of the spectrum, since Cerenkov emission is strongest in the UV. In Fig. 5-2 we show the quantum efficiency curve for the photocathode . One can see that the QE for the photocathode used by LAPPD, $K_2CsSb$ has a sharp cutoff due to the borosilicate window.

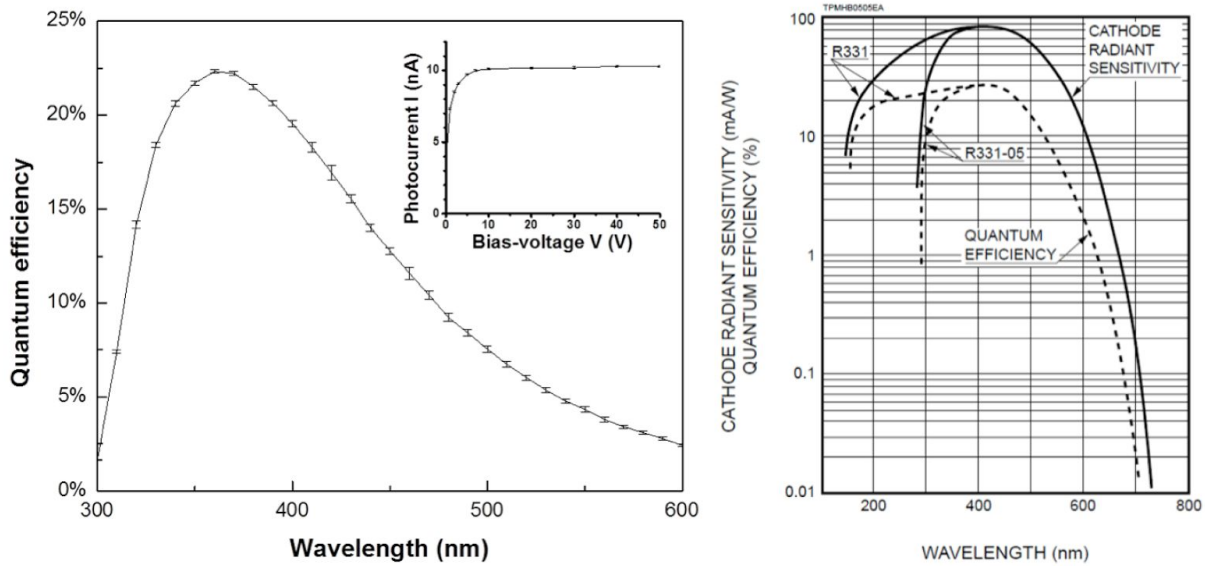


**Figure 5.2:** (left) QE measurement of photocathode grown at Argonne, which is cut-off at 330 nm due to the Borosilicate 330 window. (right) QE for Hamamatsu R331-05 (borosilicate window) and R331 (fused silica window) PMTs.

However, as can be seen in the right hand plot, the bialkali photocathode in the R331 PMT, which is the same as used by LAPPD, actually has sensitivity down to ~180 nm. Thus, one easy way to improve the MCP-PMT sensitivity is to simply replace the borosilicate window with a fused silica window. In table 5-1 we tabulate the calculation for the n.p.e. expected in various window/photocathode configurations. We expect an increase of 80% more photoelectrons by replacing the window.

There remains some uncertainty about the actual QE spectrum of $K_2CsSb$, since a measurement by a LBNL/BNL group have determined that the $K_2CsSb$ QE dies off by around 200 nm, and a calculation by John Smedley is in agreement with that cutoff [4]. Our proposed study using the fused silica window would resolve this discrepancy and determine for the first time how low the LAPPD photocathode extends in QE. In case the $K_2CsSb$ photocathode is limited at lower wavelengths, other photocathodes can also be considered. This would require some reconfiguration of the photocathode growth chamber but can be done. $Na_2KSb$, with or without Cs, seems to be the most promising option, as can be seen in table 5-1 and Fig. 5.3.

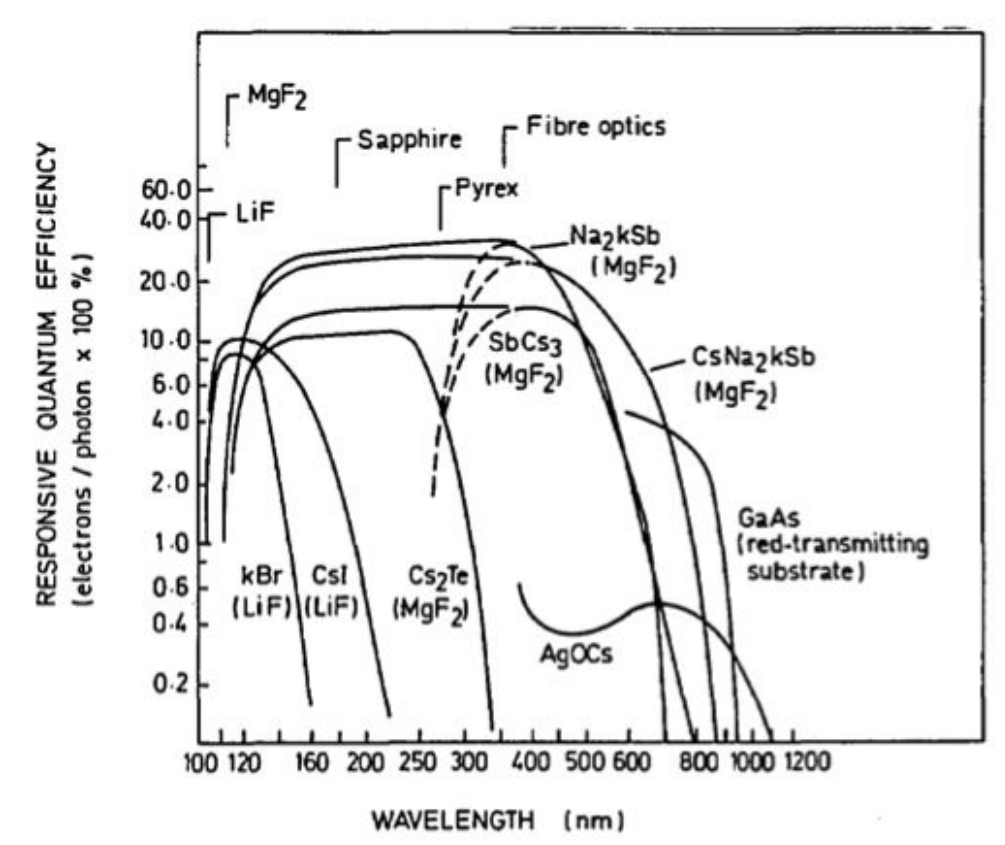


**Figure 5.3:** Example quantum efficiencies for various photocathodes, with the cut-offs for different windows [5]. The dashed lines show the quantum efficiency convoluted with the borosilicate window cutoff.

Fused silica windows have been sealed successfully by the LAPPD collaboration, so we do not expect a long learning curve before achieving success. Also, we will first try the standard photocathode ($K_2CsSb$) at first on the fused silica window, since this will minimize the number of modifications that need to be made to the assembly (which is all in vacuum and therefore not entirely trivial). These modifications proposed (changing window and photocathode), while simple, need to be tested in order to test that they work and produce quantitatively the expected number of photoelectrons. And the simplicity of the change should not detract from the major improvement that they could help to achieve, since even factors of two in the n.p.e. can make big improvements in the performance of the TOF, RICH, and DIRC detectors that have been proposed by this consortium for EIC PID.

| RadiatorWindow | Photocathode | N.P.E. |
|---|---|---|
| Borosilicate Glass | $K_2CsSb$ | 70 |
| Borosilicate Glass | $CsNa_2kSb$ | 100 |
| Fused Silica | $K_2CsSb$ | 127 |

| | | |
|---|---|---|
| Fused Silica | $CsNa_2kSb$ | 250 |
| MgF2 | $CsNa_2kSb$ | 335 |
| MgF2 | CsI | 316 |

Table 5-1: The theoretical maximum number of photoelectrons for various window and photocathode combination. The first line is the standard LAPPD photocathode. The values for CF4 are for a windowless configuration, where the photocathode is deposited on the top MCP.

# Development of Pixelated Readout for LAPPD MCP-PMTs

A more technically challenging project would be to develop a pixelated readout for the LAPPD MCP-PMT's. In Fig. 5.4, the main elements of a MCP-PMT are shown, but with the lower readout layers modified from the standard LAPPD design.

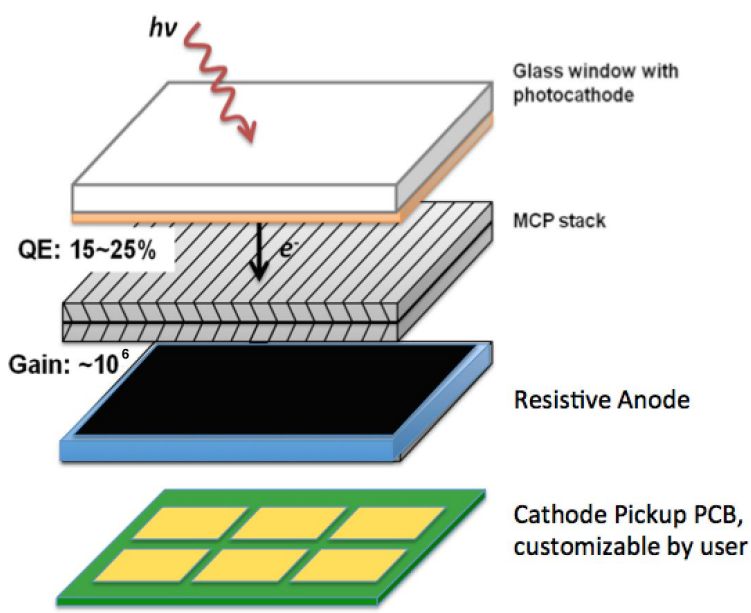


**Figure 5.4:** One possible configuration for a pixelated MCP-PMT readout.

Normally the LAPPD MCP-PMTs use silk-screened copper striplines on a glass base, with this entire base and the sidewall frit bonded in the glass lab at Argonne as a unit that only needs the top window attached in the vacuum of the tile facility to create the vacuum sealed PMT. It's not thought to be possible to use a pad geometry with this approach since then via's would be necessary through the glass bottom, though we will still explore this approach. There are two

other possibilities which we are considering which might be more feasible. The first is to coat the glass base with a somewhat resistive anode, such as graphite. A user could then design their own PCB, customized to their requirements and placed on the other side of the glass base to pick up capacitively the fast mRPC signals. This is similar to the design in the mRPC, where graphite electrodes are used to produce the ~10 kV potentials required, and the fast signals generated in the gas gaps are picked up on PCB's outside the active field regions of the detector. Whether the full timing resolution can be achieved with this approach is not known at this time.

The other possibility we are considering would be to seal the glass sidewalls to a PCB base. The pad geometry could then be easily achieved using standard PCB technology, and using direct collection of the amplified electrons from the channel plates. This would require new sealing research at Argonne since sealing glass to G-10 or other PCB compatible materials has not been something that they have worked on. It might be possible to replace the sidewalls with ceramic, which might make sealing to a PCB easier. It might also be possible to find glass-based PCBs with via's, though this is also a major R&D task by itself [6]. A glass-based PCB would make sealing the base fairly easy, however. It would also reduce risks in that there might be outgassing or other contaminaton from the standard PCB materials.

We expect developing the pixelated readout to be more technically challenging than developing the UV sensitive MCP-PMT, so we have therefore prioritized the UV sensitive MCP-PMT to give more time for us to investigate the various possibilities for a pixelated readout.

# FY2016 Plans

In the next year we propose to continue the studies from eRD11, using the standard version of the 6x6 $cm^2$ MCP-PMT tiles from Argonne. It is expected that long-lived, reliable detectors can be made from the Argonne tile facility by the end of the summer. A fairly good MCP-PMT has been provided to JLAB, from which it has been possible to see a single photo-electron peak, as shown in the eRD11 progress report. The validation studies we would like to make include

- Timing and Position Resolution: This will be done initially with laser studies and then from cosmic ray studies, and will include gain as a parameter.
- Uniformity: We want to demonstrate uniform effectiveness across the detectors. This can be done with laser scans and cosmic rays.
- Quiescent Noise: LAPPD claims less than 0.1 $Hz/cm^2$ of background noise. We want to check this and ensure that they are below the rate needed at an EIC detector.
- Operation in Magnetic Field: We want to determine the effects of a magnetic field on the operation of the MCP-PMT, particularly for the case where the field is transverse to the pore axis. Can the effects be mitigated by increasing the HV bias on the tube? This testing can be done at the test magnet facility at Argonne, or possibly JLAB.
- Rate Capability: Initial studies will be done with a laser, though final studies will have to be done in a test beam.
- Aging: We want to determine the aging characteristics of the LAPPD MCP-PMTs. Since this is potentially destructive to the MCP-PMT, we may perhaps defer this test to the LAPPD collaboration. It is of high enough importance though that we would like to address this issue as early as possible.
- Radiation Hardness: Study the resistance to radiation damage, including high particle rates as well as susceptibility to thermal neutrons. As in the aging studies, while these are destructive, it is important to try to characterize this earlier rather than later.

To elucidate a bit on the B-field testing, Argonne is currently in the process of setting up a large bore (~ 1m diameter), high field (4T), decommissioned MRI magnet that they acquired to be used for validating magnetic probes for the g-2 experiment. It can be used for studying the B-field dependence of the test MCP-PMTs. This will be an excellent addition to the HELIOS magnet at Argonne that can be used at present as experimental use schedules permit. A future possibility would be to use the proposed high field facility at JLAB constructed from a larger bore superconducting magnet currently in storage but available for use. The present JLAB facility has only a 5” diameter bore, which is too small for the current Argonne LAPPD device due to the large PCB base. The development of a smaller PCB base with a compact design would allow testing in the present high-B field test setup at JLAB, and is being considered. In any case, a pixelated 6x6 $cm^2$ readout similar to the current designs of the Photonis Planacons is being discussed for FY2017, and that will likely be able to be tested at

JLAB.

After the production of stable, long-lived, uniform and relatively high QE MCP-PMTs has been established, Argonne will produce a more UV sensitive MCP-PMT. We expect this work to commence sometime in the winter of 2015. The first step will be to simply change the window to fused silica. The QE will be measured down to ~170 nm (or as low as the fused silica window will allow). If the QE is not as good as expected, because John Smedley was right and the $K_2CsSb$ photocathode QE really is limited to 200 nm, then we will create a MCP-PMT with $Na_2KSb$.

Depending on how quickly the development proceeds, we expect to have the first UV sensitive module initially tested at Argonne, and then sent to JLAB for further testing while Argonne produces a second working module. Finally, two more will be produced with 1 cm thick fused silica windows for testing as a TOF and provided to BNL for testing in collaboration with UIUC.

# FY2017 Plans

In FY 2017 we will start on plans to produce a pixelated readout version of the MCP-PMT, using either or both of the approaches mentioned (resistive anode with external PCB or internal PCB). As mentioned previously, while it sounds simple there are many complications to overcome, in particular with respect to sealing (the PMT vacuum has to be extraordinarily good). All the modifications have to be done while maintaining the timing performance, and we suspect most of the modifications will work to reduce the performance. Therefore we expect many iterations over the year to understand how the MCP-PMT signals propagation behaves under our modifications so that we can optimize the performance for pad readout. This more compact pixelated readout should make it possible for testing in the high-B field test setup at JLAB. The JLAB, Argonne, Yale, and BNL groups will be most involved in this aspect of the R&D.

# FY2018 Plans

We expect that once there are successful versions of the MCP-PMTs produced, of either the modified designs or the standard designs, the DIRC, RICH, and TOF groups will want to incorporate them into their prototypes, and each group may want a slightly different configuration. The Argonne facility is expected to be able to produce about one MCP-PMT a week, and we expect demand of at least 10 MCP-PMTs from the EIC PID users. At some time the commercial versions from Incom will be available as well, and it would be good to test these, but it is too early to speculate when exactly these will be available.

# Requested Budget

The funding for initial characterization of the Argonne MCP-PMTS was provided to JLAB in FY15, and there are enough funds to complete most of those studies once a reliable MCP-PMT is delivered to Carl at JLAB. We request only travel funding in FY16 for Carl and for a UTFM student to go to Argonne to perform the high field tests there.

For FY16 we are requesting funding to support manpower at Argonne to produce a UV sensitive MCP-PMT. The manpower is needed to operate the production facility, and to check the produced MCP-PMTs. There is also funding requested to purchase a UV spectrometer at Argonne, which is crucial for characterizing the performance of the photocathode down into the UV. The spectrometer is based on a deuterium lamp with monochromator.

In FY17, we request funding to operate the production facility to produce MCP-PMTs with pixelated readout. This effort will funding for an Argonne technician to produce the new baseplates or PCBs that are required. If the committee deems that pixelated readout is a higher priority, optionally funding can be provided in FY16 to work on the pixelated readout. The current ordering (more UV sensitive PMT and then pixelation) was chosen since the pixelation would be much harder to implement, compared to simply changing the window and possibly changing the photocathode.

| LAPPD MCP-PMT | Institution | FY16 | FY17 | FY18 | Total |
|---|---|---|---|---|---|
| Postdoc (0.2 FTE/yr) | ANL | $25,000 | $25,000 | $25,000 | $75,000 |
| Scientist (0.1 FTE/yr) | ANL | $25,000 | $25,000 | $25,000 | $75,000 |
| Technician (1 month FTE) | ANL | $0 | $25,000 | $0 | $25,000 |
| Materials | ANL | $40,000 | $5,000 | $0 | $45,000 |
| Student (1 month FTE) | JLAB/UTFSM | $5,000 | $5,000 | $5,000 | $15,000 |
| Travel | JLAB | $5,000 | $5,000 | $5,000 | $15,000 |
| LAPPD Subtotal | | $100,000 | $90,000 | $60,000 | $250,000 |

Table 5-2: Proposed budget for the LAPPD MCP-PMT R&D.

# References


[1] LAPPD Collaboration, http://psec.uchicago.edu

[2] Bernhard Adams et al., "Measurements of the gain, time resolution, and spatial resolution of a $20$x$20cm^2$ MCP-based picosecond photo-detector," *Nucl.Instrum.Meth.*, vol. A732, pp. 392-396, 2013.

[3] Nishimura, et.al., “The time-of-propagation counter for Belle-II”, Nucl.Instrum.Meth.A639:177-180,2011 [arXiv:1009.0876]

[4] Private communication, John Smedley

[5] C. I. Coleman, "Imaging detectors for the ultraviolet," *Applied Optics*, vol. 20, pp. 3693-3703, 1981.

[6] J. Microelectron. Packag. Soc., 21(2), 53-57 (2014).

# 6. Summary

We are responding to the request of the R&D committee for a more coordinated PID effort by submitting this year's proposal as a consortium with 13 participating institutions (10 domestic and 3 international). The proposal is structured by chapters generally corresponding to the three previously funded proposals (TOF, RICH, and DIRC). Eventually, we envision a fourth chapter on sensors. However, this time we decided to break out the LAPPD work, which was part of both the TOF and RICH proposals into a separate chapter, while retaining the high-B studies as part of the DIRC chapter. In the short term, this allowed us to, on one hand, more clearly show the continuity of the FY16 budgets (in particular for the DIRC) and on the other, to present a coherent effort, with a visible total cost, for the LAPPD work. We have tried to make sure that the FY16 request stays around $0.5M. However, the falling budgets for FY17 and FY18 do not necessarily indicate that funding needs for PID R&D will diminish, rather reflects a natural development of the ongoing efforts. If some of the currently proposed R&D items are postponed, or new items are added, the requests for FY17-18 could increase in next year's proposal update.

## 6.1 Funding Request and Budget

We request $504k for FY16 and plan to request another $444k and $399k for FY17 and FY18, respectively. The tables below show the budget breakdown by activity (detector system), institution, and category (salaries, hardware, travel).

Budget by chapter/activity

| | FY16 | FY17 | FY18 | *Total* |
|---|---|---|---|---|
| TOF | $63k | $6k | $3k | *$72k* |
| RICH | $226k | $201k | $189k | *$616k* |
| DIRC + high-B | $115k | $147k | $147k | *$409k* |
| LAPPDs | $100k | $90k | $60k | *$250k* |
| *Total* | *$504k* | *$444k* | *$399k* | *$1,347k* |

Budget by institution

| | FY16 | FY17 | FY18 | *Total* |
|---|---|---|---|---|
| ANL | $90k | $80k | $50k | *$220k* |
| BNL | $6k | $6k | $6k | *$18k* |
| CUA | $8k | $8k | $8k | *$24k* |
| Duke | $2k | $2k | $2k | *$6k* |
| GSU | $99k | $69k | $69k | *$237k* |
| INFN (JLab) | $46k | $55k | $55k | *$156k* |
| JLab and GSI | $41k | $61k | $61k | *$163k* |
| LANL | $4k | $4k | $4k | *$12k* |
| ODU | $55k | $55k | $55k | *$165k* |
| UIUC | $63k | $6k | $3k | *$72k* |
| UNM | $69k | $65k | $53k | *$187k* |
| USC | $16k | $28k | $28k | *$72k* |
| UTFSM (JLab) | $5k | $5k | $5k | *$15k* |
| *Total* | *$504k* | *$444k* | *$399k* | *$1,347k* |

Budget by category

| | FY16 | FY17 | FY18 | *Total* |
|---|---|---|---|---|
| Prof/Staff | $37k | $62k | $37k | *$136k* |
| Postdocs | $251k | $200k | $200k | *$651k* |
| Students | $46k | $54k | $54k | *$154k* |
| Hardware | $112k | $65k | $48k | *$225k* |
| Travel | $58k | $63k | $60k | *$181k* |
| *Total* | *$504k* | *$444k* | *$399k* | *$1,347k* |

### Comments on budget tables

All costs listed include overhead. Payments to INFN (Italy) and UTFSM (Chile) will go through JLab. GSI (Germany) does not receive funds directly, but travel and some hardware are covered through JLab.

## 6.2 Manpower

The funds for senior personnel go primarily to ANL (74%), with the remainder going to UNM. The postdoc funds support positions (with matching funds) at ANL, GSU, ODU, UNM, UIUC (FY16 only), and internationally at INFN. The student funds support students at CUA (undergraduate), GSU, USC (one undergraduate in FY16 and two in FY17-18), UNM, and UTFSM.

## 6.3 Travel

Travel funds are distributed between many of the participating institutions. However, the key items are support for travel for sensor measurements the high-B test facility at JLab, travel for tests of LAPPDs at ANL, and travel for testing a prototype of the modular aerogel RICH in test beams at Fermilab.

## 6.4 Procurement

### FY16:

1. $35k for construction of modular aerogel RICH prototype
2. $17k items for GEM photocathode work
3. $20k high-B test facility operations
4. $40k items for LAPPD work

Total: $112k

### FY17:

1. $5k materials for modular aerogel RICH prototype
2. $13k items for GEM photocathode work
3. $25k radiation hard lens for high-performance DIRC
4. $17 high-B test facility operations
5. $5k items for LAPPD work

Total: $65k

### FY18:

1. $5k materials for modular aerogel RICH prototype
2. $1k items for GEM photocathode work
3. $30k timing upgrade for high-B test facility
4. $12k high-B test facility operations

Total: $48k

## 6.5 Responsibilities

An important goal for forming a consortium was to help coordinating various PID efforts, and to increase collaboration between the different participating groups. The specific responsibilities (contacts, co-PIs, institutions) for the different projects are listed in each chapter.